INSTABILITIES IN HIGHER-DIMENSIONAL THEORIES OF GRAVITY

by

Jordan L. Hovdebo

A thesis
presented to the University of Waterloo
in fulfillment of the
thesis requirement for the degree of
Doctor of Philosophy
in
Physics

Waterloo, Ontario, Canada, 2006

AUTHOR’S DECLARATION FOR ELECTRONIC SUBMISSION OF A THESIS

I hereby declare that I am the sole author of this thesis. This is a true copy of the thesis, including any required final revisions, as accepted by my examiners.

I understand that my thesis may be made electronically available to the public.

Abstract

A number of models of nature incorporate dimensions beyond our observed four. In this thesis we examine some examples and consequences of classical instabilities that emerge in the higher-dimensional theories of gravity which can describe their low energy phenomenology.

We first investigate a gravitational instability for black strings carrying momentum along an internal direction. We argue that this implies a new type of solution that is nonuniform along the extra dimension and find that there is a boost dependent critical dimension for which they are stable. Our analysis implies the existence of an analogous instability for the five-dimensional black ring. We construct a simple mode of the black ring to aid in applying these results and argue that such rings should exist in any number of space-time dimensions.

Next we consider a recently constructed class of nonsupersummetric solutions of type IIB supergravity which are everywhere smooth and have no horizon. We demonstrate that these solutions are all classically unstable. The instability is a generic feature of horizonless geometries with an ergoregion. We consider the endpoint of this instability and argue that the solutions decay to supersymmetric configurations. We also comment on the implications of the ergoregion instability for Mathur's 'fuzzball' proposal.

Finally, we consider an interesting braneworld cosmology in the Randall-Sundrum scenario constructed using a bulk space-time which corresponds to a charged AdS black hole. In particular, these solutions appear to 'bounce', making a smooth transition from a contracting to an expanding phase. By considering the space-time geometry more carefully, we demonstrate that generically in these solutions the brane will encounter a singularity in the transition region.

Acknowledgements

Throughout the course of my studies, I have benefitted greatly from the help of many people. First, it is a great pleasure to thank my supervisor Rob Myers. I will be ever grateful for his advice, support and patient guidance throughout these many years as both an undergraduate and graduate student.

The Perimeter Institute for Theoretical Physics has provided me with the dream of many graduate students: an office with a window and free espresso. More importantly, though, it has given me an exciting and stimulating place to work and learn, for which I am very grateful. I have had the opportunity to work on a wide range of different projects. I thank my collaborators Amjad Ashoorioon, Vitor Cardoso, Óscar Dias, Robb Mann, Rob Myers, Maxim Pospelov, Frans Pretorius, Nemani Suryanarayan and Toby Wiseman for sharing their knowledge and insight.

The willingness of my closest friends: Dave, Simon, Laura, Rick, Casey, Niranjan, Brad, Kevin, Reid, Duke, Dennis and Dave to still return my calls and email even though they occur far too infrequently has been wonderful. Their friendship and has meant much to me, helping to maintain both my perspective and sanity. I thank my family for always being there for me, and I thank my wife, Bronwyn, for making each day of these five years a joy.

Dedication

For my mother. The things you have done for me has made this possible.

CONTENTS

LIST OF TABLES

LIST OF FIGURES

Chapter **1**

Introduction

The writing of this thesis marks nearly one hundred years since the publication of Einstein's general theory of relativity. His theory dramatically modified the prevailing notions of space and time. Since then, the scientific community has often replied in kind by modifying Einstein's notion of space-time in the continuing search for an ultimate theory of nature.

One of the earliest of these modifications, the addition of an extra dimension beyond the observed four[1], was suggested by Kaluza [3] only five years after general relativity was introduced [4]. He found, by what he interpreted as a purely formal construction, that four-dimensional Einstein-Maxwell theory could be obtained as the dimensional reduction of pure gravity in five dimensions. To arrive at this result required the assumption that the extra coordinate was a Killing vector for the five-dimensional space, and that the proper length of the extra dimension was a constant. This simple idea was the seed for many fruitful years of research up to and including writing of this thesis. For a description of that history, we follow the excellent review given by Appelquist, Chodos, and Freund [5].

---

[1] Note, however, this was not the first gravitational theory to incorporate extra dimensions. In fact, even before general relativity, Gunnar Nordström had proposed a scalar theory of gravity [1]. He was able to unify his theory with Electromagnetism by adding an extra dimension and identifying the fifth component of the gauge field with the scalar [2].

It was later, in 1926, that Klein [6] and Mandel [7] independently rediscovered Kaluza's theory. Klein came closer to interpreting the extra dimension as having physical significance, discussing higher harmonics of scalar fields in the internal dimension leading to quantized charge. Einstein and Bergmann [8] continued in this direction, advancing the idea closer to our modern interpretation that the extra dimension should be interpreted as physical, but compactified on a circle sufficiently small so as to require exceedingly high energy to excite derivatives of the fields in that direction. This, it could be said, was the start of the paradigm of studying higher-dimensional theories of gravity as a route toward the unification of gravity with the other forces in nature.

Progress in this direction included the generalization to non-abelian gauge fields [9–15] by adding even more dimensions. These constructions suffered from an important problem not found in the five-dimensional theory. While the simple solution consisting of four-dimensional Minkowski space and a flat internal circle was a solution of Kaluza-Klein theory in five dimensions, the same could not be said of these higher-dimensional constructions with non-abelian gauge groups. One finds that when the gauge fields vanish, requiring both the higher-dimensional and four-dimensional spaces be flat implies that the internal space has no curvature. This, however, is inconsistent with the requirement of non-trivial structure constants for the non-abelian gauge group which must have their origin in the curvature of the internal space.

What was needed was a method of "spontaneous compactification", whereby the theory contained solutions corresponding to a four-dimensional Minkowski base times an internal compact space. Cremmer and Scherk [16] first addressed the problem by pointing out that such solutions could exist if one included Yang-Mills and scalar matter fields in the higher-dimensional theory. This was later generalized by Luciani [17] to a larger class of internal spaces.

While the additions suggested by Cremmer and Scherk were a departure from the original Kaluza-Klein idea of pure gravity in higher dimensions, there is a natural arena where they find a home. In eleven dimensions there is a unique supergravity [18], the bosonic sector of which consists solely of a graviton and a four-form field strength. Moreover, there are no matter or Yang-Mills supermultiplets in eleven dimensions. The compactification of gravity theories in d dimensions containing a p-form field strength have been studied by Freund and Rubin

[19]. They observed that there were preferred compactifications to $d-p$ and p dimensions that arose when looking for configurations in which the uncompactified part of the space-time was maximally symmetric. In a sense then the extension of the Kaluza-Klein idea to supergravity is quite natural in eleven dimensions where the observed four dimensions of space-time arise as a consequence.

This, however, is not the only context in which eleven dimensions has appeared. Witten realized [20] that in order to obtain, by compactification, a realistic model containing the standard model gauge group, the minimum dimensionality of the internal space was seven. Further, simply producing the required gauge group is not sufficient. One needs chiral fermions, which were shown to be impossible to obtain in the eleven dimensional compactifications [20]. In fact, this result was later extended to arbitrary dimension [21], showing that although higher dimensions may be an important part of a potential theory, Kaluza-Klein theory alone will be insufficient to produce the known phenomenology.

Around the time pure Kaluza-Klein theory was shown to be insufficient for producing realistic phenomenology, string theory was developing as a potential theory of quantum gravity which unified all known forces. The bosonic theory was only consistent in twenty-six dimensions, but its spectrum contained a tachyon. This caused attention to shift to the superstring where the requirement of supersymmetry in the target space projected the tachyon out of the spectrum. Again, consistency of the theory requires that it exist in a critical dimension, this time ten.

More recently, superstring theory received a boost as a result of the progress being made in understanding the microphysics of black holes. The discovery in the 1970's of the laws of black hole mechanics — for a review see [22] — and their formal similarity to the laws of thermodynamics led Bekenstein [23] to conjecture that one could associate to a black hole an entropy proportional to its horizon area. Strength was later given to this conjecture by Hawking who showed that particle creation took place near horizons causing them to effectively radiate as a blackbody and thus could be associated with a temperature [24]. The next logical step, as it was in the transition from thermodynamics to statistical mechanics, was to find a microscopic description of the black holes in which the entropy counted the number of degenerate microstates that are indistinguishable on a macroscopic level.

In 1995, it was discovered that string theory is not just a theory of strings, but also contains D-branes [25], extended objects upon which strings can end. As they are endowed with tension, bringing together many D-branes can result in the formation of an event horizon. For certain (nearly) supersymmetric black holes, one is able to show that the Bekenstein-Hawking entropy as computed in the strongly-coupled supergravity description, can be reproduced as a statistical entropy in a weakly-coupled D-brane description as the degeneracy of the relevant microstates [26] — for reviews, see [27–29]. The AdS/CFT correspondence [30, 31] provides further insights into these issues by providing a dictionary relating the geometric description of the physics in the near-horizon region of many coincident D-branes with the physics of a dual conformal field theory — see [32] for a review. In particular, the AdS/CFT indicates that Hawking evaporation should be a unitary process, in keeping with the basic tenets of quantum theory.

As noted earlier, it has not just been the search for a unified theory which has led to extra dimensions. While the standard model of particle physics has been hugely successful, there are indications that it is incomplete. For example, recent observations of neutrino oscillations [33] imply that they have mass, but Majorana mass terms for the neutrinos are forbidden in the standard model by B-L symmetry [34]. One may obtain a Majorana mass for the neutrinos by including a dimension-five operator, but this implies we should only regard the standard model as an effective low-energy theory. Indeed, one could also arrive at such a conclusion from purely theoretical considerations as QED is not asymptotically free, implying its interactions must become strong at some scale. Ensuring that the quadratic running of the Higgs mass does not interfere with the electroweak symmetry breaking mechanism places the scale of the new physics on the order of a few TeV [35].

While the UV completion of the standard model is not yet known, increasingly the phenomenology community has been turning to models that posit extra dimensions to address many of its outstanding puzzles. Braneworlds [36–40] for example, have generated an enormous amount of interest in higher-dimensional space-times among particle theorists. Inspired by D-branes, a key ingredient in these brane models is that the standard model particles remain confined to a (3+1)-dimensional brane, while only the gravitational excitations propagate through the full space-time. Such scenarios provide a new framework in which to address many longstanding puzzles in particle physics, such as the hierarchy problem. The cosmology community has also shown an increasing interest in braneworlds [41–62], since this is another field where brane models have the potential to provide novel solutions to many of the perennial questions.

In all these braneworld scenarios, the size of the extra dimensions are larger than the fundamental Planck scale. Their low energy behavior will then be described by classical general relativity. It is in this arena that we may understand much of the phenomenology of these models.

It seems then, whether one's interest lies in unification or phenomenology, the study of higher-dimensional relativity will be important. One of the most striking results of such studies is that general relativity in dimension greater than four has a much richer structure than its lower-dimensional counterpart. Studying black holes in higher dimensions, for example, it has been discovered that a large number are unstable at the classical level. The prototypical example of this being the black string: the direct product of a Schwarzschild black hole and a flat circle. One finds that for a sufficiently large internal circle, the solutions are unstable against a class of perturbations to the metric that grow exponentially in time [63, 64]. The discovery of such instabilities by Gregory and Laflamme suggested there were previously undiscovered black hole solutions, which were nonuniform along the internal dimension, to be found [65, 66]. Such solutions were later constructed both in perturbation theory [67] and in a fully nonlinear regime [68].

These new nonuniform black hole solutions were not the only new black hole solutions waiting to be found in higher dimensions. Even before the nonuniform solutions were constructed any hope of extending black hole uniqueness theorems from four [69–72] to higher dimensions was dashed by the discovery of a second type of asymptotically flat black hole solution in five dimensions [73]. The new solution was a black ring, a black hole with horizon topology $S^2 \times S^1$ in five dimensions. The angular momentum supports the ring against collapse by the tension and also the gravitation self-attraction [74]. There is a range of angular momentum such that there are two solutions which have energy and angular momentum that is degenerate with a five-dimensional black hole spinning in one axis. If one additionally allows the ring to carry a dipole charge, this discreet degeneracy becomes a continuous, infinite one

[75]. Though there is no upper Kerr bound on the angular momentum for the black ring, it appears one may be dynamically enforced by instabilities that occur for larger spin [74].

Further, a recent proposal by Mathur and collaborators for understanding black hole entropy has been advanced, for a review see [76, 77]. They argue that individual microstates correspond to smooth, horizon free geometries that differ only out to a distance corresponding to the horizon size. The black hole is dual to an ensemble of these microstates, and so the horizon only emerges in a coarse grained average over the exponential number of microstates. For this proposal to be true, there must be families of new solitonic solutions of gravity which form the ensemble of microstates. Though of course if true, these microstates must also exist in four dimensions. Such microstate geometries have been constructed for supersymmetric black holes [78–93], and more recently the first steps have been taken toward their construction for nonsupersymmetric black holes [94].

The focus of this thesis will be one of the very common problems that occur in higher-dimensional theories: instabilities arising at the classical level. We begin in Chapter 2 by examining the Gregory-Laflamme instability for black strings carrying momentum along an internal direction. We demonstrate a simple kinematical relation between the thresholds of the classical instability for the boosted and static black strings. We argue that this implies a new type of solution and find that there is a boost dependent critical dimension for which these solutions are stable. Our analysis implies the existence of an analogous instability for the five-dimensional black ring of Emparan and Reall. We also use our results for boosted black strings to construct a simple model of the black ring and argue that such rings exist in any number of space-time dimensions.

Next, in Chapter 3, we turn our attention to the Mathur proposal and the nonsupersymmetric microstate geometries which have recently been constructed [94]. It is found that these also suffer from a classical instability, though its nature is quite different than that occurring for the boosted strings. It is a generic feature of horizonless geometries with an ergoregion. We argue that this instability holds strong implications for the Mathur proposal.

Finally, before giving some concluding remarks, we consider in Chapter 4 an aspect of the braneworld description of cosmology. Recently, a model has been constructed within the

Randall-Sundrum scenario of a codimension-1 brane in the background of an AdS-Reissner-Nordström black hole, producing a cosmological evolution which appeared to result in a non-singular bounce between contracting and expanding phases. By considering the space-time geometry more carefully, we demonstrate that the evolution of this solution will always encounter a curvature singularity in the transition region resulting from an exponential flux of perturbations generated in the external space-time.

Chapter 2

Black Rings, Boosted Strings and Gregory-Laflamme

There has been a great deal of activity studying "black objects" in higher dimensions, particularly in string theory [95–98]. There is clear evidence that our four-dimensional intuition leads us astray in thinking about the physics of event horizons in higher-dimensional gravity. For example, an interesting corollary of the early theoretical investigations of black holes in four dimensions was that each connected component of a stationary horizon must have the topology of a two-sphere [99]. However, this result is easily evaded in higher dimensions. As a simple example, consider the four-dimensional Schwarschild metric combined with a flat metric on R^m. This space-time is an extended black hole solution of Einstein's equations in 4+m dimensions, and the topology of the horizon is $S^2 \times R^m$. Clearly, this straightforward construction is easily extended to constructing many other higher-dimensional black holes whose horizons inherit the topology of the "appended" manifold.[1] These solutions describe extended objects in that the geometry is not asymptotically flat in all 3+m spatial directions and so one might have conjectured that all localized black objects would have a spherical horizon. However, this hope was eliminated by Emparan and Reall [73], who constructed an explicit five-dimensional metric describing a black ring with horizon topology $S^2 \times S^1$. The circle direction in these solutions is supported against collapse by the angular momentum carried in this direction, as was anticipated much earlier in [104].

---

[1] Similar solutions arise for four dimensions in the presence of a negative cosmological constant [100–103].

These black ring solutions also eliminated any possibility of extending the usual black hole uniqueness theorems beyond four dimensions. In four-dimensional general relativity, work on black hole uniqueness theorems began with the pioneering work of Israel [69, 70]. The no-hair results are now rigorously established for Einstein gravity coupled to Maxwell fields and various other simple matter systems [71, 72]. While in string theory, we study more complicated matter field couplings (as well as space-time dimensions beyond four), the plethora of new solutions [95–98] still respected the spirit of the no-hair theorems in that the black hole geometries are still completely determined by some small set of charges. However, the black rings [73] explicitly provided two solutions for which the mass and spin were degenerate with five-dimensional spinning black holes [104]. This nonuniqueness was further extended to a continuous degeneracy with the introduction of dipole charges [75].

One open question is whether or not such black rings exist in more than five dimensions. One argument suggesting that five dimensions is special comes from considering the scaling of the Newtonian gravitational and centripetal forces. In this sense, five dimensions is unique in that it is only for $D = 5$ that these forces scale in the same way and can be stably balanced. Of course, this is purely a classical argument which need not be true in the fully relativistic theory, and further it ignores the tension of the ring. It is part of the goal of this chapter to address this question.

In considering spinning black holes and rings, four dimensions is also distinguished from higher dimensions by the Kerr bound. While there is an upper bound on the angular momentum per unit mass of a four-dimensional black hole, no such bound exists for black holes in dimensions higher than five [104]. The five-dimensional black rings also remove this bound in higher dimensions [73].

Even more strikingly, in contrast to the stability theorems proven for four-dimensional black holes [105–108], Gregory and Laflamme [63, 64] have shown that extended black branes are unstable. The spectrum of metric perturbations contains a growing mode that causes a ripple in the apparent horizon. The endpoint of the instability is not completely clear, however, a fascinating picture is emerging [66]. Interestingly, it was shown in [109] the Gregory-Laflamme instability dynamically enforces the “Kerr bound” for $D \geq 6$. Perhaps a stability criterion will restore some of the restrictions which are seen to apply to black holes in four dimensions.

In the present chapter, we investigate the Gregory-Laflamme instability for black strings carrying Kaluza-Klein (KK) momentum. These solutions are easily constructed by boosting the static black string metrics. We begin in Section 2.1 with a review of the Gregory-Laflamme instability for static black strings. The discussion of boosted black strings begins in Section 2.2, where we first present the solutions carrying KK momentum and then consider their stability with global thermodynamic arguments. We then adapt the usual numerical analysis of the Gregory-Laflamme instability to these boosted solutions. We demonstrate a simple kinematical relation between the thresholds of the instability for boosted and static black strings with a fixed horizon radius. Comparing the numerical results with the previous global analysis, we find that Sorkin's critical dimension [110] depends on the boost velocity. In Section 2.3, we apply our results to a discussion of the stability of the black ring solutions of Emparan and Reall [73]. As already anticipated there, we find that large black rings will suffer from a Gregory-Laflamme instability. Our analysis allows us to argue that black rings will exist in any dimension higher than five as well.

2.1 Gregory-Laflamme instability

The detailed calculation of the instability of the boosted black strings will be an extension of the original analysis of Gregory and Laflamme [63, 64]. Hence we begin here by reviewing theprovide no barrier stability analysis for static black strings.[2] For the static string in $D = n+4$ dimensions, the background metric is an extrema of the Einstein-Hilbert action

$$I = \frac{1}{16\pi G}\int d^D x\sqrt{-g}R \ ,$$

and can be written as

$$ds^2 = -f(r)\,dt^2 + \frac{dr^2}{f(r)} + r^2 d\Omega_{n+1}^2 + dz^2 \ , \tag{2.1}$$

---

[2] Note, however, that our gauge fixing follows [111] which differs from that in the original analysis of [63, 64]. The present gauge fixing [111] has the advantages that it succeeds in completely fixing the gauge and it is well-behaved in the limit of vanishing k.

where $d\Omega^2_{n+1}$ is the metric on a unit $(n+1)$-sphere and

$$f(r) = 1 - \left(\frac{r_+}{r}\right)^n \ . \tag{2.2}$$

The event horizon is situated at $r = r_+$ and we imagine that the z direction is periodically identified with $z = z + 2\pi R$.

Now we seek to solve the linearized Einstein equations for perturbations around the above background (2.1). The full metric is written as

$$g_{\mu\nu} = \tilde{g}_{\mu\nu} + h_{\mu\nu} \ , \tag{2.3}$$

where $\tilde{g}_{\mu\nu}$ is the background metric (2.1) and $h_{\mu\nu}$ is the small perturbation. We will restrict the stability analysis to the *S*-wave sector on the $(n+1)$-sphere as it can been be proven that modes with $\ell \neq 0$ are all completely stable. This is apparent following the line of argument originally presented in [112]. Assume the threshold for any instability corresponds to a time-independent mode. This mode could then be analytically continued to a negative mode of the Euclidean Schwarzschild solution. However, by a direct calculation involving an expansion in scalar, vector and tensor spherical harmonics, Gross, Perry and Yaffe [113] have shown that the existence of such a mode is unique to the *S*-wave sector. Recently, this stability has also been proven by a more direct analysis [114]. Hence we write the perturbations as

$$h_{\mu\nu} = \mathcal{R}e\left[e^{\Omega\, t + ik\, z} a_{\mu\nu}(r)\right] \ , \tag{2.4}$$

where Ω and k are assumed to be real and $a_{\mu\nu}$ is chosen to respect the spherical symmetry, *e.g.*, $a_{z\theta} = 0$. Hence solutions with $\Omega > 0$ correspond to instabilities of the static black string. The above ansatz (2.4) can be further simplified with infinitesimal diffeomorphisms. Using a diffeomorphism with the same t and z dependence as above, the perturbation may be reduced to a form where the only nonvanishing components of $a_{\mu\nu}$ are:

$$\begin{aligned} a_{tt} = h_t(r)\ , \quad a_{rr} = h_r(r)\ , \quad a_{zz} = h_z(r)\ , \\ a_{tr} = \Omega\, h_v(r)\ , \quad a_{zr} = -ik\, h_v(r)\ . \end{aligned} \tag{2.5}$$

Note that even though $a_{\theta\theta} = 0 = a_{\phi\phi}$, these perturbations can cause rippling in the position of the *apparent* horizon along the internal direction [64].

The linearized Einstein equations give a set of coupled equations determining the four radial profiles above. However, we may eliminate h_v, h_r and h_t from these equations to produce a single second order equation for h_z:

$$h_z''(r) \;+\; p(r)\, h_z'(r) \;+\; q(r)\, h_z(r) = \Omega^2 w(r) h_z(r) \tag{2.6}$$

$$\begin{aligned} p(r) &= \frac{1}{r}\left(1 + \frac{n}{f(r)} - \frac{4(2+n)\,k^2 r^2}{2\,k^2 r^2 + n(1+n)\left(\frac{r_+}{r}\right)^n}\right) \\ q(r) &= \frac{1}{r^2}\left(-\frac{k^2 r^2}{f(r)}\,\frac{2\,k^2 r^2 - n(3+n)\left(\frac{r_+}{r}\right)^n}{2\,k^2 r^2 + n(1+n)\left(\frac{r_+}{r}\right)^n}\right) \\ w(r) &= \frac{1}{f(r)^2} \end{aligned} \tag{2.7}$$

Next we must determine the appropriate boundary conditions on $h_z(r)$ at the horizon and asymptotic infinity for a physical solution. First near the horizon, the radial equation (2.6) simplifies considerably yielding solutions

$$h_z = A e^{\Omega\, r_*} + B e^{-\Omega\, r_*}\ . \tag{2.8}$$

Here r_* is the tortoise coordinate defined by $dr_*/dr = 1/f$ and with which the horizon appears at $r_* \to -\infty$. Now in principle, we would choose initial data for the perturbation on a Cauchy surface extending to the future horizon and demand that the perturbation be finite there. Hence we require that $B = 0$ for physical solutions.[3]

Eq. (2.6) also simplifies as $r \to \infty$. The asymptotic solutions behave differently depending on whether $n = 1$ or $n \geq 2$. For $n = 1$, the regular solutions take the form

$$h_z \sim e^{-\mu\, r} r^{2 - \frac{\Omega^2+\mu^2}{2\mu} r_+}\ , \tag{2.9}$$

where $\mu^2 \equiv \Omega^2 + k^2$. For $n \geq 2$, they are

$$h_z \sim e^{-\mu\, r} r^{\frac{n+3}{2}}\ , \tag{2.10}$$

with the same definition for μ. Hence we expect that the unstable perturbations are localized near the horizon with a characteristic size μ^{-1}.

---

[3] While the present argument is somewhat superficial, a more careful treatment yields the same result [63, 64].

n	1	2	3	4	5
$k_{\max} r_+$	0.876	1.269	1.581	1.849	2.087

Table 2.1: Maximum wavenumber corresponding to the marginally unstable mode of the static black string in various dimensions $D = n + 4$.

The instabilities can be determined as follows: For a fixed value of k, we choose Ω and set the asymptotic conditions according to eq. (2.9) or (2.10). The radial equation (2.6) is integrated in numerically to $r \approx r_+$. Here we match the numerical solution to the near-horizon solution (2.8) which determines the ratio B/A for the chosen value of Ω. By varying Ω, we may tune this ratio to satisfy the physical boundary condition at the horizon, *i.e.*, $B = 0$. We find solutions for a range of k from 0 up to a maximum value $k_{\max}$. Figure 2.1 shows the resulting solutions for various space-time dimensions. The critical value $k_{\max}$ corresponds to the threshold of the Gregory-Laflamme instability and is set by the only dimensionful parameter in the background, r_+, up to a factor of order one. Table 2.1 tabulates $k_{\max}$ for different values of n.

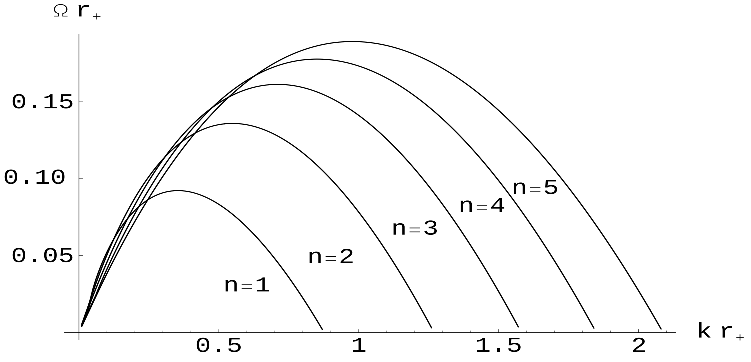

Figure 2.1: Unstable frequencies and wavenumbers for the static black string.

When the coordinate along the string is periodic, the allowed values of k are discrete, *i.e.*, for $z = z + 2\pi R$, $k = n/R$ with n an integer. Hence for small R, the system is stable when $k_{\max} \geq 1/R$. However, for $R > 1/k_{\max}$, the lowest wavenumber, allowed by periodicity, falls in the unstable range and the black string is unstable.

2.2 Boosted black strings

Our focus at present is "boosted black strings," *i.e.*, stationary black string solutions carrying momentum along their length. Such solutions can be obtained by simply boosting the static solution (2.1) along the z direction

$$ds^2 = -dt^2 + \frac{dr^2}{f(r)} + r^2 d\Omega_{n+1}^2 + dz^2 + (1-f)\cosh^2\beta\,(dt + \tanh\beta\,dz)^2 \ , \tag{2.11}$$

where the boost velocity is given by $v = \tanh\beta$, and as before

$$f(r) = 1 - \left(\frac{r_+}{r}\right)^n \ . \tag{2.12}$$

Again, we assume that in the new solution the z direction is periodically identified with $z = z + 2\pi R$. This solution has an event horizon situated at r_+ and an ergosurface at $r = r_+ \cosh^{2/n}\beta$, where ∂_t becomes spacelike.

To see quantitatively that this solution carries both mass and momentum, we calculate the ADM-like stress tensor for the string with the following asymptotic integrals [115]

$$T_{ab} = \frac{1}{16\pi G}\oint d\Omega_{n+1}\,\hat{r}^{n+1}\,n^i\left[\eta_{ab}\left(\partial_i h^c{}_c + \partial_i h^j{}_j - \partial_j h^j{}_i\right) - \partial_i h_{ab}\right] \ . \tag{2.13}$$

Here n^i is a radial unit vector in the transverse subspace and $h_{\mu\nu} = g_{\mu\nu} - \eta_{\mu\nu}$ is the deviation of the asymptotic metric from flat space. Note that the index labels $a, b, c \in \{t, z\}$, while i, j run over the transverse directions. To apply this formula, the asymptotic metric must approach that of flat space in Cartesian coordinates. This is accomplished with the coordinate transformation $r = \hat{r}(1 + (r_+/\hat{r})^n/2n)$ which yields

$$\begin{aligned} ds^2 \simeq & -\left(1 - \left(\frac{r_+}{\hat{r}}\right)^n \cosh^2\beta\right) dt^2 + 2\left(\frac{r_+}{\hat{r}}\right)^n \sinh\beta\cosh\beta\,dtdz \\ & + \left(1 + \left(\frac{r_+}{\hat{r}}\right)^n \sinh^2\beta\right) dz^2 + \left(1 + \frac{1}{n}\left(\frac{r_+}{\hat{r}}\right)^n\right) dx^i dx_i \ , \end{aligned} \tag{2.14}$$

keeping only the leading order corrections. Here $\hat{r}^2 = \sum_{i=1}^{n+2}(x^i)^2$. Hence applying eq. (2.13), we find the stress energy for the boosted black string is:

$$\begin{aligned} T_{tt} &= \frac{\Omega_{n+1}}{16\pi G} r_+^n (n\cosh^2\beta + 1) \,, \\ T_{tz} &= \frac{\Omega_{n+1}}{16\pi G} r_+^n \, n\cosh\beta \, \sinh\beta \,, \\ T_{zz} &= \frac{\Omega_{n+1}}{16\pi G} r_+^n (n\sinh^2\beta - 1) \,, \end{aligned} \tag{2.15}$$

where Ω_{n+1} is the area of a unit $(n+1)$-sphere. Integrating over z, the total energy and momentum of the string are then

$$E_{\rm BS} = \frac{\Omega_{n+1}R}{8G} r_+^n (n\cosh^2\beta + 1) \,, \tag{2.16}$$

$$P_{\rm BS} = \frac{\Omega_{n+1}R}{8G} r_+^n \, n\cosh\beta \, \sinh\beta \,. \tag{2.17}$$

The limit of maximal boost $\beta \to \infty$ results in divergent $E_{\rm BS}, P_{\rm BS}$, but these can be kept finite if r_+ vanishes sufficiently fast. In particular taking the large β limit while holding $r_+^n \cosh^2\beta$ fixed produces finite charges. However, the limiting background has a naked null singularity at the center of a finite-size ergosphere.

2.2.1 Comparing black strings and black holes

Gregory and Laflamme [63, 64] originally gave a simple argument favoring instability of the static black string by comparing its entropy to that of a spherical black hole with the same energy. This argument also plays a role in deducing the full phase structure of black strings and black holes in a compactified space-time [66, 116]. So we begin here by extending this discussion of the global thermodynamic stability to the boosted black string. The analysis for the case at hand becomes slightly more complicated because, as well as matching the energy, we must also explicitly match the KK momentum along the z circle in our comparison.

We compare the boosted black string solution (2.11) to a D-dimensional spherical black hole of radius r'_+ moving along the z axis with velocity $v' = \tanh\beta'$. At rest, the energy of the spherical black hole is [104]

$$M_{\text{BH}} = \frac{(n+2)\Omega_{n+2}}{16\pi G} {r'_+}^{n+1} . \tag{2.18}$$

Now to a distant observer, the spherical black hole behaves like a point particle and so when boosted, its energy and momentum are given by

$$E_{\text{BH}} = M_{\text{BH}} \cosh\beta' , \quad P_{\text{BH}} = M_{\text{BH}} \sinh\beta' . \tag{2.19}$$

Equating the above to those for the black string given in eqs. (2.16) and (2.17), the black hole must have:

$$\tanh\beta' = \frac{n\cosh\beta\,\sinh\beta}{1+n\cosh^2\beta} , \quad {r'_+}^{n+1} = 2\pi r_+^n R \frac{\sqrt{1+n(n+2)\cosh^2\beta}}{n+2} \frac{\Omega_{n+1}}{\Omega_{n+2}} . \tag{2.20}$$

It is interesting to note that with the usual relation $v = \tanh\beta$, the first expression above can be rewritten as

$$v' = v \frac{n}{n+1-v^2} . \tag{2.21}$$

Hence we always have $v' < v$, with v' approaching v (from below) as $v \to 1$.

We now need to calculate the horizon entropy $S = A/4G$ for each configuration. For the boosted string, we find

$$S_{\text{BS}} = \frac{\pi R \Omega_{n+1}}{2G} r_+^{n+1} \cosh\beta . \tag{2.22}$$

The $\cosh\beta$ dependence arises here because proper length along the z direction at the horizon expands with increasing β, as can be seen from eq. (2.11). In contrast, the horizon area of the black hole is invariant under boosting. This invariance is easily verified in the the present case by explicitly applying a boost along the z direction to the black hole metric in isotropic coordinates. However, this is a general result [117]. Hence for the boosted black hole, we have

$$S_{\text{BH}} = \frac{\Omega_{n+2}}{4G} {r'_+}^{n+2} . \tag{2.23}$$

Setting $S_{\text{BH}}/S_{\text{BS}} = 1$ and solving for R, we find

$$R_{\text{min}} = \frac{r_+}{2\pi\cosh\beta} \frac{(n+2)^{n+2}}{(n(n+2)+\cosh^{-2}\beta)^{n/2+1}} \frac{\Omega_{n+2}}{\Omega_{n+1}} . \tag{2.24}$$

Hence we might expect that the boosted black string is unstable for $R > R_{\rm min}$. Fixing r_+, $R_{\rm min}$ scales like $1/\cosh\beta$ for large β. It should be remembered that the large β limit with r_+ fixed has divergent energy. Rescaling r_+ while taking the large β limit can make the energy finite, but this causes $R_{\rm min}$ to vanish even more quickly. In any event, this naive analysis suggests that the instability will persist for $\beta \to \infty$. Again, note that the black string horizon becomes a null singularity in this limit.

2.2.2 Instability of boosted strings

Turning now to the instability of boosted strings, a natural choice of coordinates in which to perform the analysis are those for which the string appears at rest:

$$\tilde{t} = \cosh\beta\, t + \sinh\beta\, z \ , \quad \tilde{z} = \cosh\beta\, z + \sinh\beta\, t \ . \tag{2.25}$$

In the following we shall refer to this as the “static frame”, and our original frame (2.11) having periodic boundary conditions in z, will be called the “physical frame”.

Let us begin in the static frame with perturbations having functional form $\exp(\tilde{\Omega}\tilde{t} + i\tilde{k}\tilde{z})$. Now transforming back to the physical frame, this becomes $\exp(\Omega t + ikz)$ where

$$\Omega = \cosh\beta\, \tilde{\Omega} + i\sinh\beta\, \tilde{k} \ , \quad k = \cosh\beta\, \tilde{k} - i\sinh\beta\, \tilde{\Omega} \ . \tag{2.26}$$

For real $\tilde{k}$ and $\tilde{\Omega}$, the imaginary part of k induced by the boost is inconsistent with the periodic boundary conditions on z which are imposed in the physical frame. Hence consistency requires that we add an imaginary part to $\tilde{k}$, $i\tanh\beta\,\tilde{\Omega}$, which ensures that the resulting k is real. In practice, finding solutions also requires adding a small imaginary part to $\tilde{\Omega}$ — see below. Hence in the static frame, our perturbations have a $\tilde{t}, \tilde{z}$ dependence of the form

$$\exp[(\tilde{\Omega} + i\tilde{\omega})\tilde{t} + i(\tilde{k} + i\tanh\beta\,\tilde{\Omega})\tilde{z}] \ , \tag{2.27}$$

where $\tilde{\Omega}, \tilde{\omega}, \tilde{k}$ are all real. In the physical frame, the t, z dependence of the perturbations becomes $\exp(\Omega t)\exp\ i(\omega t + kz)$ where

$$\Omega = \tilde{\Omega}/\cosh\beta \ , \quad \omega = \cosh\beta\,\tilde{\omega} + \sinh\beta\,\tilde{k} \ , \quad k = \cosh\beta\,\tilde{k} + \sinh\beta\,\tilde{\omega} \ . \tag{2.28}$$

Again all of the above are real numbers. Provided we ensure that k is a multiple of $1/R$, this ansatz is now consistent with the periodicity of z. As before, solutions with $\Omega > 0$ will correspond to instabilities.

Including the complex part, $i\tilde{\omega}$, in the near-horizon form of the solution (2.8) turns the terms respectively into in and outgoing modes at the future-event horizon. When $\tilde{\Omega} > 0$, regularity of the solution requires that we set $B = 0$, as before. For the special case that $\tilde{\Omega}$ vanishes, neither solution diverges on the future-event horizon, however, the limit of the second is undefined there. In this case, we continue to impose $B = 0$ as our boundary condition for $\tilde{\Omega} = 0$ as this corresponds to a boundary condition of purely ingoing modes at the future-event horizon.

Hence the problem of finding instabilities of the boosted string reduces to finding instabilities of the static string with the complex frequencies defined by (2.27). With these frequencies, the perturbations have a time dependent phase. The boundary condition must therefore be imposed on both the real and imaginary parts of the unknown function. This means that for each value of $\tilde{k}$ there are two constraints that must be solved on the horizon, precisely matching the number of free parameters $\tilde{\omega}, \tilde{\Omega}$. Apart from these complications, the solutions were found numerically using the method outlined in Section 2.1.

The numerical results for the frequencies $\tilde{\Omega}$ and $\tilde{\omega}$ in the static frame are displayed as a function of $\tilde{k}$ in Figure 2.2 for $n = 1$. The results in other dimensions are similar. On the left, we see that $\tilde{\Omega}(\tilde{k})$ is almost independent of the boost velocity v. This result might be interpreted as arising because even when $v = 0$, $\tilde{\Omega}$ is suppressed relative to $\tilde{k}$ and so making v nonzero (but small) only yields a small perturbation on the unboosted results. Further, we note that the behavior of $\tilde{\Omega}(\tilde{k})$ near $\tilde{k} = 0$ and $\tilde{k}_{\max}$ is independent of v — a point we return to below.

More dramatic differences are seen when the results are transformed to the the physical frame with eq. (2.28). We display $\Omega(k)$ in Figure 2.3a for $n = 1$. Again, the behavior for other values of n is similar. We might note that the comparison is made here for boosted strings with a fixed value of r_+. Hence the total energy (2.16) increases with the boost velocity and diverges as $\beta \to \infty$.

In fact, one can predict the threshold for the Gregory-Laflamme instability of the boosted string without the numerical analysis above. The revised ansatz (2.27) in the static frame was

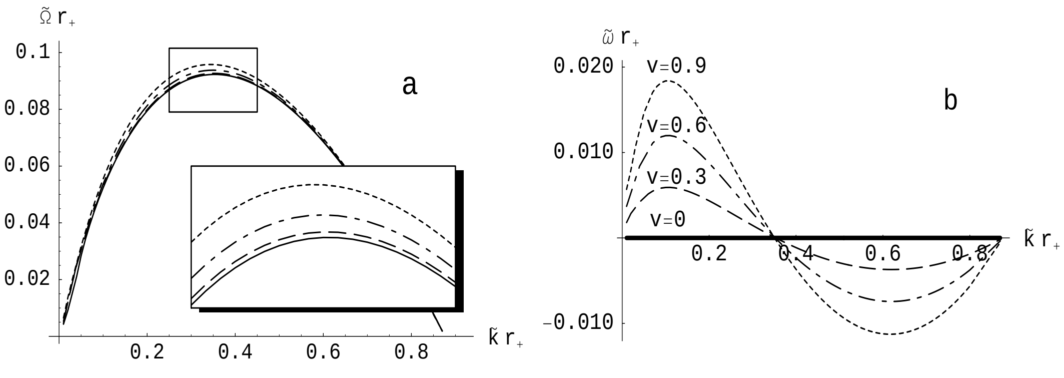

Figure 2.2: Frequencies $\tilde{\Omega}(\tilde{k})$ and $\tilde{\omega}(\tilde{k})$ leading to instabilities, as observed in static $(\tilde{t}, \tilde{z})$ frame, for $n = 1$.

introduced to accommodate the time dependence of these modes upon boosting to the physical frame. However, the threshold mode is defined as that for which the timescale of the instability diverges, *i.e.*, $\tilde{\Omega} = 0$. Hence there is no obstruction to boosting the threshold mode originally found by Gregory and Laflamme. Hence there is a simple kinematical relation between the thresholds for the boosted and static black strings. In the physical frame, this marginal mode has

$$k_{\max} = \cosh\beta\, \tilde{k}_{\max}\ , \quad \omega = \sinh\beta\, \tilde{k}_{\max} \tag{2.29}$$

where $\tilde{k}_{\max}$ is the threshold for a static black string, listed in Table 2.1. Hence these threshold modes are travelling waves in the z direction having precisely the same speed as the boosted string.

One may ask whether there are more general modes with $\tilde{\Omega} = 0$, but nonzero $\tilde{\omega}$. For example an exactly marginal mode in the physical frame would require that $\tilde{\Omega} = 0$ and $\tilde{\omega} = -\tanh\beta\tilde{k}$, but in fact such a solution is inconsistent with the equations of motion. The linearity of (2.7) allows us to arbitrarily choose a normalization in which h_z is real at a point. When we set $\tilde{\Omega} = 0$, the real and imaginary parts of h_z decouple, implying that h_z is real everywhere. If $\tilde{\omega}$ is nonzero, the only choice of A and B in the near-horizon solution (2.8) consistent with h_z real is $A = B^*$, so that the boundary condition $B = 0$ is not possible. We then conclude that the only solution with $\tilde{\Omega} = 0$ is time-independent in the static frame ($\tilde{\omega} = 0$), which is then a

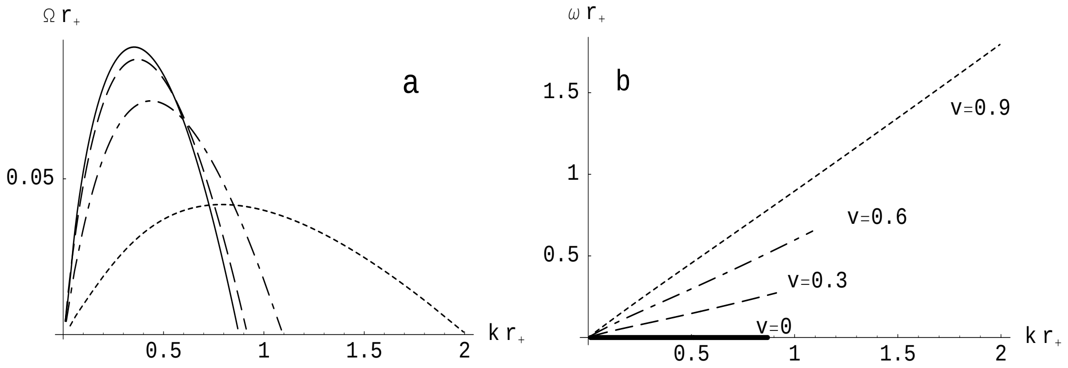

Figure 2.3: Plot of physical frequencies $\Omega(k)$ and $\omega(k)$ leading to boosted string instabilities for fixed horizon size, at various boost velocities and with $n = 1$.

travelling wave of constant amplitude in the physical frame.

To close this section, we observe that in the static frame, $\tilde{\omega}(\tilde{k})$ shows some interesting structure, as shown in Figure 2.2b. The zeros of $\tilde{\omega}$ seem to be independent of v. The vanishing at $\tilde{k}_{\rm max}$ (and $\tilde{k} = 0$) is understood from the discussion above, but there is also a fixed intermediate zero which seems to coincide with the maximum value of $\tilde{\Omega}$. We do not have a physical explanation for the latter.

Using eq. (2.28), the phase velocity of the unstable modes in the physical frame can be written as

$$\frac{\omega}{k} = \frac{v + \tilde{\omega}/\tilde{k}}{1 + v\,\tilde{\omega}/\tilde{k}} \simeq v + (1 - v^2)\frac{\tilde{\omega}}{\tilde{k}} + \cdots \ . \tag{2.30}$$

The last approximation uses our numerical result that generically $\tilde{\omega}/\tilde{k} \ll 1$. Hence we see that to a good approximation all of the perturbations travel along the string with the boost velocity — a result which is verified by the numerical results in Figure 2.3b. However, given $\tilde{\omega}(\tilde{k})$ in Figure 2.2b, we see that the deviations from this rule are such that the long (short) wavelength modes travel with a phase velocity that is slightly faster (slower) than v. Of course, the threshold mode moves along the z direction with precisely the boost velocity.

2.2.3 Comparing black strings and black holes, again

The threshold mode sets a minimum radius of the compact circle for which the boosted black string is unstable. Hence from eq. (2.29) above, we have

$$\left(\frac{R_{\min}}{r_+}\right)_{\rm BS} = \frac{1}{(k_{\max}\, r_+)_{\rm BS}} = \frac{1}{\cosh\beta\, \tilde{k}_{\max}\, r_+} \tag{2.31}$$

where again $\tilde{k}_{\max}$ is the static string threshold, given in Table 2.1. This result might be compared to that in Section 2.2.1. Recall that there we compared the entropy of the boosted black string to that of a small black hole boosted along the z-direction. In this case, we found

$$\left(\frac{R_{\min}}{r_+}\right)_{\rm BH} = \frac{1}{(k_{\max}\, r_+)_{\rm BH}} = \frac{1}{2\pi\cosh\beta}\, \frac{(n+2)^{n+2}}{(n(n+2)+\cosh^{-2}\beta)^{n/2+1}}\, \frac{\Omega_{n+2}}{\Omega_{n+1}}\, . \tag{2.32}$$

Hence the simple scaling with $1/\cosh\beta$ in eq. (2.31) is modified here by corrections in powers of $1/\cosh^2\beta$. The two results are plotted together in Figure 2.4 for various space-time dimensions.

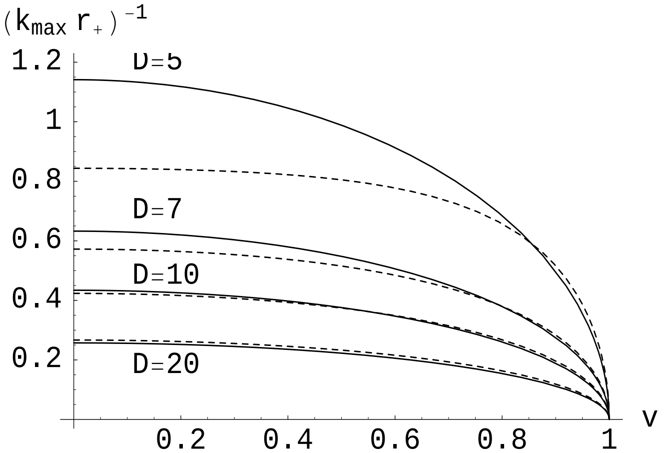

Figure 2.4: Comparison of the threshold wavenumber calculated numerically (2.31) (solid line) to that predicted by global entropy considerations (2.32) (dashed) for $D = 5, 7, 10, 20$

Considering the static results (*i.e.*, $v = 0$ or $\cosh\beta = 1$), Figure 2.4 shows that $(R_{\min})_{\rm BS} > (R_{\min})_{\rm BH}$ for smaller values of D, but $(R_{\min})_{\rm BS} < (R_{\min})_{\rm BH}$ for larger values. Sorkin [110] first observed this transition occurs between $D = 12$ and $D = 13$. This result seems to indicate that there is an interesting phase diagram [66, 116], for small D, with a regime $(R_{\rm min})_{\rm BS} > R > (R_{\rm min})_{\rm BH}$ where the black string is locally stable, but the black hole solution is a global maximum of the entropy. These global considerations then suggest that in this regime, the two solutions are separated by an unstable nonuniform black string phase [68] — this structure has been verified with numerical calculations for $D = 6$ [118], and more recently for $D = 5$ [119]. In contrast, for large D, it appears that the nonuniform black string becomes stable and can appear as the end state of the decay of the uniform black string in the regime $(R_{\rm min})_{\rm BS} < R < (R_{\rm min})_{\rm BH}$. Interestingly, one may actually construct the nonuniform strings perturbatively for R near $(R_{\rm min})_{\rm BS}$ [110] and the critical dimension at which the nonuiform strings become stable is found to be slightly higher than predicted by the above argument, occuring between $D = 13$ and $D = 14$.[4]

Now we observed that $(R_{\rm min})_{\rm BS}$ and $(R_{\rm min})_{\rm BH}$ in eqs. (2.31) and (2.32) do not have the same dependence on the boost velocity. This leads to an interesting effect which we observe in Figure 2.4. In the regime $D < 13$, we start with $(R_{\rm min})_{\rm BS} > (R_{\rm min})_{\rm BH}$ for small $\cosh\beta$, but there is a transition to $(R_{\rm min})_{\rm BS} < (R_{\rm min})_{\rm BH}$ for large boosts. Figure 2.5 displays the critical boost velocity (for the uniform black strings) at which this crossover occurs in various dimensions. This behavior can also be verified using the analytic approximation for the static threshold provided in [110], which yields

$$\left(\frac{R_{\rm min}}{r_+}\right)_{\rm BS} = \frac{1}{(k_{\rm max}\, r_+)_{\rm BS}} \simeq \frac{1}{2\pi\cosh\beta}\left(\frac{16\pi\, a\,\gamma^{n+4}}{(n+1)\Omega_{n+1}}\right)^{1/n} \tag{2.33}$$

where $a \simeq 0.47$ and $\gamma \simeq 0.686$ are constants.

To visualize these phases, it is perhaps more intuitive to examine the known solutions on a phase diagram. For static solutions, Harmark and Obers [121–123] have suggested a diagram constructed from the mass and tension. By deriving a Smarr formula for an arbitrary solution one is immediately able to completely determine the thermodynamics from such a plot. For boosted solutions, we must also take into consideration the momentum in the circle direction, P. In the supplementary material for this chapter, we give a derivation of the Smarr formula in this case.

---

[4] The precise value of the critical dimension may depend on the thermodynamic ensemble considered [120].

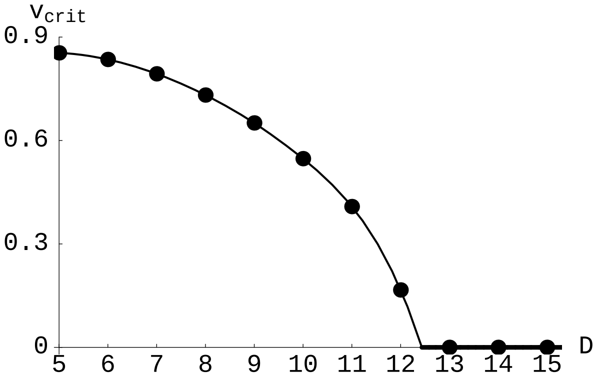

Figure 2.5: The critical boost at which nonuniform black strings become stable in various (low) dimensions. (The curve is simply a guide to the eye.)

In Figure 2.6, we have plotted a phase diagram for the boosted solutions in five dimensions. The analogous diagrams for the solutions in other numbers of dimensions less than 13 are similar. On the vertical axis we plot the dimensionless ratio P/M, which is bounded physically above and below by $|P/M| < 1$ for any solution. However, since it is symmetric about $P = 0$ we need only consider the upper half plane. While extending this plot into three dimensions by adding a direction proportional to the tension would allow one to better resolve the two dimensional surfaces corresponding to different phases, it is not necessary to do so for the heuristic arguments we present here.

The uniform strings fill this diagram from $M = 0$ up to arbitrarily high masses. For black holes, on the other hand, the finite size of the internal circle will put an upper bound on the allowed mass. We indicate this by the alternating dot-dash line in Figure 2.6. It is an approximation derived by setting the size of the black hole ($2r'_+$) equal to the size of the internal circle in the static frame ($2\pi R \cosh \beta'$), and calculating the energy and momentum using eqs. (2.18) and (2.19). The allowed region for black holes then sits above and to the left of this line and the forbidden region is labeled E. Finally the solid line, which we describe shortly, marks the precise beginning of a phase of nonuniform strings that extends, approximately, to the boundary of region E. Below we shall explore further the global argument suggesting this new nonuniform phase.

Note that it is not simply the approximation made above which leads us to treat region E as an approximate bound on the nonuniform string phase. In fact, when one considers the phases at zero boost in the fully nonlinear regime, it is found that the nonuniform string phase appears to connect to the black hole phase at a mass smaller than the maximum allowed value for a black hole, but larger than that for which the uniform string and the black hole have the same entropy — see [118, 119]. In other words, the nonuniform phase appears to end between the dashed and dot-dashed lines in the region labelled C. It should be noted, however, that the exact structure near the point where the nonuniform string and black hole phases appear to meet is still an open question. In the original construction it appeared that one phase would connect to the other at a cusp [118], however a more recent construction [119] appears to show that the mass of the nonuniform string also reaches at least one maximum before it may join onto the black hole phase.

On diagrams such as Figure 2.6, the expressions for $(R_{\rm min})_{\rm BS}$ and $(R_{\rm min})_{\rm BH}$, are constraints defining curves that each divide the phase diagram into two sections. In Figure 2.6 the solid curve is defined by eq. (2.31). It divides the phase space into two regions according to the stability of the uniform strings. Below the curve the strings are stable, while above they are unstable due to the Gregory-Laflamme instability. Recall that the mode defined by $(R_{\rm min})_{\rm BS}$ was a time-independent perturbation of the uniform string. Hence there are static strings precisely on this line which are nonuniform along the internal dimension.

The second, dashed, curve defined by $(R_{\rm min})_{\rm BH}$, corresponds to black holes which have the same energy, momentum and entropy as a uniform black string. This curve then subdivides the phase diagram into a different set of sections. Below the dashed curve a black hole with the same mass and momentum as a black string will have less entropy, and above it will have more. In 13 dimensions and above, this line sits completely to the left of the solid line and the two no longer cross.

A consideration of the region of phase space above or below both curves is what Gregory and Laflamme originally had in mind when they presented their thermodynamic argument predicting the instability [63, 64]. For example, above both curves in the area labeled A, a uniform black string is likely unstable in the microcanonical ensemble because a black hole would have more entropy. A heuristic sketch of the entropy is shown in Figure 2.7. At the far

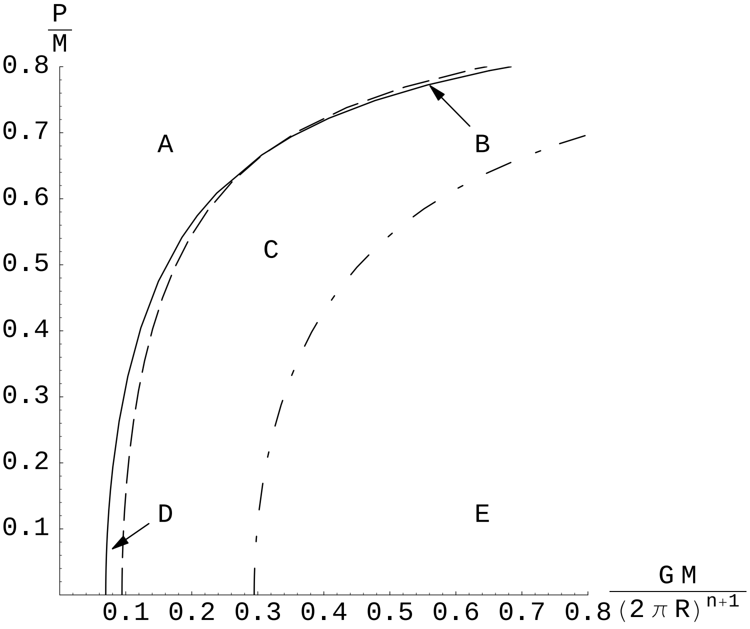

Figure 2.6: Phase diagram for boosted black strings. The solid line is the marginally unstable black string and the dashed are black holes constrained to have the same energy, momentum and entropy as a uniform black string. The alternating dot-dash line is the boundary of the disallowed region, E, for black holes.

left is the uniform boosted string and at the right is the black hole. In this situation there can be no other solutions between these two as new extrema could only be added in pairs. Similar arguments hold for the region labeled C in which the uniform string is a global maximum of the entropy and is therefore stable. In region E, the disallowed region for black holes, the uniform black string should be the single global maximum for the entropy.

To discuss the new nonuniform string phase we focus attention on the region between the two curves. The region labeled D is the situation above where $(R_{\text{min}})_{\text{BS}} > R > (R_{\text{min}})_{\text{BH}}$. Since the uniform string is stable and the black hole has more entropy they must be separated

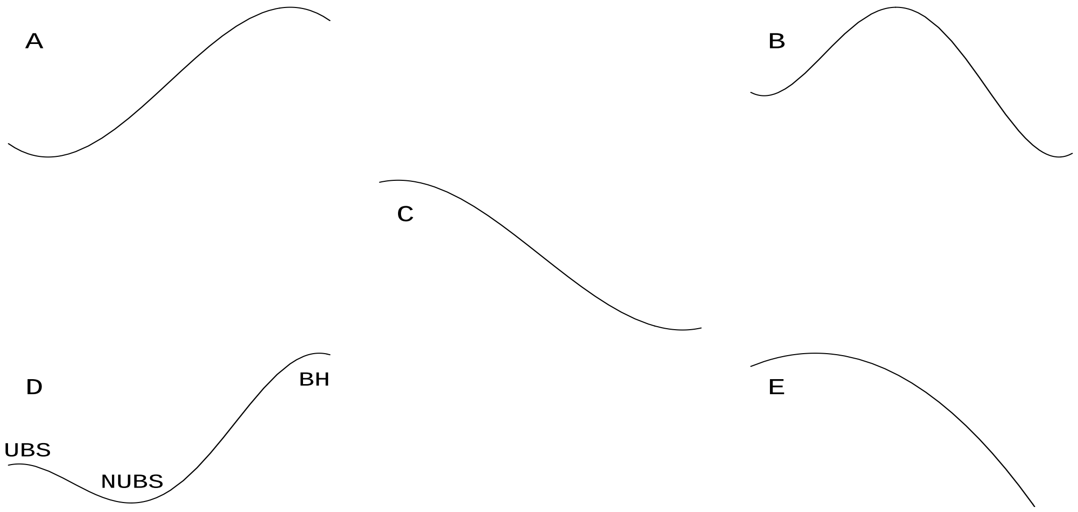

Figure 2.7: Speculative sketches of the entropy for various solutions corresponding to the different regions in Figure 2.6. In each case, the uniform black string is on the far left and the black hole is on the right.

by a local minimum of the entropy, *i.e.*, there is a new unstable phase that separates the two known solutions. This situation is again depicted in Figure 2.7. A similar argument applies in the region labeled B where the uniform black strings are locally unstable, but have greater entropy than black holes with the same momentum and mass. The new solution separating these phases is therefore a stable maximum of the entropy which can be reached as a result of the decay of an unstable uniform black string or black hole.

The point where these two regions meet may be a critical boost at which point the nonuniform strings change from unstable to stable. From the consideration of static solutions, we know that as the mass increases, these arguments only explain the behavior of the various phases approximately. So, while the arguments we have presented were global in that they involved the black hole phase, we expect them to be most accurate for describing the nonuniform string phase very near the point where it meets the uniform phase. Note that this is the context in which the critical dimension was first discovered [110].

Of course, this argument in favor of a boost dependent critical dimension strongly depends on there actually being a crossing point for the two curves. The analysis in Section 2.2.1 leading to eq. (2.32) treats the black hole as being spherical sitting inside a fixed internal circle. For very small black holes this is an acceptable approximation, but as the size increases, the interactions with the 'image' black holes in the covering space become important and lead to mass-dependent corrections for the entropy of black holes [124–128]. However, as β increases, so too does the proper separation of the black hole and its images (along the z direction) in their static frame, *i.e.*, $\Delta\tilde{z} = 2\pi\, R\, \cosh\beta'$ where the boost factors are related as in eq. (2.20) but for large boosts, $\cosh\beta' \simeq \cosh\beta$. Naively, eq. (2.20) shows that the size of the black holes grows at a much slower rate as β increases. However, near the boundary where $S_{\rm BH} = S_{\rm BS}$, one finds that r'_+ grows as $\cosh\beta$ for large β, precisely the same rate as $\Delta\tilde{z}$.

In Figure 2.8, we have plotted the size of the horizon relative to the size of the internal dimension in the static frame when we set the energy, momentum and entropy as for the dashed line in Figure 2.6. We see that at no point is the black hole small relative to the internal circle. In fact, the black hole grows in size relative to the extra dimension as the boost is increased. Generally then we expect the size of the corrections will also grow with the boost.

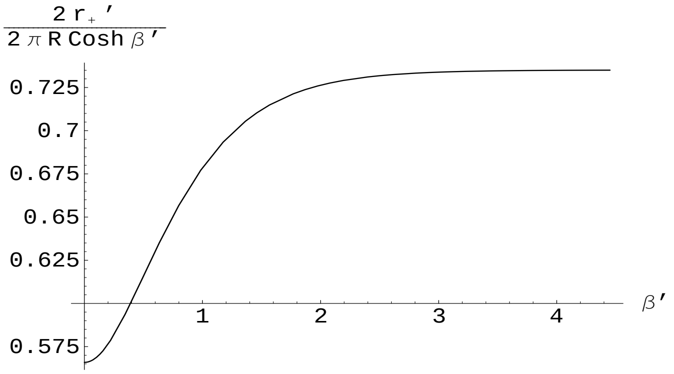

Figure 2.8: Size of the black hole with the same energy, momentum and entropy as a black string relative to the size of the internal circle in the static frame.

It seems then we should take into account the corrections that result when the black hole is placed in a compactified space time. Of course, incorporating the compactification corrections for small black holes [124–128] will allow one to produce a more accurate value for the critical boost in various dimensions [129]. For now we instead follow Kol and Sorkin [130], and assume that the entropy for the black hole is larger than that of a Schwarzschild solution by a factor $(1+\epsilon)$, *i.e.*,

$$S_{\rm BH} \equiv (1+\epsilon) S_{\rm Schw} \ . \tag{2.34}$$

Now if we set the mass, momentum and entropy for the black hole equal to that of a black string, we find that the critical boost at which the two curves in Figure 2.6 cross is strongly dependent on ϵ. In fact, there is a range of only a few percent for which a critical boost exists. In Figure 2.9 we have plotted the resulting critical boost as we vary the value of ϵ used. While we have allowed for both positive and negative values of ϵ, the results of [124–128] seem to indicate that positive values of ϵ are to be expected. Interestingly, positive values of ϵ imply larger values of the critical boost which, as we have already observed, implies larger corrections.

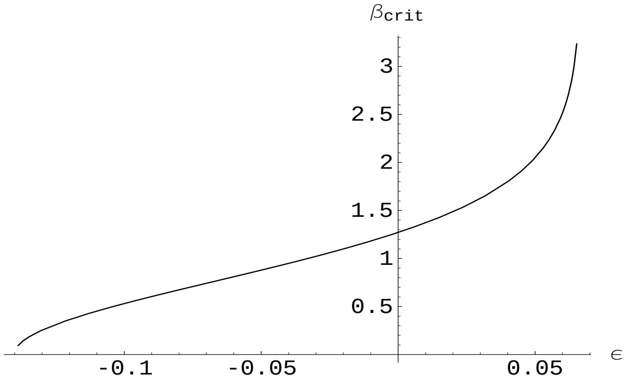

Figure 2.9: Variation of the crossing point between Gregory-Laflamme and black hole lines with the variation of the size of entropy corrections for the black hole.

All of these results seem to imply that although it works well for predicting the critical dimension in the static case, the naive evaluation of the black hole entropy may be giving misleading results about the stability zones in the boosted case. However, tentatively our results show that the critical dimension discovered in [110] depends on the boost velocity and in fact disappears for large values of $\cosh\beta$. Of course though, these are just simple heuristic arguments which are no substitute for an actual construction either perturbatively following the method of Gubser, [67] or in a fully nonlinear regime such as was done by Wiseman [68]. At present, however, this remains a work in progress [129].

2.3 Black rings

The question of black hole uniqueness in dimension greater than four was answered decisively by Emparan and Reall with the construction of an explicit counterexample [73]. Their solution is completely regular on and outside a horizon having topology $S^2 \times S^1$, a black ring. For the metric, we consider the form presented in [131]:

$$\begin{aligned} ds^2 &= -\frac{F(x)}{F(y)}\left(dt + R\sqrt{\lambda\nu}(1+y)d\psi\right)^2 \\ &\quad + \frac{R^2}{(x-y)^2}\left[-F(x)\left(G(y)d\psi^2 + \frac{F(y)}{G(y)}dy^2\right) + F(y)^2\left(\frac{dx^2}{G(x)} + \frac{G(x)}{F(x)}d\phi^2\right)\right] , \end{aligned} \tag{2.35}$$

where

$$F(\xi) = 1 - \lambda\xi \quad \text{and} \quad G(\xi) = (1-\xi^2)(1-\nu\xi) . \tag{2.36}$$

Requiring the geometry be free of conic singularities when F or G vanish determines the periods of the angles ϕ and ψ to be

$$\Delta\phi = \Delta\psi = 2\pi\frac{\sqrt{1+\lambda}}{1+\nu} , \tag{2.37}$$

and sets the value of λ to one of two possibilities

$$\lambda = \begin{cases} \frac{2\nu}{1+\nu^2} & \text{black ring} , \\ 1 & \text{black hole} . \end{cases} \tag{2.38}$$

With the former choice, (x, ϕ) parameterize a two-sphere while ψ is a circle. When $\lambda = 1$, ψ joins with x and ϕ to parameterize a three-sphere and the solution is a five-dimensional Myers-Perry black hole [104] spinning in one plane.

The family of black ring solution is therefore described by two free parameters, ν and R. The first, ν, can be chosen in the range from 0 to 1 and roughly describes the shape of the black ring. For $\nu \to 0$, the ring becomes increasingly thin and large. In the opposite limit, $\nu \to 1$, the ring flattens along the plane of rotation, becoming a naked ring singularity at $\nu = 1$. R can be roughly thought of as the radius of the ring in a manner that will become apparent shortly.

The ADM energy and spin, as well as the horizon area, are found to be

$$\begin{aligned} M &= \frac{3\pi R^2}{4G}\frac{\lambda(1+\lambda)}{1+\nu}\,, && (2.39)\\ J &= \frac{\pi R^3}{2G}\frac{(\lambda\nu)^{1/2}(1+\lambda)^{5/2}}{(1+\nu)^2}\,, && (2.40)\\ A &= 8\pi^2 R^3\frac{\lambda^{1/2}(1+\lambda)(\lambda-\nu)^{3/2}}{(1+\nu)^2(1-\nu)}\,. && (2.41)\end{aligned}$$

A more convenient set of variables for visualizing the various phases of these solutions are the reduced spin, j^2, and area, a_h, defined by

$$j^2 = \frac{27\pi}{32G}\frac{J^2}{M^3} \quad = \quad \begin{cases} \frac{(1+\nu)^3}{8\nu} & \text{black ring} \\ \frac{2\nu}{1+\nu} & \text{black hole} \end{cases} \qquad (2.42)$$

$$a_h = \frac{3}{16}\sqrt{\frac{3}{\pi}}\frac{A}{(GM)^{3/2}} \quad = \quad \begin{cases} 2\sqrt{\nu(1-\nu)} & \text{black ring} \\ 2\sqrt{2\frac{1-\nu}{1+\nu}} & \text{black hole} \end{cases} \qquad (2.43)$$

We plot the corresponding quantities in Figure 2.10. Note that the black holes are described by $a_h = 2\sqrt{2(1-j^2)}$. The black rings lie on two branches, labeled “large” and “small”, which meet at the critical point $\nu = 1/2$.

The “large” branch corresponds to solutions where the radius of the ring grows more quickly than it’s thickness, locally approaching the geometry of a boosted string. To see this explicitly, we may take $R \to \infty$, $\nu \to 0$ while keeping $R\nu$ fixed. In this limit, we introduce [131]

$$\begin{aligned} \nu R &= r_+ \sinh^2\beta\,, \quad \lambda R = r_+\cosh^2\beta\,, && (2.44)\\ r &= -R\frac{F(y)}{y}\,, \quad \cos\theta = x\,, \quad z = R\psi\,, \end{aligned}$$

and obtain precisely the metric of the boosted black string (2.11). The similarity is in fact more than just local, comparing the horizon area of the black ring in this limit we find that it matches

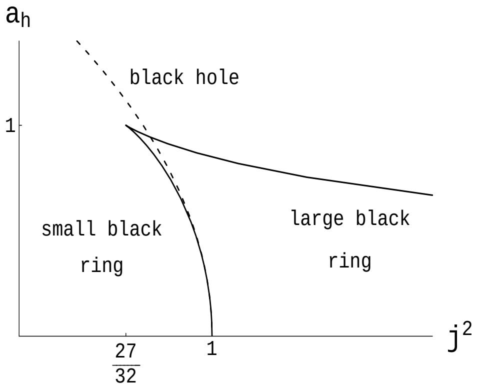

Figure 2.10: Reduced spin and area for the black ring (solid line) and black hole (dashed) solutions described by the metric (2.35).The large (small) ring branch corresponds to $\nu < 1/2$ ($\nu > 1/2$).

the boosted string result (2.22), implying that we should indeed take R as a measure of the radius of the ring.

Given the similarity between boosted black strings and very large black rings, Emparan and Reall expected that the latter should be subject to a Gregory-Laflamme type instability [73]. Using (2.29), the wavenumber for the marginal mode of the five-dimensional boosted string is $k_{\rm max}\, r_+ \approx 0.876\, \cosh\beta$. Translating this result to the black ring variables using (2.44) yields

$$k_{\rm max} \approx \frac{0.876}{R}\frac{\lambda^{1/2}}{(\lambda-\nu)^{3/2}} \approx \frac{1.239}{R\nu}\ , \tag{2.45}$$

where the last expression applies only for $\nu \to 0$. Now $k_{\rm max} \gtrsim 1/R$ should be the condition for the Gregory-Laflamme instability to appear in the black ring.[5] Hence the above result confirms that the black ring is unstable in the vicinity of small ν. Further, considering the second expression above for arbitrary ν, one finds that $k_{\rm max} > 1/R$ everywhere which suggests that all of the black rings are unstable. However, we should not think these calculations are reliable for all values of ν. We consider this question in more detail below by studying a simple model of the black ring.

---

[5] It is important here that the unstable mode is localized near the horizon, which is a point we return to later.

2.3.1 From black strings to black rings

Here we would like to construct a simple model of the black ring that captures its important features. To identify these, we consider the ratio of the mass and spin of the ring from eqs. (2.39) and (2.40). For small ν, this ratio approaches a constant

$$\begin{aligned} \frac{MR}{J} &= \frac{3}{\sqrt{2}}\left[1-2\nu+4\nu^2+\mathcal{O}(\nu^3)\right] \\ &= \frac{3}{\sqrt{2}}\left[1-2\frac{\sqrt{2}GJ}{\pi R^3}+10\frac{2G^2J^2}{\pi^2R^6}+\mathcal{O}\left(\frac{\sqrt{2}GJ}{\pi R^3}\right)^3\right] , \end{aligned} \tag{2.46}$$

where implicitly we have expanded the dimensionless quantity $\sqrt{2}GJ/\pi R^3 = \nu+3\nu^2+O(\nu^4)$. Our goal is to reproduce this expression with a simple string model. So let us assume we have a spinning loop of string where the loop has a radius R and the string has a linear "rest mass" density λ. Then we expect that, up to a boost-dependent factor, the spin is given by $J \sim \lambda R^2$. This allows us to identify the origin of the most important contributions to the energy of the black ring by reexpressing the contributions in terms of λ and R.

The constant term in eq. (2.46) corresponds to a contribution to the total energy λR, linear in both factors. Hence remembering to include the boost dependence, this leading term is simply a combination of the string's rest mass and a kinetic energy. That this term dominates may have been expected since we are considering a limit in which the radius of the ring is large. The next term in the expansion gives an R-independent contribution coming from the gravitational self-energy of the ring in five dimensions, $-G\lambda^2$. The final term in eq. (2.46) yields a $1/R$ potential which would keep the string from shrinking to zero size when formed in a ring. We can interpret such a contribution as due to rigidity of the string.

Rigidity has appeared before in various string models. In particular, it was argued to be necessary to successfully model the QCD string and was introduced by modifying the Nambu-Goto action by a term dependent on the extrinsic curvature of the worldsheet [132, 133]. It was suggested that such a term can emerge when the string is constructed as the compactification of a higher-dimensional brane [134]. Compactifying a three-brane on a two-sphere of radius ρ and forming a loop of string with radius R yields a configuration where the ratio between the tension and rigidity energies is R^2/ρ^2. Comparing this to the ratio of the first and third terms in (2.46) implies that $G\lambda \sim \rho$, whereas for a boosted black string in five dimensions, we have $GT_{tt} \sim r_+$ from eq. (2.15). This intriguing coincidence suggests that the rigidity of black strings may be accommodated by an extension of the "membrane paradigm" [135, 136] to higher dimensions.

Hence we have argued that the gravitational self-interaction and rigidity of the black string play a minor role in determining the configuration for large rings. Now we would like to proceed further in modelling the behavior of such a large black ring by approximating the latter as a loop of black string and using our results for the energy and momentum densities given in eq. (2.15). For a loop of string with radius R, these yield a mass and spin

$$\begin{aligned} M \equiv 2\pi R\, T_{tt} &= x\, n\, r_+^n R \left(\cosh 2\beta + 1 + \frac{2}{n}\right) , && (2.47)\\ J \equiv 2\pi R^2\, T_{tz} &= x\, n\, r_+^n R^2 \sinh 2\beta\ , && (2.48)\end{aligned}$$

where for notational convenience, we have introduced the constant $x \equiv \Omega_{n+1}/16G$. Hence we see that our model has three independent parameters: R, r_+ and β, which correspond to the size and thickness of the loop and the tangential boost velocity which determines its angular velocity. Given a configuration with fixed M and J, the above equations give two relations between these parameters but one is left free. Our approach to fixing this last parameter will be demanding that the ring configure itself to maximize its entropy:

$$S = \frac{A}{4G} = 8\pi\, x\, r_+^{n+1} R \tag{2.49}$$

This is a straightforward although somewhat tedious exercise. Hence we only show the salient steps below.

First, we find it useful to replace R by the dimensionless parameter

$$y \equiv \frac{J}{MR} = \frac{\sinh 2\beta}{\cosh 2\beta + 1 + \frac{2}{n}} \tag{2.50}$$

where the last expression comes from combining eqs. (2.47) and (2.48). One then determines

β and r_+ in terms of y as

$$e^{2\beta} = \frac{y\left(1+\frac{2}{n}\right)+\sqrt{1+\frac{4}{n}\left(1+\frac{1}{n}\right)y^2}}{1-y}\,, \tag{2.51}$$

$$r_+^n = \frac{M^2}{4xJ}\frac{y}{1+\frac{1}{n}}\left[1+\frac{2}{n}-\sqrt{1+\frac{4}{n}\left(1+\frac{1}{n}\right)y^2}\right]\,. \tag{2.52}$$

From these expressions, one can also see that physical solutions are restricted to the range $0 \leq y \leq 1$. Substituting these expressions into eq. (2.49) then yields $S(y)$. Plotting the entropy, one finds that it vanishes[6] at $y = 0$ and 1 and that it has a single maximum in between. The value of $y_{\max}$ can be determined analytically to be:

$$y^2_{\max} = \frac{\sqrt{\left(1+\frac{2}{n}\right)\left(1+\frac{1}{n}+\frac{1}{4n^2}+\frac{1}{2n^3}\right)}-1+\frac{1}{2n}+\frac{1}{n^2}}{4\left(1+\frac{1}{n}\right)\left(1+\frac{2}{n}\right)}\,. \tag{2.53}$$

Now we would like to compare our results to those for the five-dimensional solution (2.35). For $n = 1$, eq. (2.53) yields $y_{\max} \simeq .375$ for our loop of black string while eq. (2.46) yields $y \simeq \sqrt{2}/3 \simeq .471$ for the large radius limit of the exact solution. Hence our model does not precisely reproduce the leading result for the large ring, however, the discrepency is only of the order of 20%. Given the simplifying assumptions of our black string model, it seems to work surprisingly well.

We have found another interesting verification of our model as follows: In the limit of large n, eq. (2.53) yields $y^2_{\max} \simeq 1/2n$ and further eqs. (2.51) and (2.52) indicate that $\beta \simeq 1/\sqrt{2n}$ and $r_+^n \propto 1/\sqrt{2n}$, respectively. Hence in this limit (of a large space-time dimension), the string loop is very large and thin while its tangential velocity is small. Therefore it seems reasonable to treat the loop as a nonrelativistic mechanical string whose equilibrium configuration can be analysed with Newton's law: $pv/R = T_{tot}/R$ where the right-hand side is the centripetal acceleration of a small element of string with a linear momentum density p while the force on the left-hand side is determined by the total tension. Now applying a nonrelativistic limit to the

---

[6] This vanishing occurs because r_+^n vanishes at these points, as can be seen in eq. (2.52).

stress tensor of the black string (2.15) yields

$$\begin{aligned} T_{tz} &= \rho v \ , \\ T_{zz} &= -T + \rho v^2 \ , \end{aligned} \tag{2.54}$$

where we distinguish the mass density ρ and the tension T of the string. For the black string, eq. (2.15) gives $T = \rho/n = \Omega_{n+1} r_+^n / 16\pi G$ and so we note that we have $T \ll \rho$ for large n, as expected for a nonrelativistic string. Now setting $p = T_{tz}$ and $T_{tot} = -T_{zz}$, the force law yields $v^2 = T/2\rho = 1/2n$ which precisely matches the model result quoted above.

Hence it seems that we already have a fairly reliable model of the black string. Further this model is constructed for an arbitrary space-time dimension and so we conclude that black rings also exist in dimensions higher than five. In fact, for large dimensions, it seems that a large black ring will be spinning nonrelativistically.

Of course, our simple string model will only capture the leading behavior of eq. (2.46) and not the gravitational or rigidity corrections. While we do not do so here, one could try improving our calculations to take these effects into account. In fact, one indication of the importance of these effects comes from the black ring solution itself. Note that it has been observed [131] that in the limit of large radius, the five-dimensional black rings are fairly relativistic in that $\sinh^2\beta \to 1$, in contrast to our results for large dimensions above. It is interesting that this boost corresponds precisely to where the tension (2.15) of the five-dimensional black string vanishes [131], *i.e.*, $T_{zz} = 0$. Further, however, looking at (2.44) more carefully, we find

$$\sinh^2\beta = \frac{1+\nu^2}{1-\nu^2} \simeq 1 + 2\nu^2 \tag{2.55}$$

and the black ring actually seems to approach $\sinh^2\beta = 1$ from above as $\nu \to 0$, where the tension of the string would be negative. Of course, our model only results in a boost where the black string tension is positive and so can stabilize the spinning loop. However, the implication of eq. (2.55) is that the stress tensor of the black string (2.15) must receive "rigidity" corrections, *e.g.*, $1/R^2$ terms, as in [132, 133], when the string is drawn into a loop so that the tension remains positive in this limit. Similarly, the gravitational self-interaction may play a more important role here.

We can also use the black string model to extend our results for the Gregory-Laflamme instability of boosted black strings to black rings. In particular, the string loop will be subject to a Gregory-Laflamme instability when $k_{\rm max}R \gtrsim 1$. Using eq. (2.29) and Table 2.1, we have $k_{\rm max} = \cosh\beta\,\tilde{k}_{\rm max} \simeq .876\,\cosh\beta/r_+$. Further, evaluating these expressions with eqs. (2.51–2.53) with $n=1$ gives an instability for

$$j^2 \gtrsim .239\,, \tag{2.56}$$

where j^2 is the reduced spin introduced in eq. (2.42). There we also showed that for the five-dimensional black ring, the minimum value was $j^2_{\rm min} = 27/32 \simeq .844$ at $\nu = 1/2$. Hence in accord with the result at the end of the previous section, these calculations seem to indicate that all of the black ring solutions will be unstable. However, our model calculations need not be reliable for small values of j^2, *i.e.,* for small black rings.

Before addressing the latter question, let us consider a slightly different approach to evaluating the threshold for the instability of the black ring. We reconsider our model of a loop of black string with three independent parameters. As above, we fix the mass and angular momentum which leaves one free parameter, which we take to be the radius of the loop. Now rather than extremizing the entropy, here we require that the proper area of the horizons be the same. Again this gives three equations determining the model parameters, $R_{\rm model}, r_+, \beta$, now in terms of the two free parameters of the black ring R and ν.

This system of equations fixes the rapidity to be

$$\sinh\beta = 1\,. \tag{2.57}$$

It is interesting that this corresponds to the boost for which the five-dimensional black string becomes tensionless, *i.e.,* $T_{zz}=0$, as is appropriate for the large-ring limit. Note here though that we have not explicitly taken such a limit. The remaining parameters are found to be

$$R_{\rm model} = \frac{(1+\nu)^2}{1+\nu^2}R\,, \tag{2.58}$$

$$r_+ = \frac{\sqrt{1-\nu^2}}{1+\nu^2}\nu R\,. \tag{2.59}$$

Note that $R_{\rm model}$ and R agree in the large-ring limit, $\nu \to 0$, but in general $R_{\rm model} > R$.

Returning to the Gregory-Laflamme instability, the string loop will suffer from the instability when $k_{\max} R_{\rm model} \simeq 1$ with

$$k_{\max} = \tilde{k}_{\max} \cosh \beta = \frac{1.239}{\nu R} \frac{1+\nu^2}{\sqrt{1-\nu^2}} \tag{2.60}$$

where again we have used the five-dimensional result for $\tilde{k}_{\max}$. Let use consider this threshold more carefully here. The validity of this model calculation (and that above) requires that the unstable modes are localized near the horizon on a scale much smaller than the size of the ring. This is, of course, because our calculations for the instability of the boosted string assumed an asymptotically flat metric and so we may only apply these results here if the perturbation is insensitive to the geometry at the antipodal points on the ring. Here we are considering the characteristic size of the modes in the direction orthogonal to the string and hence orthogonal to the boost direction. Therefore this profile is independent of the boost velocity and for the threshold mode, we can again use the results from Section 2.1. The radial falloff of this perturbation was determined by the scale: $\tilde{\mu} = \sqrt{\tilde{\Omega}^2 + \tilde{k}^2_{\max}} = \tilde{k}_{\max}$ since $\tilde{\Omega}$ vanishes for the threshold mode. Given the boost factor (2.57) is order one, the wavelength and the radial extent of the threshold mode are about the same size.[7] Hence to be confident of our calculations for the black ring instability, the estimate above must be revised to $k_{\max} R_{\rm model} \gg 1$, which is equivalent to

$$\frac{\nu\sqrt{1-\nu^2}}{(1+\nu)^2} \ll 1.239\ . \tag{2.61}$$

Notice that the expression on the left-hand side has a maximum of 0.192 at $\nu = 1/2$ and hence we can be confident that this inequality will be satisfied in general.

To summarize then, for any black ring on either branch in Figure 2.10, one can find a corresponding black string model that has the same energy, spin and area. This version of the calculation again suggests that the black rings are unstable with a Gregory-Laflamme instability for any value of the parameters. However, we must note that this calculation is not always reliable. Recall that our underlying assumption was that the dominant black ring dynamics were simply determined by the rest energy and tension of the string. While this is indeed valid

---

[7] Note that we expect the threshold mode has the least radial extent of the unstable modes.

for the large black ring (small ν), eq. (2.46) clearly shows that this assumption becomes invalid when ν grows. In particular, there is no reason that it should be trusted when $\nu \geq 1/2$ where the gravitational self-interaction will be important. For a conservative bound, we might require that ignoring the gravitational correction introduces less than a 10% error in the total energy, which means that we require $\nu \leq 0.05$. Of course, this bound is subject to the reader's taste in the admissible error and in any event, it only represents a bound on one's confidence in the validity of our model. However, these calculations certainly do indicate the black rings in Figure 2.10 already experience a Gregory-Laflamme instability when the reduced spin j^2 is of order one.

2.4 Discussion

We have considered the Gregory-Laflamme instability for boosted black strings. In the static frame, the results are largely unchanged compared to the instability of a static black string, although the boundary conditions required a complex frequency with a small imaginary component. However, the instability is strongly dependent on the boost velocity in the physical frame, as shown in Figure 2.3a for $n = 1$. Since the threshold mode is by definition time-independent, the mode found for the static black string is also a solution satisfying the appropriate boundary conditions in the static frame of the boosted string. As a result, for a fixed horizon size, there is a simple kinematical relation (2.29) between the threshold wavenumber of the static and boosted black strings. For the boosted black string, the threshold mode is a travelling wave moving in the z direction with precisely the same speed as the boosted string.

In the static case, Sorkin [110] showed that *stable* black strings and small black holes on a compact circle only coexist below a critical space-time dimension, of approximately 13. For the boosted case, in which there is internal momentum in the circle direction, we seem to find that the critical dimension is boost dependent and in fact vanishes for large boosts. This result is illustrated in Figure 2.4 by the crossing of the curves for the minimal radius found from the Gregory-Laflamme analysis and from a comparison of the entropy of the black holes and strings.

Sorkin's result has interesting implications for the phase diagram for black objects in a compactified space-time [66, 116]. For $5 \leq D \leq 13$, there is a regime where black holes and stable black strings coexist. These families of solutions are connected by a family of unstable and nonuniform black strings. For $D > 13$, the stable black strings and black holes do not coexist and the family of nonuniform black strings connecting these two phases is now expected to be stable.

Interest in the nonuniform black strings alluded to above began with the discussion of [65]. Such nonuniform solutions were first constructed perturbatively by Gubser in five dimensions [67] and this construction is straightforwardly extended to any number of space-time dimensions. Wiseman used numerical techniques to find such strings in a fully non-linear regime in six dimensions [68]. A similar construction has recently been performed in five dimensions [119]. Here we observe that these nonuniform strings can be boosted to carry KK momentum in the internal direction. First, note that these solutions are static and periodic in, say, the $\tilde{z}$ direction with period $2\pi\tilde{R}$. Hence one can compactify these solutions by imposing the identification:

$$(\tilde{t}, \tilde{z}) = (\tilde{t} + 2\pi\tilde{R}\tanh\beta, \tilde{z} + 2\pi\tilde{R})\,. \tag{2.62}$$

Now upon boosting as in eq. (2.25), one arrives in a boosted frame where the identification is now $(t, z) = (t, z + 2\pi R)$ where $R = \tilde{R}/\cosh\beta$. Hence in the physical (t, z) frame, one has a nonuniform string moving with velocity $\tanh\beta$ along the z direction. Note, however, that we would not compare nonuniform and uniform black strings with the same boost factor. As in Section 2.2.1, any comparison would fix the total mass and KK momentum, as well as the circle radius, and since the ratio of the energy density and tension of the nonuniform and uniform strings is different so would be the boost factors for each.

Now our observation on the boost dependence of the critical dimension would have interesting implications for the nonuniform strings. As in the static case, it would seem that for $D > 13$ these strings are stable for any value of the boost. On the other hand for $5 \leq D \leq 13$, the nonuniform strings would apparently be unstable for low values of the boost, however, they become stable for large boosts. Note that in contrast to the uniform string which has a continuum of unstable modes, the static nonuniform string is expected of have a single unstable mode below the critical dimension reflecting the periodicity of the solution [66]. While imposing the "boosted" boundary condition (2.62) did little to modify the spectrum of unstable modes for the uniform black string, it seems to be enough to remove the unstable mode in the nonuniform case. It would be interesting then that these nonuniform boosted black strings may form the end state for the decay of the uniform black strings with KK momentum.

We also applied our results for the instability of boosted strings to consider the analogous instability of the black rings of Emparan and Reall [73]. Both the naive discussion around eq. (2.45) and the more detailed analysis in Section 2.3.1 seems to indicate that the entire branch of large-ring solutions is unstable. However, these are both expected to be reliable for small ν and so one must limit the application of our calculations. However, our results certainly indicate that Gregory-Laflamme instabilities will afflict the black rings already when the reduced spin j^2 is of order one. Hence it seems that this instability will enforce a Kerr-like bound on this particular family of solutions. This is then similar to the results of [109] where it was argued that the Gregory-Laflamme instability played a role in destabilizing ultraspinning black holes in $D \geq 6$, *i.e.*, the only stable spinning black hole solutions in higher dimensions would have $J^{n+1} \lesssim GM^{n+2}$, *i.e.*, $j^2 \lesssim 1$ for $D = 5$. There it was also argued that the five-dimensional spinning black holes may also become unstable near $j^2 = 1$ since there exist large black rings with the same spin and mass but a larger horizon area. Recently, it has also been argued that the small-ring branch is unstable using a thermodynamic treatment [137–139]. This result may have been anticipated since again there are always spinning black holes and large rings with the same mass and angular momentum but a larger horizon area.

Regarding the internal KK momentum as a charge, it is interesting to compare our instability results with those for black strings carrying a gauge-charge [64, 140], *i.e.*, an electric three-form charge or a magnetic (n+1)-form. In common with the gauge-charged string, the maximum value of the growth rate Ω of the unstable modes decreases (in the physical frame) as the KK momentum is increased, as illustrated in Figure 2.3a. However, one should actually think of the boosted strings as becoming more unstable as the KK momentum grows, since the physical threshold wavenumber $k_{\max}$ grows as the boost factor is increased, as described above. In contrast, increasing the gauge-charge makes the black string more stable by decreasing the wavenumber of the threshold mode and it is expected to be absolutely stable in the extremal limit [140]. Note that the boosted string does not have an extremal limit as $v \to 1$, rather the horizon becomes a null singularity in this limit.

We may also contrast our results with those in [111, 141–143], which study the Gregory-Laflamme instability for various black branes in string theory with D0-brane charge smeared over their worldvolume. In this case, the D0 charge is introduced by lifting the black brane from ten to eleven dimensions and boosting in the extra dimension. In contrast to the present case, there the boost direction and the directions along which the unstable modes form are orthogonal. In accord with the discussion here then, the threshold for the boosted solution is unchanged from that for the original solution, *i.e.,* with and without the D0 charge [141]. Similar boosts of nonuniform black strings have also been considered to generate new brane solutions in string theory [144].

Both t and z remain Killing coordinates for the gauge-charged strings and it is straightforward to consider boosting these solutions to form black strings carrying both KK momentum and gauge-charge. In this case, the threshold for the Gregory-Laflamme instability would again satisfy the same kinematical relation (2.29) with that for the static string, if we fix the positions of the inner and outer horizons, $r_\pm$. Hence the extremal string ($r_+ = r_-$) will remain stable even after boosting. One should note that just as boosting increases the energy density of the static string, it also increases the gauge-charge density.

The stability of the latter is then relevant for the large radius limit of the "dipole-charged" black rings [75]. The latter are five-dimensional black rings providing a local source for an electric three-form charge. This dipole charge is not a conserved charge and so these solutions introduce an infinite degeneracy of solutions with the same mass and angular momentum [75]. Given the above comments, we expect that introducing a dipole charge on the black rings will make them more stable. In particular, there should be a family of extremal rings which are exactly stable for any radius. If one adds further monopole charges, there also exist supersymmetric black rings [87, 145–148] which must also be absolutely stable.

Unlike the vacuum solutions, there are no dipole-charged rings for which J^2/GM^3 becomes arbitrarily large [75]. Hence the stability of these solutions does not rule out the possibility of a dynamical Kerr-like bound holding in general. However, if there is such a bound in higher dimensions, it must be a more refined version of Kerr bound, perhaps defined in terms of angular momentum confined to a finite-size system. Certainly there is no problem producing configurations with an arbitrarily large (orbital) angular momentum by taking slowly moving bodies with very large separation, even in four dimensions, but, of course, we do not expect any such Kerr bound to apply to such systems.

While our discussion has focused on the Gregory-Laflamme instability affecting black rings, it is possible that these solutions may suffer from other instabilities as well. For example, rapidly rotating stars (as modelled by self-gravitating incompressible fluids) are subject to non-axisymmetric "bar-mode" instabilities when the ratio of the kinetic and gravitational potential energies is sufficiently large [149]. Given the discussion of Section 2.3.1, large black rings are certainly in this regime and so one may suspect that they suffer from a similar instability. It might be that such instabilities restore the Kerr bound for black rings with dipole charges but they can not play this role in general, as again the supersymmetric black rings must be absolutely stable.[8]

To consider bar-mode instabilities, one might extend the discussion of Section 2.3.1 to produce a model of the black ring which is not inherently axisymmetric. The analysis of Section 2.2 yields the energy density and tension of a boosted black string and so one might consider a model in which the black ring is described by a loop of string with the same mechanical properties — this is essentially our model for a uniform spinning loop. However, this information is insufficient to model general non-axisymmetric loops. Basically, one still requires an equation of state for the string. For example, the mechanical string could be considered a relativistic string characterized by its fundamental tension plus some internal degrees of freedom. However, there are many possibilities for the latter, *e.g.*, massive or massless excitations, which would lead to different equations of state but which could still match the same properties for a uniform boosted string. Hence progress in this direction requires a greater understanding of the dynamical properties of the black string.

---

[8] One can consider non-axisymmetric deformations of the supersymmetric black rings [87] but one finds that the resulting solutions do not have smooth event horizons [150].

2.5 Supplementary material for Chapter 2

2.5.1 A Smarr formula for boosted solutions

Harmark and Obers [121–123] have proposed that one may conveniently visualize the phases of black objects in a D-dimensional compactified space-time in terms of the total mass, M, and the tension $\gamma = -T_{zz}$. Note that, in contrast to the rest of the text, we have called the tension here γ, as we will soon use T to denote the temperature. Then, the Smarr formula derived by Harmark and Obers takes the form

$$(n+2)TS = (n+1)M - 2\pi R\,\gamma \, , \tag{2.63}$$

where, as before, we take $n = D - 4$.

The first law of black hole thermodynamics for the most general solution would contain a term $\gamma\, dR$ to account for the energy stored in tension. However, these expressions will only be used in situations where we fix the size of the internal circle, so we shall drop this term. The first law for solutions with an internal space of fixed size is therefore

$$TdS = dM \, . \tag{2.64}$$

One may then use the Smarr formula (2.63) to eliminate the temperature from the first law to obtain the differential equation

$$\frac{d\log S}{d\log M} = \frac{n+2}{(n+1) - 2\pi R\,\gamma/M} \, . \tag{2.65}$$

Using these, one can determine all the thermodynamic properties of an arbitrary solution simply by considering a plot of M vs γ/M.

As a first step in a similar direction we may derive a Smarr formula for an arbitrary boosted solution on a cylinder. We start in the static frame and choose an ansatz of the form

$$ds^2 = -e^{2A}d\tilde{t}^2 + e^{2B}\left(dr^2 + d\tilde{z}^2\right) + e^{2C}r^2 d\Omega^2_{n+1} \, , \tag{2.66}$$

where $d\Omega_{n+1}$ is the metric on a unit $(n+1)$-sphere. We then boost into the physical frame, where we shall perform all calculations, by making the coordinate transformation in eqs. (2.25).

The modes of the functions A, B and C carrying KK momentum are exponentially damped at infinity and therefore will not contribute to the asymptotic integrals in eq. (2.13) for the total energy and momentum. Inserting the ansatz (2.66) into Einstein's equations, assuming the unknowns have only radial dependence and linearizing leads to decoupled first order equations for the derivatives of A and B. The constants may always be chosen to vanish by a rescaling of the coordinates, so we set them to zero. The remaining solution is therefore

$$A \sim \frac{A_\infty}{r^n} \,, \tag{2.67}$$

$$B \sim \frac{B_\infty}{r^n} \,. \tag{2.68}$$

The first derivative of C is described by a first order equation sourced by derivatives of A and B. Hence there will be three terms in the solution: a constant which we again set to zero; a solution of the homogeneous equation; and a term to account for the source. The solution is then given by:

$$C = \frac{C_0}{r} + C_\infty \tilde{C}(r) \,. \tag{2.69}$$

The coefficient C_0 labels the solution of the homogeneous equation. It is the leading behavior at large r and small C of the diffeomorphism $C = \log\left(\frac{r+C_0}{r}\right)$, which shifts the origin of the coordinate r by an amount C_0. We may therefore always arrange that this term also vanishes by a choice of coordinates. The second term results from the sourcing by A and B. It's coefficient, C_∞, is thus uniquely determined. The exact form, however, depends on the dimension

$$\tilde{C} = \begin{cases} \frac{\log r}{r} & C_\infty = A_\infty + 2B_\infty \\ \frac{1}{r^n} & (1-n)C_\infty = A_\infty + 2B_\infty \end{cases} \,. \tag{2.70}$$

As before, we calculate the interesting physical quantities by using the asymptotic integrals of eq. (2.13). Asymptotically, we make the change of coordinates

$$\hat{r} = r\left(1 + \frac{A_\infty + B_\infty}{n}\tilde{C}(r)\right) \,, \tag{2.71}$$

and the corrections to the flat metric become

$$\begin{aligned} h_{tt} &= -\frac{2}{\hat{r}^n}(A_\infty + (A_\infty - B_\infty)\sinh^2\beta)\ , && (2.72)\\ h_{tz} &= -\frac{2}{\hat{r}^n}(A_\infty - B_\infty)\sinh\beta\cosh\beta\ , && (2.73)\\ h_{zz} &= \frac{2}{\hat{r}^n}(B_\infty - (A_\infty - B_\infty)\sinh^2\beta)\ , && (2.74)\\ h_{ii} &= -\frac{2}{n\hat{r}^n}(A_\infty + B_\infty)\ . && (2.75) \end{aligned}$$

The energy and momentum density as well as the tension are then given by

$$\begin{aligned} T_{tt} &= -\frac{2\Omega_{n+1}}{16\pi G}\left((n+1)A_\infty + B_\infty + n(A_\infty - B_\infty)\sinh^2\beta\right)\ , && (2.76)\\ T_{tz} &= -\frac{2n\Omega_{n+1}}{16\pi G}\,(A_\infty - B_\infty)\sinh\beta\cosh\beta\ , && (2.77)\\ T_{zz} &= \frac{2\Omega_{n+1}}{16\pi G}\left(A_\infty + (n+1)B_\infty - n(A_\infty - B_\infty)\sinh^2\beta\right)\ . && (2.78) \end{aligned}$$

Following Harmark and Obers [121], we now consider the following Komar integral:

$$I = -\frac{1}{16\pi G}\int_\Sigma dS_{ab}\nabla^a\xi^b\ , \qquad (2.79)$$

where Σ is an $S^{n+1}\times S^1$ hypersurface and $\xi = \partial_t + \tanh\beta\partial_z$. We may evaluate this integral on an S^{n+1} of any radius since

$$\frac{1}{16\pi G}\left(\int_\Sigma dS_{ab}\nabla^a\xi^b - \int_{\Sigma'} dS_{ab}\nabla^a\xi^b\right) = \frac{1}{8\pi G}\int_V dS_a\nabla_b\nabla^a\xi^b\ , \qquad (2.80)$$

where V is the $(D-1)$-dimensional volume bounded by Σ and Σ'. Since ξ is a Killing vector, $\nabla_b\nabla^a\xi^b = R^a_{\ b}\xi^b$ which vanishes because we are considering vacuum solutions of Einstein's equations.

Since this integral is the same on any surface, we evaluate it both at infinity and on the horizon and equate the two values. At the horizon, the result is known to be [121, 151]

$$I_h = TS\ . \qquad (2.81)$$

If the solution was uniform in the z direction, ∂_t and ∂_z would individually be Killing vectors and we could express the integral at infinity in terms of individual Komar integrals for these vectors, giving contributions dependent on the total mass and momentum of the space-time. For the general solution this is no longer possible, but we do know the asymptotic behavior of the solutions. Using these we may evaluate the integral to be

$$\begin{aligned} I_\infty &= -\frac{\Omega_{n+1}}{16\pi G}(2\pi R)\, 2nA_\infty \,, && (2.82) \\ &= \frac{2\pi R}{n+2}\left[(n+1)\left(T_{tt} - \tanh\beta T_{tz}\right) + T_{zz} - \tanh\beta T_{tz}\right] \,. && (2.83) \end{aligned}$$

In the last line we have inverted eqs. (2.76–2.78) to eliminate A_∞ in favor of the components of the stress tensor.

We can simplify this further by noting that the combinations

$$T_{\tilde{t}\tilde{t}} = T_{tt} - \tanh\beta\, T_{tz} \,, \qquad T_{\tilde{z}\tilde{z}} = T_{zz} + \tanh\beta\, T_{tz} \,, \tag{2.84}$$

are simply the components of the stress tensor for an unboosted solution. In terms of these, the integral becomes

$$I_\infty = 2\pi R \frac{(n+1)T_{\tilde{t}\tilde{t}} + T_{\tilde{z}\tilde{z}}}{n+2} \,. \tag{2.85}$$

Finally, equating the values of the integral when evaluated on the horizon and at infinity we have

$$(n+2)TS = (n+1)2\pi R T_{\tilde{t}\tilde{t}} + \, 2\pi R T_{\tilde{z}\tilde{z}} \,. \tag{2.86}$$

When written this way, the Smarr formula is very similar to that for static solutions (2.63). This is no coincidence. On general grounds, we expect that the entropy is invariant under boosting [117]. The temperature, on the other hand, will gain a factor of $1/\cosh\beta$ when we apply a boost. For the right-hand side we recall that the size of the internal circle differs between the physical and static frames such that

$$R = \frac{\tilde{R}}{\cosh\beta} \,. \tag{2.87}$$

Hence the remaining combinations appearing on the right-hand side of the Smarr formula, for example $2\pi R\, T_{\tilde{t}\tilde{t}} = 2\pi \tilde{R} T_{\tilde{t}\tilde{t}}/\cosh\beta$, are simply the variables appearing in eq. (2.63) evaluated in the static frame then divided by a factor of $\cosh\beta$.

Chapter 3

Instability of Nonsupersymmetric Smooth Solutions

In recent years, Mathur and collaborators have advanced a radical revision of the stringy description of black holes — for a review, see [76, 77]. They argue that each of the CFT microstates corresponds to a separate space-time geometry with no horizon. The black hole is dual to an ensemble of such microstates and so the black hole geometry only emerges in a coarse-grained description which 'averages' over the $e^{S_{\rm BH}}$ microstate geometries. In particular, this averaging should produce an effective horizon at a radius where the individual microstate geometries start to 'differ appreciably' from one another [78, 152]. Therefore in this scenario, quantum gravity effects are not confined close to the black hole singularity, rather the entire interior of the black hole is 'filled' by fluctuating geometries — hence this picture is often referred to as the 'fuzzball' description of black holes. The first support for this proposal came from finding agreement between the propagation time of excitations in the throat of certain microstate geometries and in the dual brane description [78, 153]. A further remarkable feature, that has drawn attention to these ideas, is that there is growing evidence that the microstate geometries may be smooth, as well as horizon-free.[1] In the case of the D1-D5 system, smooth asymptotically flat geometries can be constructed corresponding to all of the RR ground states in the dual CFT [78–83]. Despite their large degeneracy, this two-charge system will not pro-

---

[1] 'Smooth' means the curvature is finite everywhere up to orbifold singularities. The curvatures in the throat may also be very large.

duce a macroscopic black hole horizon. However, a large horizon can be produced by introducing a third charge, Kaluza-Klein momentum [154–157]. Recently progress has been made in constructing smooth microstate geometries in the D1-D5-P system [84–89]. While large families of such solitons are now known, a complete understanding of the three-charge case remains to be found. Further, preliminary work on the four charge system of D1-D5-P-KK has also appeared [90–93].

In general, the preceding discussion connecting microstates with smooth geometries focuses on supersymmetric configurations. This raises the interesting question of how the fuzzball proposal would be extended to nonsupersymmetric black holes. In particular, are there nonsupersymmetric versions of the smooth horizon-free geometries corresponding to non-BPS microstates? Remarkably, Jejjala, Madden, Ross and Titchener [94] recently extended the known set of D1-D5 microstate geometries by adding a family of nonsupersymmetric solutions, hereafter referred to as JMaRT solitons. The JMaRT solutions comprise a five-parameter family of nonsupersymmetric smooth geometries which are asymptotically flat.[2] These solutions may be parameterized by the D1-brane and D5-brane charges, the (asymptotic) radius of the internal circle with Kaluza-Klein momentum, and by two integers m and n which fix the remaining physical parameters. These integers also determine a spectral flow in the CFT which allows the underlying microstate to be identified. For $m = n + 1$, the JMaRT solitons reduce to supersymmetric solutions found previously in [79–85].

An important feature which distinguishes the JMaRT solitons from any of the analogous supersymmetric solutions is the presence of an ergoregion. As a consequence, in these nonsupersymmetric geometries, there is an inner region (that extends to the origin) where states of negative energy are allowed. This then leads naturally to the question of whether or not the ergoregion produces an instability of the background. One possibility is that the ergoregion may lead to superradiant scattering which can produce a catastrophic instability in some situations [158–160]. However in the present case, this possibility is easily dismissed [94] because the solutions are horizon-free. Since the seminal work of Zel'dovich [161, 162] on superradiant amplification of electromagnetic waves incident upon an absorbing cylinder, it has been known

---

[2] By considering orbifolding, this family can extended by a third integer [94] but we will focus on the original five-parameter solutions.

that key ingredients for superradiance are the existence of an ergoregion *and* an absorbing surface. For black holes, the horizon plays the latter role, but certainly the JMaRT geometries lack such a surface.

Quite interestingly, there is another class of instabilities, which we simply refer to as 'ergoregion instabilities', that generically afflict space-time geometries with an ergoregion, but no horizon. These instabilities were first discovered by Friedman [163], who provided a very general discussion. Explicit computations of the instability were later made in [164, 165] for the case of rotating stars with an ergoregion. There the existence of this instability was explicitly verified for a free scalar field in the background of a rotating star. According to Friedman's general arguments however, the instability should also exist for electromagnetic and gravitational waves. Since the JMaRT solutions [94] have an ergoregion but no horizon, one might suspect that a similar ergoregion instability would arise in these geometries. The present chapter explicitly verifies the presence of an ergoregion instability for the JMaRT backgrounds with a variety of techniques. Further, we consider the endpoint of the resulting decay and argue that it should be a smooth supersymmetric solution.

Our results have immediate consequences for the endpoint of tachyon decay discussed in [166]. There, Ross extended the discussion of [167] to D1-D5 black strings for which he identified tachyonic string modes in a particular winding sector. He argued that the condensation of these tachyons would transform the space-time to a JMaRT soliton. In conjunction with the above results, we see that these solutions cannot be the final endpoint of these decays but rather they should end with a supersymmetric microstate geometry. Our analysis and the ergoregion instability may also have interesting implications for Mathur's fuzzball proposal more generally.

The remainder of this chapter is organized as follows: Section 3.1 provides a brief exposition on Friedman's analysis [163]. In Section 3.2, we briefly review some of the features of the JMaRT solutions and present the main equations used in the subsequent analysis, namely the radial and angular equations for a free massless scalar field, as well as some of their properties. In Section 3.3 we compute the details of the instability using a WKB approach [164]. We show explicitly that the instability exists for a general nonsupersymmetric geometry of [94], and that it disappears for supersymmetric objects, as expected. In Section 3.4, we use an alternative method, that of matched asymptotic expansions, to investigate the instability and its properties. The methods of Sections 3.3 and 3.4 are complementary, *i.e.*, their regime of validity is different. We then perform a numerical analysis of the wave equation in Section 3.5 to complement the analytical calculations. We find that the results of both analytical analyses agree remarkably well with the numerical results. In Section 3.6, after summarizing the main properties of the ergoregion instability, we discuss various related topics: the endpoint of this instability; its consequences for Ross's tachyon condensation [166]; general implications for the fuzzball picture of black holes.

3.1 Ergoregion instabilities

There are two classes of instabilities that are of potential interest for the JMaRT backgrounds [94] (or nonsupersymmetric geometries in general), namely: the superradiant instability, and the ergoregion instability. In this section, we demonstrate why superradiance is not present in these geometries, as first noted in [94]. Then we introduce the general argument of [163] which suggests an ergoregion instability is present in the JMaRT solutions.

3.1.1 Geometries with an ergoregion and horizon: superradiance

For a stationary, asymptotically flat black hole, the equations describing a massless[3] spin-s fields may be written as

$$\frac{d^2\Psi}{dr_*^2} + V(\omega,\, r)\Psi = 0 \ , \tag{3.1}$$

where ω was introduced with a Fourier transform with respect to the asymptotic time coordinate: $\Psi(t) = e^{-i\omega t}\Psi(\omega)$. The radius r_* is a convenient tortoise coordinate and in one finds:

$$\begin{cases} r_* \sim r\,, & V \sim \omega^2 \quad \text{as } r \to \infty\,, \\ e^{r_*} \sim (r-r_+)^\alpha\,, & V \sim (\omega-\Phi)^2 \quad \text{as } r \to r_+\,, \end{cases} \tag{3.2}$$

---

[3] We stress massless here, as it is only for such fields that the separation of variables and asymptotic behavior of the potential (3.2.) is guaranteed.

where α is a positive constant. The potential Φ can be a rotational potential (in the Kerr geometry $\Phi = m\Omega$, with m an azimuthal number, and Ω the angular velocity at the horizon) or a chemical potential (in the Reissner-Nordström geometry, $\Phi = qQ$, where q is the charge of the field and Q the charge of the black hole).

For a wave scattering in this geometry, eq. (3.1) yields the following asymptotic behavior:

$$\Psi_1 \sim \begin{cases} \mathcal{T}\,(r-r_+)^{-i\alpha(\omega-\Phi)} & \text{as } r \to r_+\,, \\ \mathcal{R}\,\mathrm{e}^{i\omega r} + \mathrm{e}^{-i\omega r} & \text{as } r \to \infty\,. \end{cases} \tag{3.3}$$

These boundary conditions correspond to an incident wave of unit amplitude from $+\infty$ giving rise to a reflected wave of amplitude $\mathcal{R}$ going back to $+\infty$ and a transmitted wave of amplitude $\mathcal{T}$ at the horizon — the boundary condition allows only ingoing waves at the horizon. Now assuming a real potential, the complex conjugate of the solution Ψ_1 satisfying the boundary conditions (3.3) will satisfy the complex-conjugate boundary conditions:

$$\Psi_2 \sim \begin{cases} \mathcal{T}^*(r-r_+)^{i\alpha(\omega-\Phi)} & \text{as } r \to r_+\,, \\ \mathcal{R}^*\mathrm{e}^{-i\omega r} + \mathrm{e}^{i\omega r} & \text{as } r \to \infty\,. \end{cases} \tag{3.4}$$

Now, these two solutions are linearly independent, and the standard theory of ordinary differential equations tells us that their Wronskian, $W = \Psi_1\partial_{r_*}\Psi_2 - \Psi_2\partial_{r_*}\Psi_1$, is a constant (independent of r). If we evaluate the Wronskian near the horizon, we find $W = -2i(\omega-\Phi)|\mathcal{T}|^2$, and near infinity we find $W = 2i\omega(|\mathcal{R}|^2 - 1)$. Equating the two we get

$$|\mathcal{R}|^2 = 1 - \frac{\omega-\Phi}{\omega}|\mathcal{T}|^2\,. \tag{3.5}$$

Now, in general $|\mathcal{R}|^2$ is less than unity, as is to be expected. However, for $\omega - \Phi < 0$ we have that $|\mathcal{R}|^2 > 1$. Such a scattering process, where the reflected wave has actually been amplified, is known as superradiance. Of course the excess energy in the reflected wave must come from that of the black hole, which therefore decreases.

Superradiant scattering can lead to an instability if, *e.g.*, we have a reflecting wall surrounding the black hole that scatters the returning wave back toward the horizon. In such a situation, the wave will bounce back and forth, between the mirror and the black hole, amplifying itself each time. The total extracted energy grows exponentially until finally the radiation pressure destroys the mirror. This is Press and Teukolsky's black hole bomb, first proposed in [158]. This instability can arise with an effective 'mirror' in a variety of situations: a scalar field with mass $\mu > \omega$ in a Kerr background creates a potential that can cause flux to scatter back toward the horizon [168]; infinity in asymptotically AdS spaces also provides a natural wall [169] that leads, for certain conditions, to an instability; a wave propagating around rotating black branes or rotating black strings may similarly find itself trapped [170].

3.1.2 Geometries with an ergoregion but no horizon: ergoregion instability

Suppose now there is no horizon in the background space-time[4]. The boundary conditions must therefore be modified since there is no longer a surface absorbing the ingoing modes. In this case, the absorption boundary condition (3.3) at the horizon is replaced by some kind of regularity condition at the origin. We suppose the radial coordinate r now ranges from zero to infinity and we impose the following boundary condition:

$$\Psi \sim A f(r)\ ,\ \ r \to 0\,, \tag{3.6}$$

where $f(r)$ is some well-behaved *real* function. This ansatz encompasses for instance typical regularity requirements where, *e.g.*, one chooses $f(r) \sim r^{\beta}$ with $\beta > 0$. Repeating the above calculation, one finds $|\mathcal{R}|^2 = 1$. Therefore the absence of a horizon, which precludes any absorption, prevents superradiance and hence the superradiant instability.

Nevertheless, geometries with an ergoregion but without horizons are the arena of another class of instability. This ergoregion instability was discovered by Friedman [163]. Even though his discussion was made in four dimensions only, it is trivial to extend it to any number of dimensions. The instability arises because of the following [163]: Given the test field energy-momentum tensor T^{ab}, we can associate a canonical energy

$$\mathcal{E}_S = \int_S t^a\, T_a{}^b dS_b\,, \tag{3.7}$$

---

[4] In fact, one can be slightly more general here as the ergoregion instability has also been found to exist for some models of 2-D black holes in which there is a horizon that is causally disconnected from the ergoregion [171]. However, since the JMaRT solutions are horizon-free we shall only concern ourselves with this situation.

where t^a is the background Killing vector which generates time translations in the asymptotic geometry. Now, because t^a is space-like within an ergosphere, initial data can be chosen on a Cauchy surface S which makes $\mathcal{E}_S$ negative. Moreover, it is shown in [163] that the energy can be negative only when the test field is time dependent. Then, since the field is time dependent and only positive energy can be radiated at future null infinity, the value of $\mathcal{E}_S$ must decrease from one asymptotically null hypersurface S to another, say, S', in the future of S. Thus the energy $\mathcal{E}_S$ will typically grow negative without bound. This instability was computed analytically using a WKB approximation in [164] for rotating stars. There it was shown that the instability timescale is usually very large (typically larger than the age of the universe). The analysis of [164] was improved in [165] where further details of the instability were computed numerically.

A key assumption above is that the system can not settle down to a negative energy configuration which, while time dependent, is nonradiative. Friedman [163] was able to rule out such marginal cases where $\mathcal{E}_S$ is negative but constant for a four-dimensional massless scalar or electromagnetic fields. However, in fact, one is able to identify negative energy bound states for the JMaRT backgrounds — see the supplementary material 3.7.4 — and so a more thorough analysis is called for. Hence in the following, we apply a variety of techniques to explicitly show that these microstate geometries suffer from an ergoregion instability.

3.2 Formalism

We now consider wave propagation of a free massless scalar field in the JMaRT backgrounds [94], and in subsequent sections identify an ergoregion instability. As the JMaRT solutions are quite complicated, we provide a brief discussion of some of their properties here, but refer the reader to [94] for more detail.

The JMaRT solitons are solutions of type IIB supergravity corresponding to three-charge microstate geometries of the D1-D5-P system. The system is compactified to five dimensions on $T^4 \times S^1$ with the D5-branes wrapping the full internal space and the D1-branes and KK momentum on the distinguished S^1. In the construction of these solitons, one begins with the general solutions of [156, 157] which contain eight parameters: a mass parameter, M, spin parameters in two orthogonal planes, a_1, a_2, three boost parameters, $\delta_1, \delta_5, \delta_p$, fixing the D1-brane, D5-brane and KK momentum charges, the radius of the S^1, R, and the volume of the T^4. In the string frame, the geometry is described by the six-dimensional line element [94]

$$\begin{aligned} ds^2 \;=\; & \frac{1}{\sqrt{\tilde{H}_1 \tilde{H}_5}} \Big\{ \\ & -(f-M)\left[d\tilde{t} - (f-M)^{-1} M \cosh\delta_1 \cosh\delta_5 (a_1 \cos^2\theta d\psi + a_2 \sin^2\theta d\phi)\right]^2 \\ & +f\left[d\tilde{y} + f^{-1} M \sinh\delta_1 \sinh\delta_5 (a_2 \cos^2\theta d\psi + a_1 \sin^2\theta d\phi)\right]^2 \Big\} \\ & +\sqrt{\tilde{H}_1 \tilde{H}_5} \Big\{ \frac{r^2 dr^2}{(r^2+a_1^2)(r^2+a_2^2) - M r^2} + d\theta^2 \\ & +(f(f-M))^{-1}\left[\big(f(f-M) + f a_2^2 \sin^2\theta - (f-M) a_1^2 \sin^2\theta\big) \sin^2\theta d\phi^2 \right. \\ & +2 M a_1 a_2 \sin^2\theta \cos^2\theta d\psi d\phi \\ & \left. + \big(f(f-M) + f a_1^2 \cos^2\theta - (f-M) a_2^2 \cos^2\theta\big) \cos^2\theta d\psi^2\right] \Big\} . \end{aligned} \tag{3.8}$$

The dilaton is given by

$$e^{2\Phi} = \frac{\tilde{H}_1}{\tilde{H}_5} , \tag{3.9}$$

and the 2-form gauge potential sourced by the branes is

$$\begin{aligned} C_2 \;=\; & \frac{M \cos^2\theta}{\tilde{H}_1} \left[(a_2 c_1 s_5 c_p - a_1 s_1 c_5 s_p) dt + (a_1 s_1 c_5 c_p - a_2 c_1 s_5 s_p) dy\right] \wedge d\psi \\ & + \frac{M \sin^2\theta}{\tilde{H}_1} \left[(a_1 c_1 s_5 c_p - a_2 s_1 c_5 s_p) dt + (a_2 s_1 c_5 c_p - a_1 c_1 s_5 s_p) dy\right] \wedge d\phi \\ & - \frac{M s_1 c_1}{\tilde{H}_1} dt \wedge dy - \frac{M s_5 c_5}{\tilde{H}_1} (r^2 + a_2^2 + M s_1^2) \cos^2\theta d\psi \wedge d\phi , \end{aligned} \tag{3.10}$$

where $f(r) = r^2 + a_1^2 \sin^2\theta + a_2^2 \cos^2\theta > 0$ and $\tilde{H}_i(r) = f(r) + M s_i^2$, $i = 1, 5$.

One then imposes a series of constraints to ensure that the solutions are free of singularities, horizons and closed time-like curves. In particular, one focuses on a low-mass regime, $M^2 < (a_1 - a_2)^2$, in which no black holes exist. Then one finds solitonic solutions where the y circle shrinks to zero at the origin and the constraints ensure that this happens smoothly. First, M and R can be fixed in terms of the remaining parameters — see eqs. (3.15) and (3.20) of [94]. Two quantization conditions constrain the remaining parameters in terms of two integers m, n [94]:

$$\frac{j+j^{-1}}{s+s^{-1}} = m-n\,, \qquad \frac{j-j^{-1}}{s-s^{-1}} = m+n\,, \tag{3.11}$$

where $j = \sqrt{\frac{a_2}{a_1}} \leq 1$ and $s = \sqrt{\frac{s_1 s_5 s_p}{c_1 c_5 c_p}} \leq 1$. We are using the notation here that $c_i \equiv \cosh\delta_i$ and $s_i \equiv \sinh\delta_i$. Without loss of generality, one assumes $a_1 \geq a_2 \geq 0$ which implies $m > n \geq 0$. We also note here that the special case $m = n+1$ corresponds to supersymmetric solutions.

This leaves a five-parameter family of smooth solitonic solutions. We can think of the independent parameters as the D1-brane and D5-brane charges, Q_1, Q_5; the (asymptotic) radius of the y-circle, R; and the two integers, m and n, which fix the remaining physical parameters as [94]

$$Q_P = nm\frac{Q_1 Q_5}{R^2}\,, \quad J_\phi = -m\frac{Q_1 Q_5}{R}\,, \quad J_\psi = n\frac{Q_1 Q_5}{R}\,. \tag{3.12}$$

Of course, depending on the specific application, it may be more appropriate and/or simpler to describe the solutions using a different set of quantities. In our case, when we make explicit calculations of the ergoregion instability, we will fix the parameters n, m, a_1, c_1 and c_5 or c_p. As we are interested in nonsupersymmetric backgrounds, we also impose $m \geq n+2$. To conclude our discussion of notation, we add that the roots of g^{rr}, r_+ and r_-, will also appear in the following but they are determined by M and the spin parameters — see eq. (3.2) of [94].

The key ingredient producing the instability in the JMaRT solutions is the existence of an ergoregion. To verify the presence of the ergoregion, one takes as usual the norm of the Killing vector $V = \partial_t$ and using eq. (2.12) of [94], calculates

$$g_{\mu\nu}V^\mu V^\nu = -\frac{f - Mc_p^2}{\sqrt{\tilde{H}_1 \tilde{H}_5}}\,. \tag{3.13}$$

It is then clear that $V = \partial_t$ becomes space-like for $f(r) < M$ and thus an ergosphere appears at $f(r) = M$. An inspection of the metric also allows one to conclude the geometry rotates along ϕ, ψ and y since $g_{t\phi} \neq 0$, $g_{t\psi} \neq 0$ and $g_{ty} \neq 0$. The supersymmetric limit of the JMaRT solitons corresponds to the limit $M \to 0$ and $\delta_i \to \infty$, while keeping the other parameters fixed, including the conserved charges $Q_i = M s_i c_i$ [94]. So, in the supersymmetric limit the norm becomes $|V|^2 = -f/\sqrt{\tilde{H}_1 \tilde{H}_5}$, which is always negative and thus the ergoregion is not present.

Now consider the Klein-Gordon equation for a massless scalar field propagating in the JMaRT geometries,

$$\frac{1}{\sqrt{-g}}\frac{\partial}{\partial x^\mu}\left(\sqrt{-g}\, g^{\mu\nu}\frac{\partial}{\partial x^\nu}\Psi\right) = 0\,. \tag{3.14}$$

We are using the string-frame metric in which case one can think of eq. (3.14) as the linearized equation of motion for the Ramond-Ramond scalar. As described above, these backgrounds can be thought of as special cases of the general D1-D5-P solutions found earlier [156, 157] and so one may apply separation of variables following [172]. Introducing the following ansatz[5]

$$\Psi = \exp\left[-i\omega\frac{t}{R} - i\lambda\frac{y}{R} + im_\psi\psi + im_\phi\phi\right]\,\chi(\theta)\,h(r)\,, \tag{3.15}$$

one obtains an angular equation

$$\begin{split}\frac{1}{\sin 2\theta}\frac{d}{d\theta}\left(\sin 2\theta\,\frac{d\chi}{d\theta}\right)+ \\ \left[\Lambda - \frac{m_\psi^2}{\cos^2\theta} - \frac{m_\phi^2}{\sin^2\theta} + \frac{\omega^2-\lambda^2}{R^2}(a_1^2\sin^2\theta + a_2^2\cos^2\theta)\right]\chi = 0\,,\end{split} \tag{3.16}$$

and a radial equation[6]

$$\begin{split}\frac{1}{r}\frac{d}{dr}\left[\frac{g(r)}{r}\frac{d}{dr}h\right] - \Lambda h + \left[\frac{(\omega^2-\lambda^2)}{R^2}(r^2+Ms_1^2+Ms_5^2) + (\omega c_p + \lambda s_p)^2\frac{M}{R^2}\right]h \\ -(r_+^2-r_-^2)\frac{(\lambda - nm_\psi + mm_\phi)^2}{(r^2-r_+^2)}\,h + (r_+^2-r_-^2)\frac{(\omega\varrho + \lambda\vartheta - nm_\phi + mm_\psi)^2}{(r^2-r_-^2)}\,h = 0\,,\end{split} \tag{3.17}$$

where $g(r) = (r^2-r_+^2)(r^2-r_-^2)$, and $\sqrt{-g} = r\sin\theta\cos\theta\sqrt{\tilde{H}_1\tilde{H}_5}$ (the determinant of the metric in eq. (3.8)). If we introduce a dimensionless variable

$$x = \frac{r^2-r_+^2}{r_+^2-r_-^2}, \tag{3.18}$$

we can rewrite the radial equation in the form

$$\partial_x[x(x+1)\partial_x h] + \frac{1}{4}\left[\kappa^2 x + 1 - \nu^2 + \frac{\xi^2}{x+1} - \frac{\zeta^2}{x}\right]h = 0\,, \tag{3.19}$$

---

[5] Note that the negative sign for λ corrects a typo found in [94]

[6] Note the factor $(r_+^2 - r_-^2)$ that appears in the two last terms of the left-hand side of (3.17), which are necessary for dimensional consistency, corrects the typo appearing in eq. (6.4) of [94]

with

$$\begin{aligned}
\kappa^2 &= (\omega^2 - \lambda^2)\frac{r_+^2 - r_-^2}{R^2}\,, \\
\xi &= \omega\varrho + \lambda\vartheta - m_\phi n + m_\psi m\,, \\
\zeta &= \lambda - m_\psi n + m_\phi m\,, \\
\varrho &= \frac{c_1^2 c_5^2 c_p^2 - s_1^2 s_5^2 s_p^2}{s_1 c_1 s_5 c_5}\,, \\
\vartheta &= \frac{c_1^2 c_5^2 - s_1^2 s_5^2}{s_1 c_1 s_5 c_5}\, s_p c_p\,,
\end{aligned} \tag{3.20}$$

and

$$\nu^2 = 1 + \Lambda - \frac{\omega^2 - \lambda^2}{R^2}(r_+^2 + M s_1^2 + M s_5^2) - (\omega c_p + \lambda s_p)^2 \frac{M}{R^2}\,. \tag{3.21}$$

The quantities ω, λ, m_ψ, m_ϕ are all dimensionless — the last three being integers. Again, we refer the reader to [94] for a detailed account of the quantities appearing above. The reader should take note that our notation is not in complete accord with that of [94]. That is, to simplify our formulae in the following, we have defined $\kappa \equiv 1/\sigma$, the inverse of the quantity σ used there.

Of critical importance in characterizing the solutions of the radial equation is the sign of κ^2. The term $x\kappa^2$ dominates at large x, determining the asymptotic behavior of the solution. In this chapter we will mainly be interested in outgoing modes so we choose κ^2 to be positive. The two remaining possibilities: $\kappa^2 = 0$ and $\kappa^2 < 0$, will be considered in the appendices.

The angular equation (3.16) (plus regularity requirements) is a Sturm-Liouville problem. We can label the corresponding eigenvalues Λ with an index l, $\Lambda(\omega) = \Lambda_{lm}(\omega)$ and therefore the wavefunctions form a complete set over the integer l. In the general case, the problem at hand consists of two coupled second order differential equations: given some boundary conditions, one has to compute *simultaneously* both values of ω and Λ that satisfy these boundary conditions. However, for vanishing a_i^2 we get the (five-dimensional) flat space result, $\Lambda = l(l+2)$, and the associated angular functions are given by Jacobi polynomials. For nonzero, but small $\frac{\omega^2-\lambda^2}{R^2}a_i^2$ we have

$$\Lambda = l(l+2) + \mathcal{O}\left(a_i^2 \frac{\omega^2 - \lambda^2}{R^2}\right)\,. \tag{3.22}$$

The integer l is constrained to be $l \geq |m_\psi| + |m_\phi|$. We will always assume $a_i^2 \frac{\omega^2-\lambda^2}{R^2} \ll \max(m_\psi^2, m_\phi^2)$ (with $i = 1, 2$), thus $\Lambda \simeq l(l+2)$. Making this assumption implies we may neglect the terms proportional to a_i in the angular equation, but given the way Λ and ω appear in the radial equation, the corrections to Λ may not be negligible when we determine ω. To ensure that fixing $\Lambda = l(l+2)$ is consistent in both the angular and radial equations we must additionally require

$$a_i^2 \ll \max\left(|r_+^2 + M(s_1^2 + s_5^2)|, Mc_p^2\right) \,, \tag{3.23}$$

so that the contribution to ν from the a_i dependent corrections of Λ are negligible (see (3.21)).

Taking the complex conjugate of eq. (3.16) we can see that the exact solution to the angular equation has the symmetry

$$\Lambda_{lm}(-\omega^*) = \Lambda_{lm}^*(\omega) \,. \tag{3.24}$$

With this symmetry, one can also check the following:

$$(\nu^2)^*(\omega, \lambda) = \nu^2(-\omega^*, -\lambda) \,, \tag{3.25}$$

$$(\xi^2)^*(\omega, \lambda, m_\psi, m_\phi) = \xi^2(-\omega^*, -\lambda, -m_\psi, -m_\phi) \,, \tag{3.26}$$

$$(\zeta^2)^*(\lambda, m_\psi, m_\phi) = \zeta^2(-\lambda, -m_\psi, -m_\phi) \,. \tag{3.27}$$

Therefore, from the wave equation (3.19) it follows that if ω is an eigenvalue for given values of m_ψ, m_ϕ, λ with eigenfunction h, then $-\omega^*$ is an eigenvalue for $-m_\psi, -m_\phi, -\lambda$ with eigenfunction h^*. Furthermore, if $he^{-i\omega t}$ is outgoing unstable, so is $h^* e^{i\omega^* t}$. Since the symmetry simultaneously flips all the signs of m_ψ, m_ϕ, λ, without loss of generality, we can only fix the sign of one, *e.g.*, $\mathcal{R}e(\omega) \leq 0$.

To conclude this section, we point out that the angular equation (3.16) can be recast in the somewhat more familiar form:

$$\frac{1}{\sin\theta\cos\theta}\frac{d}{d\theta}\left(\sin\theta\cos\theta\frac{d\chi}{d\theta}\right) + \left[\hat{\Lambda} - \frac{m_\psi^2}{\cos^2\theta} - \frac{m_\phi^2}{\sin^2\theta} + \frac{\omega^2-\lambda^2}{R^2}(a_2^2 - a_1^2)\cos^2\theta\right]\chi = 0 \,, \tag{3.28}$$

where

$$\hat{\Lambda} = \Lambda + \frac{\omega^2-\lambda^2}{R^2}a_1^2 \,. \tag{3.29}$$

This is just the equation for a five-dimensional scalar spheroidal harmonic [173–176] which arises, *e.g.*, in the separation of Klein-Gordon equation in the background of a five-dimensional rotating black hole [104].

3.3 WKB analysis

We now explicitly show that the JMaRT geometries [94] suffer from an ergoregion instability. As described above, this instability is due to the fact that the geometry has an ergoregion but no horizon. We shall identify modes of the scalar field that are regular at the origin, represent outgoing waves at infinity and grow with time. In this section, we follow the WKB analysis of [164] and show that it applies to the nonsupersymmetric JMaRT solutions, with the same qualitative conclusions.

To begin, we want to write the radial equation in the form of an effective Schrödinger equation. In order to do so, we first transform to a new 'wavefunction' H defined by

$$h(x)=\frac{1}{\sqrt{x(1+x)}}\,H(x)\,. \tag{3.30}$$

Inserting this in (3.19), we get

$$-\partial_x^2 H+U_{\rm eff}\,H=0\,, \tag{3.31}$$

where

$$U_{\rm eff}=-\frac{\kappa^2x^3+(1-\nu^2+\kappa^2)x^2+(1-\nu^2+\xi^2-\zeta^2)x+1-\zeta^2}{4x^2(1+x)^2}\,. \tag{3.32}$$

Now in order to simplify our analysis, we choose: $\lambda=0$, $m_\phi=0$, and large m_ψ. With $\lambda\neq 0$, the waves see a constant potential at infinity and thus the amplitude of the outgoing waves can be suppressed there. We also consider $l=m_\psi$ modes, which are expected to be the most unstable. Modes with $l\gg m_\psi$ must be similar to modes with $m_\psi=0$ for some l and these are not unstable. With these choices, we have

$$\begin{aligned}\kappa^2 &= \omega^2\frac{r_+^2-r_-^2}{R^2}\,,\quad \zeta^2=n^2m_\psi^2\,,\quad \xi^2=m^2m_\psi^2+\omega^2\varrho^2+2\omega\varrho m m_\psi\,, && (3.33)\\ 1-\nu^2 &\simeq -m_\psi^2+\omega^2\frac{r_+^2+Ms_1^2+Ms_5^2+Mc_p^2}{R^2}\,. && (3.34)\end{aligned}$$

Instead of working directly with the frequency of the wave, it will be convenient to work with the pattern speed along the ψ direction, which is the angular velocity at which surfaces of constant phase rotate. This velocity is proportional to

$$\Sigma_\psi = \frac{\omega}{m_\psi}\,, \tag{3.35}$$

where the proportionality constant R^{-1} is always positive. It is important to compare the sign of the pattern speed along ψ with the sign of the angular velocity of the geometry along ψ defined, as usual, by[7]

$$\begin{aligned}\Omega_\psi = -\frac{g_{t\psi}}{g_{\psi\psi}} &= -\frac{2Ms_p\,c_p\,\cos^2\theta}{\sqrt{\tilde{H}_1\tilde{H}_5}}\frac{R/n}{g_{\psi\psi}} \\ &= -\frac{2Q_p\,\cos^2\theta}{\sqrt{\tilde{H}_1\tilde{H}_5}}\frac{\cos^2\theta R/n}{g_{\psi\psi}} < 0, \quad \forall\, x > 0\,,\end{aligned} \tag{3.36}$$

where $Q_p = Ms_p\,c_p$ is the Kaluza-Klein momentum charge. So, when Σ_ψ is negative, the wave is propagating in the same sense as the geometry.

Now it is useful to introduce the polynomial

$$\mathcal{P} = Bx^3 + (A+B)x^2 + (\varrho^2 + A)x\,, \tag{3.37}$$

which is positive definite in the range of interest (positive x). We also define

$$T = -\frac{U_{\rm eff}}{m_\psi^2}\,, \quad A \equiv \frac{r_+^2 + M(s_1^2 + s_5^2 + c_p^2)}{R^2}\,, \quad B \equiv \frac{r_+^2 - r_-^2}{R^2}\,. \tag{3.38}$$

Then, we can write the effective Schrödinger equation (3.31) as

$$\partial_x^2 H + m_\psi^2\, T\, H = 0\,, \tag{3.39}$$

with

$$T = \frac{\mathcal{P}}{4x^2(1+x)^2}\left[\Sigma_\psi^2 + \frac{2\varrho m x}{\mathcal{P}}\Sigma_\psi - \frac{x^2 - x(m^2 - n^2 - 1) + n^2}{\mathcal{P}}\right], \tag{3.40}$$

---

[7] Note that the geometry rotates simultaneously along the ψ, ϕ and y directions. We find Ω_ψ using of (2.1), (3.17) and (3.19) of [94].

where we have dropped certain small contributions to T.[8] Now it is straightforward to factorize the potential T and write it in the form

$$T = \frac{\mathcal{P}}{4x^2(1+x)^2}(\Sigma_\psi - V_+)(\Sigma_\psi - V_-)\,, \tag{3.41}$$

with

$$V_\pm = -\frac{\varrho m x}{\mathcal{P}} \pm \left[\left(\frac{\varrho m x}{\mathcal{P}} \right)^2 + \frac{x^2 - x(m^2 - n^2 - 1) + n^2}{\mathcal{P}} \right]^{\frac{1}{2}}. \tag{3.42}$$

For general $m\,,n$ the behavior of the potentials V_+ and V_- (see Figure 3.1) is exactly the same as the one studied in [164], so we do expect an instability to arise, as will be shown below. However, and this is a key point, for the case $m = n+1$ which is the supersymmetric case, we have

$$V_+ = -\frac{\varrho m x}{\mathcal{P}} + \left[\left(\frac{\varrho m x}{\mathcal{P}} \right)^2 + \frac{(x-n)^2}{\mathcal{P}} \right]^{\frac{1}{2}}, \qquad m = n+1\,, \tag{3.43}$$

which is always positive. Thus this WKB analysis indicates that the supersymmetric solutions are stable, as expected.

Hence our radial equation has been reduced to a Schrödinger equation (3.39) with a potential dependent on the pattern speed given by eq. (3.41). The problem of finding the unstable modes thus becomes tuning Σ_ψ in order that a ‘zero-energy’ solution can be found with the appropriate boundary conditions: regularity at the origin and outgoing at infinity. Note that in a region where Σ_ψ is above V_+ or below V_- (allowed regions), the solutions have an oscillatory behavior. In those intervals where Σ_ψ is in between the curves of V_+ and V_- (forbidden regions), the solutions have a real exponential behavior.

We proceed following [164] and study the scattering of waves in the effective potential constructed above. Consider a wave that comes from infinity with an amplitude $C_{\rm in}$, scatters in the ergoregion and returns to infinity with an amplitude $C_{\rm out}$. In particular, we introduce the scattering amplitude defined as

$$S \equiv \frac{C_{\rm out}}{C_{\rm in}}. \tag{3.44}$$

---

[8] More precisely, we have dropped a term $1/(m_\psi^2 \mathcal{P})$. This remains a very good approximation in the high-m_ψ limit in which we are working. As an example, for $n = 10$ and $m_\psi = 10$ the factor that we dropped is 10^{-4} smaller than the last term of (3.40).

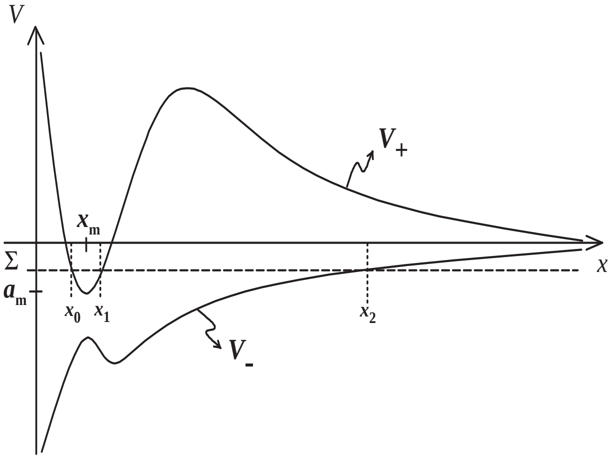

Figure 3.1: Qualitative shape of the potentials V_+ and V_- for the case in which an instability is present. An example background that yields these kinds of potentials is described by $(m = 14\,, n = 10\,, a_1 = 32\,, c_1 = 5\,, c_p = 5)$. The unstable modes are those whose pattern speed Σ_ψ is negative and approach the minimum of V_+ from above. Thus they are nearly bound states of the potential well in V_+ that can however tunnel out to infinity through V_-. Choosing $\lambda = 0$, the potentials V_+ and V_- approach zero as $x \to \infty$, which makes a tunnelling through V_- easier.

The presence of a pole in S (*i.e.*, of a resonance) signals the existence of an instability. Indeed, a pole in S occurs when $C_{\text{in}} = 0$ and $C_{\text{out}} \neq 0$, and this means that we have finite outgoing radiation for zero incoming radiation. Near the pole frequency ω_{p}, the scattering amplitude can be written to lowest order as [164]

$$S \simeq e^{i2\delta_0}\,\frac{\omega - \omega_{\text{p}}^*}{\omega - \omega_{\text{p}}}\,, \tag{3.45}$$

where δ_0 is a constant scattering phase shift and ω_{p}^* is the complex conjugate of ω_{p}. Note that this expression guarantees that when the frequency of the wave is real, one has $S(\omega)[S(\omega)]^* = 1$, as required by energy conservation. Generically, we can write the pole or resonant frequency as

$$\omega_{\text{p}} = \omega_{\text{r}} + i/\tau\,, \tag{3.46}$$

where $\omega_{\rm r}$ and $1/\tau$ are, respectively, the real and imaginary parts of $\omega_{\rm p}$. With this convention, a mode with positive τ represents an instability, and $\tau < 0$ represents a damped mode, since the time dependence[9] of the resonant wave is given by $e^{-i\omega_{\rm p}t} = e^{-i\omega_{\rm r}t}e^{t/\tau}$. We can then write

$$S \simeq e^{i2\delta_0}\,\frac{\omega - \omega_{\rm r} + i/\tau}{\omega - \omega_{\rm r} - i/\tau}\,. \tag{3.47}$$

To relate the amplitudes $C_{\rm in}$ and $C_{\rm out}$ we apply a WKB analysis. As we shall learn later on, the unstable modes are those whose pattern speed Σ_ψ is negative and approaches the minimum of V_+ from above (see Figure 3.1). The scattering problem has then four distinct regions, namely: I, the innermost forbidden region ($0 < x < x_0$); II, the allowed region where V_+ is below Σ_ψ ($x_0 < x < x_1$); III, the potential barrier region where V_+ is above Σ_ψ ($x_1 < x < x_2$); and finally the external allowed region where Σ_ψ is below V_- ($x_2 < x < \infty$). The unstable modes are those that have $\Sigma_\psi < 0$. Thus they are nearly bound states of the potential well in V_+ that can tunnel out to infinity through V_-. In region I, the WKB wavefunction that vanishes at the origin $x = 0$ is

$$H_{\rm I} \simeq \frac{C_1}{m_\psi^{1/2}|T|^{1/4}}{\rm exp}\left[-m_\psi\int_x^{x_0}\sqrt{|T|}\,dx\right]\,, \tag{3.48}$$

where C_1 is a constant. Then, the usual WKB wavefunctions and connection formulae — see Section 3.7.1 — allow us to relate $H_{\rm I}$ to the wavefunctions in the other regions and, in particular, with the incoming and outgoing contributions of the wavefunction in region IV:

$$H_{\rm IV} \simeq \frac{C_6}{m_\psi^{1/2}T^{1/4}}{\rm exp}\left[i\,m_\psi\int_{x_2}^{x}\sqrt{T}\,dx\right] + \frac{C_7}{m_\psi^{1/2}T^{1/4}}{\rm exp}\left[-i\,m_\psi\int_{x_2}^{x}\sqrt{T}\,dx\right]\,. \tag{3.49}$$

The WKB analysis yields the relation between the amplitudes C_6, C_7 and C_1:

$$\begin{aligned} C_1e^{i\gamma} &= \frac{1}{2}\left[\left(2\eta+\frac{1}{2\eta}\right)C_6 + i\left(2\eta-\frac{1}{2\eta}\right)C_7\right] \\ C_1e^{-i\gamma} &= \frac{1}{2}\left[-i\left(2\eta-\frac{1}{2\eta}\right)C_6 + \left(2\eta+\frac{1}{2\eta}\right)C_7\right]\,, \end{aligned} \tag{3.50}$$

---

[9] Our conventions differ slightly from those of [164]. There waves carry a time dependence $e^{i\omega t}$ while we follow [94] which introduces the separation ansatz (3.15) with a time dependence $e^{-i\omega t}$.

where

$$\gamma \equiv m_\psi \int_{x_0}^{x_1} \sqrt{T}\, dx - \frac{\pi}{4}\,, \tag{3.51}$$

$$\ln \eta \equiv m_\psi \int_{x_1}^{x_2} \sqrt{|T|}\, dx\,. \tag{3.52}$$

The identification of the ingoing and outgoing contributions in (3.49) depends on the sign of Σ_ψ. Indeed, one has $\Psi \propto e^{-i\omega t} H_{\rm IV}(x)$. If Σ_ψ is negative the term $C_6 e^{-i(\omega t-\gamma(x))}$ represents the ingoing contribution, while the term $C_7 e^{-i(\omega t+\gamma(x))}$ describes the outgoing contribution (if $\Sigma_\psi > 0$, the terms proportional to C_6 and C_7 in $H_{\rm IV}(x)$ represent, respectively, the outgoing and ingoing modes). Henceforth we consider the $\Sigma_\psi < 0$ case (since this will be the unstable case), for which the scattering amplitude can be written as

$$S = \frac{C_7}{C_6} = \frac{i(4\eta^2-1)e^{i\gamma} + (4\eta^2+1)e^{-i\gamma}}{(4\eta^2+1)e^{i\gamma} - i(4\eta^2-1)e^{-i\gamma}}\,. \tag{3.53}$$

The resonance peaks in the scattering amplitude occur at a frequency ω_N for which $e^{-i\gamma} + ie^{i\gamma} = 0$, *i.e.*, when $\gamma(\omega) = \gamma_N$ where

$$\gamma_N(\omega_N) \equiv N\pi + \frac{\pi}{4} \tag{3.54}$$

with N being an integer usually referred to as the 'harmonic'. The easiest way to see that the resonance peaks must be near these (real) frequencies is to note that $S(\gamma_N) = -i$ while for $\eta \to \infty$, one has $S(\gamma \neq \gamma_N) = +i$. So when $\eta \to \infty$, one has generally $S(\gamma) = +i$, but when $\gamma = \gamma_N$ a peak occurs that changes the value of S from $+i$ to $-i$.

We can now perform a Taylor expansion of the functions that appear in S around $\gamma = \gamma_N$. Defining

$$\alpha = \left.\frac{d\gamma}{d\omega}\right|_{\omega=\omega_N} = \frac{d}{d\Sigma_\psi}\left[\int_{x_0}^{x_1} \sqrt{T}\, dx\right]_{\Sigma_\psi=\Sigma_{\psi,N}}\,, \tag{3.55}$$

the scattering amplitude can be written as

$$S \simeq \frac{-\alpha(\omega-\omega_N) + \frac{1}{4\eta^2} - i\left[\alpha(\omega-\omega_N) + \frac{1}{4\eta^2}\right]}{-\alpha(\omega-\omega_N) + \frac{1}{4\eta^2} + i\left[\alpha(\omega-\omega_N) + \frac{1}{4\eta^2}\right]} \tag{3.56}$$

which, using $(1+i)/(1-i) = i$, can be cast in the form

$$S \simeq i\,\frac{\omega-\omega_N+i\frac{1}{4\eta^2\alpha}}{\omega-\omega_N-i\frac{1}{4\eta^2\alpha}}\,. \tag{3.57}$$

This result takes the form (3.47). Hence the discrete spectrum of resonance frequencies ω_N is selected by condition (3.54). Further, comparing (3.47) with (3.57), one has that the growth or damping timescale is given by

$$\tau = 4\eta^2\alpha\,. \tag{3.58}$$

Now, α defined in (3.55) is always positive since as Σ_ψ increases so does T and γ defined in (3.51) (the area of the region in between the Σ_ψ line and the V_+ curve, and in between Σ_ψ line and the V_- curve both increase when Σ_ψ increases). So, we are guaranteed to have a positive τ and thus the negative Σ_ψ modes are unstable. If we redo the computations to consider the $\Sigma_\psi > 0$ case, the only difference is that in (3.49) the ingoing and outgoing waves are given instead by the terms proportional to C_7 and C_6, respectively. This changes the scattering amplitude from S to S^{-1} and thus τ to $-\tau$ implying that the positive Σ_ψ modes are damped.

Though the resonance frequencies and growth timescales can be computed with numerical methods from (3.54) and (3.58), we can still make some further progress analytically by approximating the well of V_+ by a parabola. Near the well, the potential V_+ behaves generally as

$$V_+ \simeq \frac{(x-x_{\rm m})^2}{P_{\rm m}} + a_{\rm m}\,, \tag{3.59}$$

with $a_{\rm m} < 0$. The boundaries x_0 and x_1 are the roots of $\Sigma_\psi - V_+$, namely: $x_0 = x_{\rm m} - [P_{\rm m}(\Sigma_\psi - a_{\rm m})]^{1/2}$ and $x_1 = x_{\rm m} + [P_{\rm m}(\Sigma_\psi - a_{\rm m})]^{1/2}$. Since $\sqrt{T}$ vanishes at these boundaries one has

$$\alpha = \int_{x_0}^{x_1} \frac{d\sqrt{T}}{d\Sigma_\psi}\,dx\,. \tag{3.60}$$

Moreover, near the bottom of the well, only $\Sigma_\psi - V_+$ varies significantly with x, and we can assume that all the other quantities that appear in the integral of α are approximately constants given by their value at $x = x_{\rm m}$ (the accuracy of this assumption increases as Σ_ψ approaches

$a_{\rm m}$). One then has

$$\alpha \simeq \frac{\Sigma_\psi + \frac{\varrho m x_{\rm m}}{\mathcal{P}(x_{\rm m})}}{\sqrt{\Sigma_\psi - V_-(x_{\rm m})}} \frac{\sqrt{\mathcal{P}(x_{\rm m})}}{2x_{\rm m}(1+x_{\rm m})} \int_{x_0}^{x_1} \left[\Sigma_\psi - V_+\right]^{-\frac{1}{2}} \, dx \,, \tag{3.61}$$

with V_+ given by (3.59), which yields for α the value

$$\alpha = \pi\sqrt{P_{\rm m}} \left[\Sigma_\psi + \frac{\varrho m x_{\rm m}}{\mathcal{P}(x_{\rm m})}\right] \left[\Sigma_\psi - V_-(x_{\rm m})\right]^{-1/2} \frac{\sqrt{\mathcal{P}(x_{\rm m})}}{2x_{\rm m}(1+x_{\rm m})} \,. \tag{3.62}$$

Let us illustrate the use of the WKB method we have described in this section to compute the instability parameters in a particular configuration. Take,

$$m \;\; = \;\; 14\,;\;\; n = 10\,;\;\; a_1 = 32\,;\;\; c_1 = 5\,;\;\; c_p = 5\,; \tag{3.63}$$

$$\lambda = m_\phi = 0\,;\;\; l = m_\psi = 10\,. \tag{3.64}$$

By approximating the well in V_+ by a parabola, as in (3.59), we get

$$a_{\rm m} = -0.17894\,;\;\; x_{\rm m} = 9.1537\,;\;\; P_{\rm m} = 2759.4\,. \tag{3.65}$$

The resonant frequencies are those that satisfy condition (3.54) with $\gamma(\omega)$ given by (3.51). For the fundamental harmonic ($N = 0$), we get

$$\Sigma_\psi = -0.173\,. \tag{3.66}$$

The growth timescale of the instability is given by (3.58) with $\eta(\omega_N)$ given by (3.52). Again, for $N = 0$ we get

$$\tau \sim 10^{47}\,. \tag{3.67}$$

Independently of the details of the geometry, we note that as m_ψ grows, Σ_ψ approaches $a_{\rm m}$, the value of the V_+ at its minimum. For the particular geometry parameters described in (3.63) we have (for $\lambda = m_\phi = 0$):

$$\begin{aligned} m_\psi &= 10: \;\; \Sigma_\psi = -0.173\,, \\ m_\psi &= 20: \;\; \Sigma_\psi = -0.176\,, \\ m_\psi &= 40: \;\; \Sigma_\psi = -0.177\,. \end{aligned} \tag{3.68}$$

This feature can be proven analytically, as was done in [164].

Let us verify consistency of our results. We have assumed that $a_i^2\frac{\omega^2-\lambda^2}{R^2} \ll 1$ in order to make the approximation $\Lambda \simeq l(l+2)$. Now, for the cases listed above one has $a_i^2\frac{\omega^2-\lambda^2}{R^2} \sim 10^{-2}$, which is inside the range of validity for the approximation of the angular eigenvalue.

To conclude this section, we consider the regime of validity of the WKB approximation in more detail. A standard analysis of eq. (3.31) suggests the WKB approximation is valid for $|\partial_x U_{\rm eff}| \ll |U_{\rm eff}|^2$, which can be rewritten as $|\partial_x T/T^2(x)| \ll m_\psi^2$. So, for large m_ψ, the WKB approximation seems to be valid quite generally. However, we must sound a note of caution. As we already remarked, eq. (3.68) shows that as m_ψ grows, Σ_ψ approaches $a_{\rm m}$, the value of the V_+ at its minimum — this can be proved analytically [164]. So when m_ψ becomes very large, the two turning points are very close and the WKB analysis breaks down because $T(x) \to 0$. So we conclude that the WKB approximation used in this section should be valid in a regime with large m_ψ, but not exceedingly large. In any event, it is clear that the instability is strongest for small values of m_ψ, when the WKB analysis is certainly not valid. So, in the next two sections we will compute the features of the instability using complementary methods valid for small values of m_ψ.

3.4 Matched asymptotic expansion analysis

The WKB analysis described in the last section appears to be strongest when describing solutions for which $\kappa^{-1} \sim \zeta, \xi$, but in general this corresponds to solutions with high angular momentum. In the sense that the timescale of the instability due to these modes is largest, they are the least unstable. Conversely, the matched asymptotic expansion that we use in this section becomes valid when $\kappa^{-1} > \zeta, \xi$, they are the dominant decay modes. As an additional bonus, the eigenvalues are determined explicitly through algebraic constraints. Having both approximations at our disposal allows us to accurately calculate the eigenvalues for most of the allowed parameters.

We follow a matching procedure introduced in [177–179], which has previously been used for studying scalar fields in three-charge geometries by Giusto, Mathur and Saxena [86–89], in the JMaRT backgrounds [94] and also in [160, 168–170, 180]. The space is divided into two parts: a near-region, $x \ll \beta$, and a far-region, $x \gg \alpha$, such that $\alpha \ll \beta$. The radial equation is then solved approximately and the appropriate boundary conditions applied in each of the two regions. Finally, we match the near-region and the far-region solutions in the area for which they are both valid, $\alpha \ll r \ll \beta$. This gives a set of constraints, the solution of which gives the eigenvalues. Performing this analysis for the radial equation (3.19), we shall see that the only solutions which are regular at the origin and purely outgoing at infinity are finite as $x \to \infty$, and lead to instabilities. Except when otherwise stated, the analysis in this section will hold for general values of m_ψ, m_ϕ and λ.

3.4.1 The near region solution

In the near-region, $\kappa^2 x \ll |1-\nu^2|$, one can neglect the $\kappa^2 x$ term, and the radial equation (3.19) is approximated by

$$x(1+x)\partial_x^2 h + (1+2x)\partial_x h + \frac{1}{4}\left[1-\nu^2+\frac{\xi^2}{x+1}-\frac{\zeta^2}{x}\right] h = 0\,. \tag{3.69}$$

With the definition $h = x^{|\zeta|/2}(1+x)^{\xi/2}\, w$, the near-region radial equation becomes a standard hypergeometric equation [181] of the form

$$x(1+x)\partial_x^2 w + [c+(a+b+1)x]\partial_x w + ab\, w = 0, \tag{3.70}$$

where

$$a = \frac{1}{2}\left(1+|\zeta|+\xi+\nu\right)\,, \qquad b = \frac{1}{2}\left(1+|\zeta|+\xi-\nu\right)\,, \qquad c = 1+|\zeta|\,. \tag{3.71}$$

The solution to the above in terms of hypergeometric functions allows us finally to write the solution of the radial equation in the near region as

$$\begin{aligned} h &= A\, x^{|\zeta|/2}(1+x)^{\xi/2} F(a,b,c,-x) \\ &\quad + B\, x^{-|\zeta|/2}(1+x)^{\xi/2} F(a-c+1, b-c+1, 2-c, -x)\,. \end{aligned} \tag{3.72}$$

At this point we impose the first boundary condition: the solution must be regular at $x=0$ since the geometry is smooth at the origin of the “core”. The term proportional to $x^{-|\zeta|/2}$ diverges at $x=0$, and must be discarded, *i.e.*, its coefficient, B, is set to zero.

To perform the matching we need to know the large x behavior behavior of the regular near-region solution. To this end, one uses the $x \to 1/x$ transformation law for the hypergeometric function [181]

$$\begin{aligned} F(a,b,c,-x) &= \frac{\Gamma(c)\Gamma(b-a)}{\Gamma(b)\Gamma(c-a)}\, x^{-a}\, F(a,1{-}c{+}a,1{-}b{+}a,-1/x) \\ &\quad + \frac{\Gamma(c)\Gamma(a-b)}{\Gamma(a)\Gamma(c-b)}\, x^{-b}\, F(b,1{-}c{+}b,1{-}a{+}b,-1/x)\,, \end{aligned} \tag{3.73}$$

and the property $F(a,b,c,0) = 1$. Note that this expression for the transformation is only valid when $a - b = \nu$ is non-integer. This is an assumption we will continue to make throughout this section. In the end, we shall derive a condition determining the allowed eigenvalues that will not be dependent upon this assumption and therefore we may extend our results to integer values of ν by continuity.

The large x behavior of the near-region solution is then given by

$$\begin{aligned} h \sim A\,\Gamma(1+|\zeta|)\Bigg[&\frac{\Gamma(-\nu)}{\Gamma\left[\frac{1}{2}(1+|\zeta|+\xi-\nu)\right]\Gamma\left[\frac{1}{2}(1+|\zeta|-\xi-\nu)\right]}\, x^{-\frac{\nu+1}{2}} \\ &+ \frac{\Gamma(\nu)}{\Gamma\left[\frac{1}{2}(1+|\zeta|+\xi+\nu)\right]\Gamma\left[\frac{1}{2}(1+|\zeta|-\xi+\nu)\right]}\, x^{\frac{\nu-1}{2}}\Bigg]. \end{aligned} \tag{3.74}$$

3.4.2 The far region solution

In the far-region, $\kappa x^2 \gg \max\{\xi^2-1, \zeta^2\}$, the terms $\xi^2/(x+1)$ and ζ^2/x can be neglected, and the radial equation becomes

$$\partial_x^2(xh) + \left[\frac{\kappa^2}{4x} - \frac{\nu^2-1}{4x^2}\right](xh) = 0\,. \tag{3.75}$$

The most general solution of this equation when ν is non-integer is a linear combination of Bessel functions of the first kind [181],

$$h = x^{-1/2}\left[C J_\nu(\kappa\sqrt{x}) + D J_{-\nu}(\kappa\sqrt{x})\right]\,. \tag{3.76}$$

This form does not lend itself easily to application of the boundary conditions. Instead, for large $\kappa\sqrt{x}$, the solution may be expanded as [181]

$$h \sim \frac{x^{-3/4}}{\sqrt{2\pi\kappa}}\left[e^{i\kappa\sqrt{x}}e^{-i\frac{\pi}{4}}\left(Ce^{-i\frac{\pi\nu}{2}}+De^{i\frac{\pi\nu}{2}}\right)+e^{-i\kappa\sqrt{x}}e^{i\frac{\pi}{4}}\left(Ce^{i\frac{\pi\nu}{2}}+De^{-i\frac{\pi\nu}{2}}\right)\right]. \tag{3.77}$$

As in the WKB analysis, we assume that the real part of ω is negative, and therefore the positive and negative sign exponentials give, respectively, ingoing and outgoing waves. We require that there be purely outgoing waves at infinity and so impose the constraint that the coefficient of the positive exponential vanishes, yielding

$$C = -De^{i\pi\nu}. \tag{3.78}$$

When ω becomes complex, so too does κ. Since the sign of the real part of ω is negative, the definition of κ (3.20) implies that its imaginary part has a sign opposite that of the imaginary part of ω. Therefore, requiring additionally that the solution be finite as $x \to \infty$ implies that the imaginary part of ω must be positive. This is precisely the sign for the imaginary part of the frequency that leads to instabilities. Thus we see that simply requiring the solutions with complex frequency be finite at infinity automatically guarantees they lead to instabilities.

Now, to do the matching in the overlapping region, we will need to know how the far-region solution behaves for small values of x. More specifically, for small $\kappa\sqrt{x}$, and considering only the dominant terms, the solution behaves as [181]

$$h \sim D\left[\frac{(2/\kappa)^{-\nu}}{\Gamma(1+\nu)}\,x^{\frac{\nu-1}{2}} - e^{i\pi\nu}\frac{(2/\kappa)^{\nu}}{\Gamma(1-\nu)}\,x^{-\frac{\nu+1}{2}}\right]. \tag{3.79}$$

3.4.3 Matching the solutions

We will now determine the frequencies that can appear when the geometry is perturbed by a scalar field. The frequency spectrum is not arbitrary: only those values that satisfy the matching conditions between the near-region and the far-region are allowed. We shall see that there are two solutions of the matching equations, yet only one will lead to instabilities.

Matching the powers of x between the near (3.74) and far-region solutions (3.79), and taking a ratio to eliminate the amplitudes A and D, yields

$$-e^{i\pi\nu}(\kappa/2)^{2\nu}\frac{\Gamma(1-\nu)}{\Gamma(1+\nu)}=\frac{\Gamma(\nu)}{\Gamma(-\nu)}\frac{\Gamma(\frac{1}{2}(1-\nu+|\zeta|+\xi))}{\Gamma(\frac{1}{2}(1+\nu+|\zeta|+\xi))}\frac{\Gamma(\frac{1}{2}(1-\nu+|\zeta|-\xi))}{\Gamma(\frac{1}{2}(1+\nu+|\zeta|-\xi))}\,. \tag{3.80}$$

The problem of finding the outgoing modes thus boils down to solving the single transcendental equation (3.80); we will do so by iteration. Note that the κ dependence on the left hand side means that it is suppressed. For the equation to hold, a similar suppression must also occur on the right hand side. This is only possible if one of the gamma functions in the denominator of the right side is large. Since the gamma function diverges when its argument is a non-positive integer, we take as a first iteration the choice

$$\nu+|\zeta|-\xi=-(2N+1)\,, \tag{3.81}$$

where the non-negative integer N will again be referred to as the harmonic. Note that we could also have chosen the above relation, but with the opposite sign for ξ. While this does indeed lead to a solution, one finds that the imaginary part of the frequency is always negative, *i.e.*, the modes are exponentially damped in time.

This first estimate is obviously not the end of the story as it would cause the right side to completely vanish. To go beyond this approximation, we rewrite eq. (3.80) in terms of N, then perturb $N\rightarrow N+\delta N$, where $\delta N\ll N$. This deformation appears at leading order only for the Γ function in the denominator on the right hand side that diverges, it may be neglected in all other factors. More concretely, to extract δN from the Γ function we use $\Gamma(z)\Gamma(1-z)=\pi/\sin(\pi z)$, and sine function identities to obtain the expansion

$$\Gamma(-N-\delta N)\approx-\left[(-1)^N N!\,\delta N\right]^{-1}. \tag{3.82}$$

Substituting this into (3.80), and using a number of Γ function identities, we solve for the imaginary part of the first correction

$$\mathcal{I}m(\delta N)=\pi\frac{(\kappa/2)^{2\nu}}{\Gamma^2(\nu)}[\nu]_N\,[\nu]_{N+|\zeta|}\,, \tag{3.83}$$

where $[a]_n=\prod_{i=1}^{n}(1+a/i)$. Since N is $\mathcal{O}(1)$ and $\delta N\sim\kappa^{2\nu}$, we see that we may stop after the first iteration. As a function of ν, this can have a single maximum near $\nu\sim\kappa$. In general we will have $\kappa \ll 1$ and $\nu \sim 1 + l$, so we will always be in a region where this is a monotonically decreasing function of ν. For fixed ν, the last two factors make this an increasing function of N and $|\zeta|$, but the general behavior will be dominated by the effects of changing ν.

The equation (3.81) uniquely determining ω can be exactly solved

$$(\varepsilon + \varrho^2)\,\omega = -\left(\lambda\frac{s_p c_p M}{R^2} + \varrho c\right) + \sqrt{\left(\lambda\frac{s_p c_p M}{R^2} + \varrho c\right)^2 - (\varepsilon + \varrho^2)(c^2 - \nu_0^2)}\ , \qquad (3.84)$$

where

$$\varepsilon \equiv \frac{1}{R^2}(r_+^2 + M(s_1^2 + s_5^2 + c_p^2))\ , \qquad c \equiv \xi_0 - |\zeta| - (2N+1)\ , \qquad (3.85)$$

and a variable with a subscripted 0 means we have set $\omega = 0$. Note that as long as $m \geq n+2$, one can show — see Section 3.7.3 — that $\varepsilon/\varrho^2 \ll 1$ and both quantities are positive. When $m \to n+1$, though, $\varepsilon \to -\infty$ (since $M \to 0$, $r_+^2 \to -\infty$ and R^2 stays finite), ensuring that there can be no instability for the supersymmetric solutions. This extends to arbitrary modes the conclusion from the discussion associated to equation (3.43) for modes with $m_\phi = \lambda = 0$.

When evaluated on a solution, ν is given by $\nu = \omega\varrho + c$. Since we are interested in solutions for which ω is negative, this means $c > 0$. Then, requiring that ω be negative and real, gives three more conditions. The first ensures that the result is real while the second requires that the first term of (3.84) is negative. Finally, the condition that appears to be the most difficult to satisfy ensures the contribution from the square root does not make the total result positive, *i.e.*,

$$c^2 - \nu_0^2 > 0\ . \qquad (3.86)$$

When $\lambda \neq 0$, these conditions must also be supplemented by the requirement that $\omega^2 - \lambda^2 > 0$, which ensures the asymptotic behavior of the solution is correct. With these satisfied, we may determine the effect of the correction.

The imaginary contribution to N is taken as resulting from a small imaginary correction to

ω. Then, the two are related through

$$\begin{aligned} \delta N &= \frac{\delta\omega}{2}\frac{d}{d\omega}(\xi-\omega)\Big|_N \\ &= \frac{\delta\omega}{2\nu}\left[(\varrho^2+\varepsilon)\omega+(\lambda s_p c_p M/R^2+\varrho c)\right] \\ &= \frac{\delta\omega}{2\nu}\sqrt{\left(\lambda\frac{s_p c_p M}{R^2}+\varrho c\right)^2-(\varepsilon+\varrho^2)(c^2-\nu_0^2)}\,. \end{aligned} \tag{3.87}$$

In the final line we have used the solution (3.84) to show that the sign of δN determines the sign of the correction to ω. Since $\mathcal{I}m(\delta N)$ is always positive when evaluated on the solution of (3.81), the corresponding imaginary part of ω is positive.

To summarize, whenever the constraints, in particular (3.86), are satisfied there is a corresponding outgoing mode of the scalar field equation. Further, the imaginary part of the frequency of this mode is guaranteed to be positive, indicating that it leads to an instability. The timescale for the instability generated by the mode is a monotonically increasing function of ν, which is given by

$$\begin{aligned} (\varepsilon+\varrho^2)\,\nu &= \varepsilon c-\lambda\varrho s_p c_p\frac{M}{R^2} \\ &\quad+\sqrt{\left(\varepsilon c-\lambda\varrho s_p c_p\frac{M}{R^2}\right)^2+(\varepsilon+\varrho^2)(2c\varrho\lambda s_p c_p\frac{M}{R^2}+\nu_0^2\varrho^2-\varepsilon c^2)}\,. \end{aligned} \tag{3.88}$$

A similar argument, based on the solution of equation (3.81), but with the opposite sign for ξ would lead to a set of outgoing modes with an amplitude that decays in time.

As an example, consider the particular background geometry and scalar field solution described by

$$\begin{aligned} m &= 5\,;\ n=1\,;\ a_1=19.1\,;\ c_1=5\,;\ c_p=1.05\,; \\ &\quad \lambda=m_\phi=0\,;\ l=m_\psi=2\,. \end{aligned} \tag{3.89}$$

The first two iterations with $N=0$ gives

$$\begin{aligned} \omega &= -2.8717\,, \\ \tau^{-1}=\mathcal{I}m(\delta\omega) &= 4.42\times10^{-11}\,, \end{aligned} \tag{3.90}$$

The results obtained here are consistent with the WKB analysis of the last section, *i.e.*, there are outgoing modes that rotate in the same sense as the background geometry whose amplitude grows exponentially in time. What we have gained is an explicit set of relations that allows the unstable mode frequencies to be calculated. In particular, one can now make definite statements about the relative timescales for unstable modes just by looking at equation (3.88). We leave the precise details of this to Section 3.7.3 and just give the results here. The most unstable modes are those which minimize ν. Since $\varepsilon \ll \varrho^2$ this generally means that the modes which maximize c or minimize ν_0 will be the most unstable. In general this means we should consider the lowest possible l for which the constraints can be satisfied when setting $m_\psi = l$, $m_\phi = 0$ and $N = 0$.

A second benefit of this analysis is an improvement in accuracy for the most unstable modes. For comparison, performing the WKB analysis and not neglecting any terms in the potentials or approximating the bottom of the well with a parabola gives $\omega = -3.129 + 4.00 \times 10^{-10} i$. From the full numerical solution, which we discuss next, we have $\omega = 2.8718 + 4.46 \times 10^{-11} i$. For values of ω in this range we have $\kappa^{-2} \sim 1900$, so we are well within the regime for which we may trust this solution. As κ^{-1} approaches $\max(|\zeta|, \xi)$, this analysis begins to break down, but it appears that the WKB approach becomes increasingly accurate. In the next section we will present a more detailed list of eigenvalues corresponding to instabilities and discuss the results.

3.5 Numerical results

We will now solve the radial equation (3.19) numerically to extract the instability. We begin with a description of the numerical algorithm. The only approximation used in this section concerns the angular eigenvalue, Λ, which we assume to be well described by (3.22). At the end of the calculation we always make sure the result is in the regime of validity of this approximation. Note, however, solutions can still be found even if outside this range. The easiest way to do this is by treating the eigenvalue problems for Λ and ω separately. The coupled system may then be solved by first assuming the approximation to hold and solving the radial equation for ω, this is then fed into the angular equation which is solved to obtain an improved value of Λ. This process may be iterated until the desired level of convergence is achieved. We shall give an example of this process in Section 3.7.2.

3.5.1 Numerical procedure

The method of finding solutions of the radial equation numerically is very much like performing the matched expansions. We use eqs. (3.72) and (3.76) to fix the initial conditions for two integrations of the exact radial equation. Since the equation of motion is linear, we may immediately match the two solutions at a point in the interior region by rescaling. This leaves two more conditions to be satisfied, those matching the derivative of the real and imaginary parts. Fixing all other parameters, we vary the real and imaginary parts of ω to satisfy these conditions.

Given the small size of the expected imaginary part, it is most straightforward to use a package like Mathematica [182], with its software based arbitrary precision, to perform the calculations. Solving the matching conditions can be done by treating the difference in derivatives at the interior point as a complex valued function of ω. A root may then be searched for using the built-in function `FindRoot` which, for a function without explicit derivatives, looks for the solution by constructing secants for the equations being solved.

Since the imaginary part is expected to be far smaller than the real, gradients of the matching function in the imaginary ω direction will be large only when very near a solution, but negligible elsewhere. The initial guesses at the solution are therefore very important for ensuring that iterations of the root finding procedure converge to a solution. It was found empirically that solutions could consistently be found by choosing to start the search in a region around the real value of ω for which the inner solution vanishes at the matching point. Small changes in the imaginary part of ω near this point appear to be sufficient to bring about convergence. In Figure 3.2 we show an example solution obtained in this manner. The solid line is the full numeric solution, composed on either side of the dot by the integrations which start at large and small x. The dashed lines are the near (3.72) and far (3.76) approximations used to set the initial conditions for integrating the exact radial equation. The fact that the imaginary part of

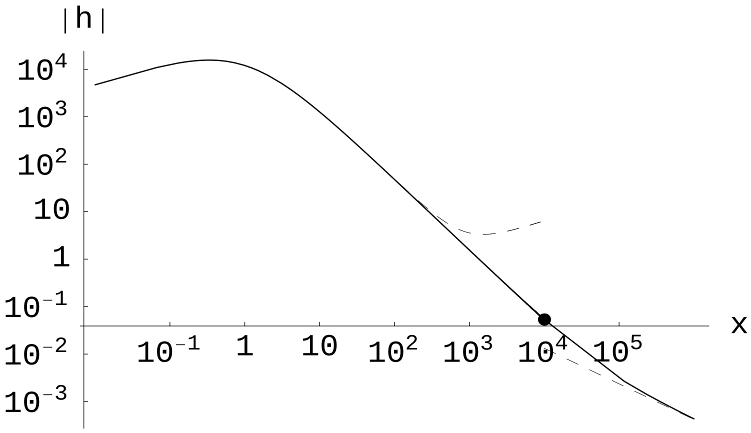

Figure 3.2: An example of an unstable mode of the scalar field showing vanishing as both $x \to 0$ and $x \to \infty$.

ω is in general very small raises non-trivial problems related to the number of digits of precision used and the exact way in which boundary conditions are applied. A discussion of these aspects is deferred to the supplementary material in Section 3.7.2.

3.5.2 Numerical results

Our numerical results are summarized in Figure 3.3 and Table 3.1. In Figure 3.3 on the left we present the numerical solutions obtained for

$$m = 5\,,\ n = 1\,,\ c_1 = 1.1\,,\ c_5 = 1.52\,,\ a_1 = 262.7\,,\ \lambda = m_\phi = 0\,. \tag{3.91}$$

We consider only the lowest harmonic, $N = 0$, but vary $l = m_\psi$. At $l = 1$, $\kappa^{-1} \sim 40$, indicating the matched solution is valid. As l grows so do ξ, ζ while κ^{-1} shrinks, meaning the approximation should soon break down. At $l = 5$, $\kappa^{-2} \sim 10$ and the approximation is becoming no longer valid. Finally, when $l = 13$, $\kappa^{-2} \sim 1$ and differences between the matched and numerically determined eigenvalues are starting to become apparent. In Figure 3.3 on the right, we use the same parameters as before, but now fix $l = m_\psi = 4$ and vary the harmonic from $N = 0$ up to 4. Increasing N leads to smaller values of ω and therefore smaller values of κ, so that the matched solutions are valid throughout. It should also be noted that if the approximation $a_1^2\omega^2/R^2 \ll m_\psi^2$ is valid for a given m_ψ, then it should be valid for all m_ψ. This is because ω scales with m_ψ, as we observed within the WKB approximation.

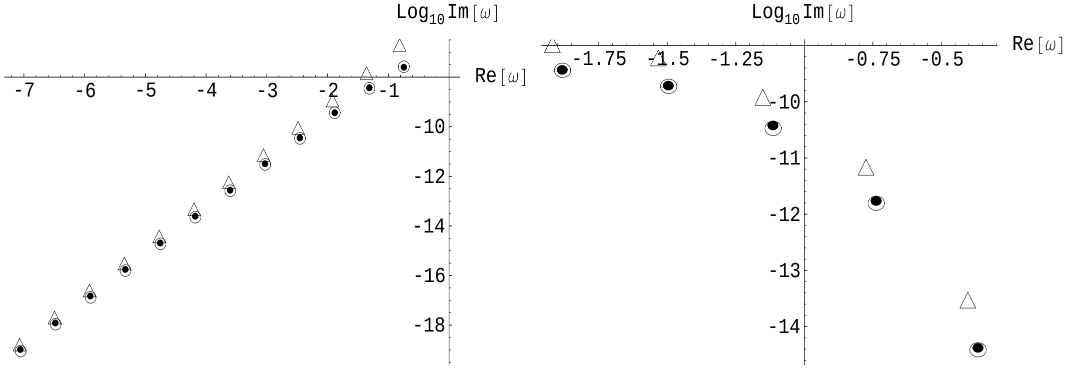

Figure 3.3: On the left we choose the lowest harmonic and vary $l = m_\psi$ from 2 to 13 from upper right to lower left. The solid circles represent the numeric solutions, while the triangles are the results of the WKB analysis and the unfilled circles correspond to the matched expansion. On the right we fix $l = m_\psi = 4$, and vary the harmonic from 0 to 4 from upper left to lower right.

In Table 3.1 we present and compare the numerical results with those obtained through the approximate analytical approaches. The values labeled as WKB stand for values obtained using the WKB approximation, formulae (3.51), (3.52), (3.54) and (3.58), and the parabolic approximation for the potential (3.59)-(3.62).

Notice first that all the different approaches yield very similar results: they are all rather accurate in their own regime of validity. As predicted by the analytic approaches, and verified numerically, the real part of the frequency scales with m_ψ, whereas the logarithm of the imaginary part scales with m_ψ, *e.g.,* see eq. (3.52). Thus the instability timescale increases rapidly as a function of m_ψ.

m_ψ	Numeric	WKB	Matching
1	$-0.184 + 3.83 \times 10^{-8} i$	$-$	$-0.184 + 3.83 \times 10^{-8} i$
2	$-0.744 + 2.51 \times 10^{-8} i$	$-0.826 + 1.89 \times 10^{-7} i$	$-0.744 + 2.64 \times 10^{-8} i$
3	$-1.312 + 3.73 \times 10^{-9} i$	$-1.371 + 1.48 \times 10^{-8} i$	$-1.312 + 3.53 \times 10^{-9} i$
4	$-1.883 + 3.69 \times 10^{-10} i$	$-1.932 + 1.17 \times 10^{-9} i$	$-1.882 + 3.63 \times 10^{-10} i$
5	$-2.456 + 3.55 \times 10^{-11} i$	$-2.499 + 9.39 \times 10^{-11} i$	$-2.454 + 3.39 \times 10^{-11} i$
6	$-3.030 + 3.22 \times 10^{-12} i$	$-3.072 + 7.62 \times 10^{-12} i$	$-3.028 + 3.02 \times 10^{-12} i$
7	$-3.605 + 2.77 \times 10^{-13} i$	$-3.647 + 6.23 \times 10^{-13} i$	$-3.602 + 2.63 \times 10^{-13} i$
8	$-4.180 + 2.47 \times 10^{-14} i$	$-4.216 + 4.88 \times 10^{-14} i$	$-4.176 + 2.24 \times 10^{-14} i$
9	$-4.755 + 2.05 \times 10^{-15} i$	$-4.794 + 4.03 \times 10^{-15} i$	$-4.751 + 1.89 \times 10^{-15} i$
10	$-5.331 + 1.76 \times 10^{-16} i$	$-5.369 + 3.26 \times 10^{-16} i$	$-5.326 + 1.58 \times 10^{-16} i$
11	$-5.907 + 1.49 \times 10^{-17} i$	$-5.947 + 2.65 \times 10^{-17} i$	$-5.902 + 1.32 \times 10^{-17} i$
12	$-6.483 + 1.22 \times 10^{-18} i$	$-6.516 + 2.07 \times 10^{-18} i$	$-6.477 + 1.09 \times 10^{-18} i$
13	$-7.059 + 1.04 \times 10^{-19} i$	$-7.102 + 1.81 \times 10^{-19} i$	$-7.053 + 8.97 \times 10^{-20} i$

Table 3.1: Some numerical values of the instability for the geometry described by (3.91), and $l = m_\psi$. In the second column, we have the results of the full numerical analysis. In the third column, labeled as WKB, the values obtained from the WKB analysis, are given. In the final column, we present the results of the matching procedure (3.81),(3.83). Notice the close agreement between all the different methods. For $m_\psi = l = 1$ and for these particular values of the parameters, the WKB analysis breaks down. Indeed, for $m_\psi = 1$, the potential V_+ has no minimum.

3.6 Discussion

In this chapter, we have shown that the nonsupersymmetric JMaRT solitons [94] are classically unstable. The relevant instabilities are quite generic to space-times which have an ergoregion but are horizon-free [163]. However, as noted in Section 3.1.2, the general proof does not strictly apply to the JMaRT solutions since the latter support nonradiative negative energy modes as shown in Section 3.7.4. Hence we have explicitly shown that the ergoregion instabilities are active in the JMaRT geometries using three different approaches, which in the end show a remarkable agreement — see Figure 3.3 and Table 3.1. Perhaps the most physically intuitive method is the WKB analysis carried on in Sec. 3.3. This approach allows us to clearly identify the nature and physical properties of the instability. However, this analysis is only expected to be valid for large angular momentum quantum numbers, *i.e.*, $m_\psi \gg 0$, which is not where the instability is strongest. The more unstable modes were studied using the matched asymptotic expansion method [177–179] in Sec. 3.4. As a final consistency check of these analytical results, we made a numerical analysis of the wave equation in Sec. 3.5.

In passing we note by considering orbifolds, the JMaRT solutions were extended to a six-parameter family which includes a third integer k characterizing the orbifold group $\mathbb{Z}_k$ [94]. Of course, it is straightforward to adapt our instability analysis so that the modes respect this orbifold symmetry in the covering space and so one concludes that the ergoregion instability arises in these orbifold geometries as well.

Let us now summarize some of the features of the ergoregion instability found for the JMaRT solutions:

(i) The general shape of the WKB potentials $V_\pm$ are sketched in Figure 3.1 for the case in which an instability is present. The key point is that when the ergoregion is present the bottom of the potential well in V_+ reaches negative values. The unstable modes are those whose pattern speed Σ_ψ is negative and approaches the minimum of V_+ from above (see Figure 3.1). Thus they are nearly bound states of the potential well in V_+ that can however tunnel out to infinity through V_-.

(ii) The fact that the unstable modes are those with negative phase velocity, $\Sigma_\psi < 0$, has a clear physical interpretation. As in the discussion of eqs. (3.35) and (3.36), modes with $\Sigma_\psi < 0$ are those that propagate in the same sense as geometry's rotation Ω_ψ. Therefore at infinity these modes carry positive angular momentum (same sense as Ω_ψ), as well as positive energy. Hence by conservation of energy and angular momentum, with the onset of the ergoregion instability, the JMaRT solutions are shedding both energy and angular momentum by an amount that increases exponentially.

(iii) The instability can be quite strong, depending on the particular combination of parameters that define the geometry. More importantly, the instability is robust, in the sense that it exists for a wide range of parameters.

(iv) With $m = n + 1$, the JMaRT solutions are supersymmetric and so must be stable. It is a consistency check of our analysis then that we find no instability in this case. As commented in Section 3.3, when $m = n + 1$ the potential V_+, as given by eq. (3.43), is always positive. Hence there are no negative Σ_ψ modes which could intersect the potential well of V_+ and the SUSY geometry is stable as required.

In our analysis, we have focused on the special case $\lambda = 0$ and $m_\phi = 0$, to simplify the relevant equations. In fact, the ergoregion instability persists when either or both of these parameters are nonvanishing. A discussion of the general situation is given in Section 3.7.3. The result is most simply understood from the point of view of the WKB approach. Then all of the additional contributions to the effective potential (3.32) introduced by a nonvanishing m_ϕ or λ are suppressed by inverse powers of m_ψ and so can certainly be neglected in the limit of large m_ψ. One can further check that the instability exists over some range even when m_ψ does not dominate the other two. One distinguishing feature of $\lambda \neq 0$ is that asymptotically the scalar modes have an effective mass in five dimensions. In our analysis, this is reflected in the fact that asymptotically $V_\pm \to \pm|\lambda/m_\psi|$ and so there is an additional barrier for the modes to tunnel out to infinity. However, for sufficiently large m_ψ, such tunnelling is possible. One other interesting point about the large m_ψ regime is that unstable modes appear with either sign of m_ϕ and λ. Hence, while the modes on which we have focused lead to an instability 'powered' by J_ψ resulting in its decrease, there are unstable modes which may at the same time increase $|J_\phi|$ and/or P.

Adding a mass for the scalar field modifies the potentials $V_\pm$ in essentially the same way as having nonvanishing λ. Hence we expect the ergoregion instability will even appear for massive fields, at least in modes with sufficiently large angular momentum. As described in Section 3.1.2, the arguments given by Friedmann [163] are quite general and so we expect the ergoregion instability to appear for higher spin fields as well. In particular, we expect the fields of the low energy type IIB supergravity will generically experience this instability. Having said that the ergoregion instability is robust, we must also add that it can be suppressed in certain parameter regions. In particular, one finds that the instability timescale becomes extremely long in the regime where Q_1 and Q_5 are much larger than the other scales. Further, we add that in the decoupling limit where one isolates an asymptotically AdS$_3$ core [94], the ergoregion instability is absent. The simplest way to understand this result is that the AdS$_3$ core has a globally timelike Killing vector [94] and so there is a 'rotating' frame where we can define all energies to be positive. One can also explicitly verify the absence of an ergoregion instability in the core solutions by directly applying the analysis used in this chapter to those backgrounds.

The JMaRT geometries (both supersymmetric and nonsupersymmetric) also have damped modes, *i.e.*, modes (3.15) for which the imaginary part of ω is negative. As per the WKB analysis, these are modes with positive Σ_ψ below the local maximum of V_+ that tunnel out to infinity through V_+ — see Figure 3.4.

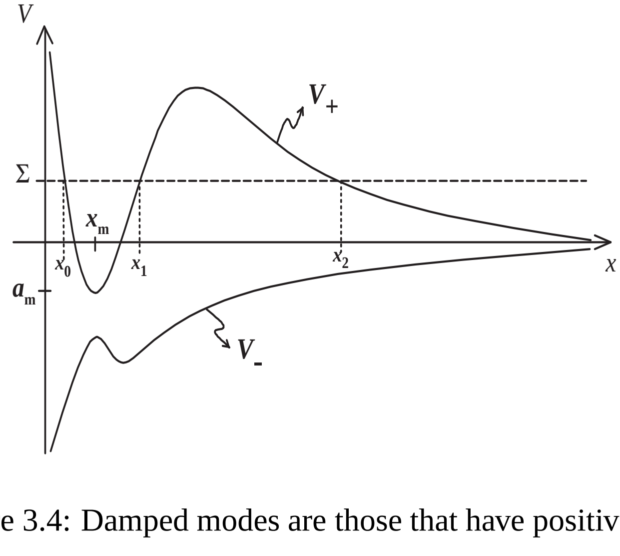

Figure 3.4: Damped modes are those that have positive Σ_ψ.

As emphasized previously, we can also find purely bound states (*i.e.*, nonradiative modes) with $\kappa^2 \propto \omega^2 - \lambda^2 < 0$. With some fine-tuning, it may also be possible to find geometries which support bound states with $\kappa = 0$. These nonradiative modes are described in the supplementary material. The typical situation for such modes is sketched in Figure 3.5. As already noted above when $\lambda \neq 0$, asymptotically $V_\pm \to \pm|\lambda|/m_\psi$ and so there is a finite potential barrier at infinity. If this barrier is sufficiently large relative to $\Sigma_\psi = \omega/m_\psi$, bound states can arise. These bound states can also be negative energy states, as can be seen with the energy integral (3.7). The absence of such negative energy modes which do not radiate at infinity was central to Friedman's general argument for the ergoregion instability. In [163], he did not find any such nonradiative modes because he only considered the massless fields for which there is no potential barrier at infinity. Note, however that the current situation is more complicated because the KK momentum of the background, as well as the angular momenta, contribute to the presence of the ergoregion.

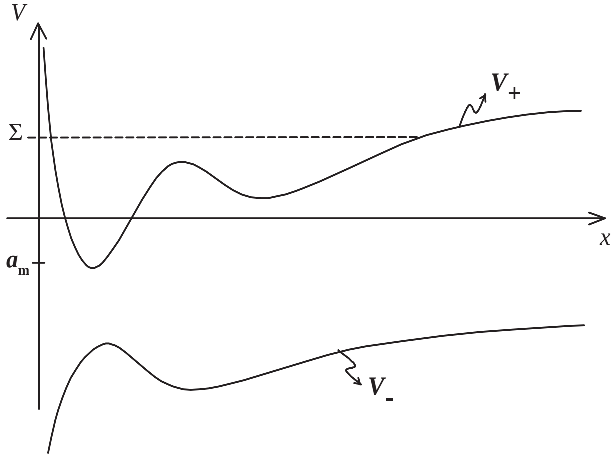

Figure 3.5: Qualitative shape of the potentials V_+ and V_- when $\omega^2 - \lambda^2 < 0$. These are the purely bound states that are discussed in Section 3.7.4.

The appearance of negative energy states in the presence of an ergoregion can be anticipated from a geodesic analysis [164]. By definition, the Killing vector t^a, which generates asymptotic time translations, becomes space-like inside the ergosphere. Hence (time-like or null) geodesics can have either positive or negative energy, $e = -t \cdot u$, in this region. However, asymptotically only positive energy (*i.e.*, future-oriented) geodesics are physical. Therefore any negative energy geodesics must be confined to circulate within the ergoregion. Of course, in a black hole background, such geodesics would ‘disappear’ behind the event horizon. However, for horizon-free geometries, such as the JMaRT solutions, they are stable bound orbits and so it is natural to find bound states in the context of a field theory analysis. However, the question then becomes whether the analogous modes of the field ‘fit’ inside the ergoregion or whether they ‘leak’ out to infinity, *i.e.*, whether a negative energy bound state or an ergoregion instability results. A more thorough examination of the bound states shows that the negative energy bound states are characterized by having $\Sigma_y = \omega/\lambda < 0$ while the ergoregion instability is associated with modes where $\Sigma_\psi = \omega/m_\psi$ and/or $\Sigma_\phi = \omega/m_\phi$ are negative – see Sections 3.7.3 and 3.7.4. Hence as the geodesic analysis would suggest the negative energy modes have a negative pattern speed or phase velocity, and the KK momentum modes tend to lead to bound states while the spinning modes are related to instabilities.

The presence of negative energy bound states can also be expected to enhance the decay of these horizon-free geometries. The analysis of the ergoregion instability (considered in this chapter) is only at the level of linearized test fields. Generically any theory coupling to gravity will also have nonlinear interactions (*e.g.*, even the free scalar considered here has nonlinear couplings with gravitons). These nonlinear couplings might be expected to lead to processes, where positive energy modes are radiated at infinity while negative energy modes are populated within the ergoregion. However, one should note that the negative energy modes are exponentially decaying at large radius — see Section 3.7.4 — while the positive energy modes are power-law suppressed inside the ergoregion. Hence the overlap of these modes is expected to be small, which will suppress this nonlinear contribution to the decay.

We now turn to consider the endpoint of the ergoregion instabilities. As emphasized before, the presence of these instabilities relies on two key ingredients, namely, the geometry has an ergoregion but it does not have an event horizon. Hence the resulting decay process could be terminated either by the disappearance of the ergoregion or the appearance of a horizon. However, the unstable modes radiate with a positive energy density asymptotically which is compensated for by a negative energy density inside the ergoregion — as could be seen in eq. (3.7). Hence the onset of the ergoregion instability produces a(n exponential) build-up of negative energy near the core of the JMaRT solutions. Therefore it seems unlikely that an event horizon will form since the latter is typically associated with a large build-up of positive energy density. This reasoning then suggests that the decay must terminate with the disappearance of the ergoregion. The supersymmetric D1-D5-P microstate geometries [79–89] are all free of an ergoregion and hence it is natural to suppose that these are at the endpoint of the ergoregion instabilities. Of course, these solutions offer a huge family of possible endpoints and the precise one that forms will depend on the details of the decay process, beyond the linear regime considered here — although as we are only considering the classical evolution, it is in principle possible given a certain set of initial conditions. Of course, we can expect that the final mass should be close to the BPS mass determined by the charges of the initial JMaRT solution, *i.e.*, $E = \pi/4G_5\,[Q_1 + Q_5 + Q_P]$. Although even here, we can only say 'close' as we know that the unstable modes with $\lambda \neq 0$ (and *either* sign of λ) occur which may modify the final value of Q_P. Similar comments apply for the angular momenta, J_ψ and J_ϕ. We also observe that there is no reason to expect that the decay process will lead to an endpoint within the family of supersymmetric JMaRT solutions. Of course, at the level of the present discussion, we cannot rule out that the endpoint is only a nearly supersymmetric solution (or that this would be the effective endpoint). Our expectation is that such solutions will have a 'small' ergoregion and that the instability might be eliminated (or strongly suppressed) before the ergoregion precisely vanishes.[10]

The stability analysis of the JMaRT solitons [94] is relevant for the stringy tachyon decays discussed recently in [166]. Originally, [167] considered tachyon condensation in certain D1-D5 black string backgrounds where tachyonic string winding modes can occur if one chooses antiperiodic boundary conditions for the fermions around the circle on which the black string is compactified. The latter choice necessarily restricts the scenario to a nonsupersymmetric sector of string theory which already suffers from various instabilities [183–185]. Ref. [166] considered adding angular momentum to the black strings. In this case, it was shown that

---

[10] We should note that the JMaRT solutions begin in a low-mass regime where $M^2 < (a_1 - a_2)^2$, however, if the ergoregion instability sheds the background momentum efficiently then the system will evolve to a regime where black holes can form. Hence we can not rule out the appearance of an event horizon – we thank Simon Ross for correspondence on this point.

string modes winding certain compact circles near the horizon can be tachyonic even when the asymptotic fermion boundary conditions are supersymmetric. The relevant point for the present discussion is that the endpoint of the tachyon condensation is in general one of the nonsupersymmetric JMaRT solitons. Now, in this chapter, we have shown that these solitons are themselves unstable and so they will not be the final endpoint of these decays. Instead, the ergoregion instability will continue the decay process and as suggested above, will likely terminate with a supersymmetric microstate geometry.

We would now like to consider the implications of ergoregion instabilities for Mathur's fuzzball program of describing black holes in terms of an ensemble of microstate geometries. If this program is to succeed it must supply a description of both supersymmetric and also nonsupersymmetric black holes. At first sight, it may appear that constructing non-BPS microstate geometries is not possible. In particular, non-BPS states will decay and so it is not clear that there should be stationary geometries to describe them. However, the JMaRT solutions provide an explicit example indicating that this is not really a problem. In fact, the decay of non-BPS microstates was already considered in the D-brane description of nonextremal black holes [27–29]. In that context, it was seen as a success of the string theoretic approach as this instability had an interpretation in terms of Hawking radiation [186–189]. Of course, Hawking radiation is a quantum effect in the black hole background and so presents no obstacle to the construction of classical supergravity solutions which are static or stationary.

It is perhaps useful to remind ourselves as to how this distinction arises. The classical limit can be understood as the limit in which the string coupling g_s is vanishingly small [187]. However, the interesting classical solutions are those which correspond to states where the various quantum numbers are extremely large. That is, $n_1, n_5 \propto 1/g_s$ and $n_p, J_\psi, J_\phi \propto 1/g_s^2$ while $g_s \to 0$. These scalings are chosen to ensure that the gravitational 'footprint', *i.e.*, Q_1, Q_5, Q_P, a_1 and a_2, associated with each of these quantum numbers remains finite. However, in this limit, the ADM energy of the system diverges with $E \propto 1/g_s^2$. As the energy is a dimensionful quantity, this can be accommodated by changing the scale to which energies are compared in the classical limit. Essentially, this divergence is associated with the divergence of the Planck mass, which does not serve as a useful reference scale in classical gravity. Now the decay rate of the nonextremal D1-D5-P black holes can be computed in a straightforward manner [187–189]. The key point, however, is that the final expression for dE/dt is expressed in terms of geometric quantities and is independent of g_s. To see the implications of this, it is somewhat more intuitive to consider the fractional rate of energy loss, $E^{-1}dE/dt$. Its inverse defines a characteristic time scale for the decay of the system. Therefore in the classical limit, the time scale of the decay diverges when measured against the fiducial scale established for classical physics, *i.e.*, $E(dE/dt)^{-1} \propto g_s^{-2} \to \infty$.

We note that the 'straightforward' calculations of the decay rate referred to above can be performed either in the framework of a microscopic D-brane perspective or of the gravitational perspective of Hawking radiation. The suprising result is that the results of both analyses agree precisely [187–189], including greybody factors, at least in the so-called 'dilute gas' approximation [156, 190]. However, even though suggestive arguments can be made in this regime [191], this remarkable agreement remains poorly understood. As the JMaRT solutions are horizon-free, the gravitational calculation of the decay rate would have to be modified. Using the connection between absorption and emission rates, it is possible that absorption calculations along the lines of those presented in [94] could be extended to yield the desired decay rate. On the other hand, the underlying microscopic states for the JMaRT solutions were already identified in [94]. Hence one can use microscopic techniques to estimate the decay rate expected for these solutions. The result is $dE/dt \sim Q_1Q_5(m-n)^6/R^6$ and again this quantity remains finite as $g_s \to 0$. Therefore we can again ignore this decay channel for the classical JMaRT solutions.

However, the ergoregion instability investigated in this chapter is a classical instability and so should not be associated with the decay discussed above. We should also note that the form of these two instabilities differs. Above one is considering the spontaneous decay of the system while the classical instability really corresponds to a decay that results when the initial data does not precisely match that of the JMaRT solutions. Of course, in the quantum regime, the same modes associated with the ergoregion instability will give rise to spontaneous decay due to quantum fluctuations of the background.[11] However, the latter will again be suppressed in the $g_s \to 0$ limit. This reflects the fact that the background can be prepared with arbitrarily

---

[11] In [94] it was erroneously assumed that all of these geometries have an AdS$_3$ core to argue that such emissions would not occur.

accurate precision in the classical limit and so it should be possible to produce an arbitrary suppression of ergoregion instability. Alternatively, working in the classical limit, we can regard the ergoregion instability as a property of how the JMaRT solutions interact with external sources. That is, generically if an external wave packet impinges on one of the nonsupersymmetric JMaRT configurations, it will produce a dramatic decay of the original background. Hence this instability seems to present a major challenge for the fuzzball description of black holes.

We have argued that the ergoregion instability is a robust feature of the nonsupersymmetric JMaRT solutions over a wide range of parameters. Given general arguments along the lines of [163], we also expect that this instability will be a generic feature of any smooth horizon-free geometries which describe microstates which are non-BPS and carry significant angular momentum (and hence have a macroscopic ergoregion). Therefore if a nonextremal D1-D5-P black hole is to be described by a coarse-grained ensemble fuzzball, it seems that that the classical black holes must suffer from an analogous instability. While the presence of an event horizon eliminates the possibility of an explicit ergoregion instability, there are, in fact, a number of potential instabilities which might afflict these black holes and possibly reproduce the same physics:

a) Superradiant Instability: Spinning nonextremal black holes will exhibit superradiant scattering, where an incident wave packet can be reflected with a stronger amplitude. Superradiance by itself does not provide a classical instability, but an instability can arise if the scattered modes are reflected back to rescatter, as described in Section 3.1. This scattering was considered for higher-dimensional spinning black branes [170] and there it was found that when the noncompact space has more than four dimensions, this instability does not arise. Explicitly analyzing the present D1-D5-P black string again seems to indicate the absence of an instability [192].

b) Gyration Instability: Considering supersymmetric D1-D5-P black strings, it was found that above a certain critical angular momentum a straight black string is unstable towards carrying the angular momentum in gyrations of the horizon [193]. This instability should also appear in nonsupersymmetric configurations and so would present an instability at large values of the angular momentum.

c) Gregory-Laflamme Instability: The relevant configurations are black strings and so are expected to suffer from the Gregory-Laflamme instability [63, 64] in two ways. The first is the usual instability of long wavelength modes along the string. Of course, this instability can be eliminated by reducing the radius of the compactification along the string. For a fixed radius, it is also suppressed by the boosting along this direction which induces the KK momentum [74]. This instability is not related to the angular momentum carried by the black string or the presence of an ergoregion, but we list it here for completeness.

d) Ultraspin Instability: In six or higher space-time dimensions, one can find black hole solutions with an arbitrarily large spin per unit mass [104]. However, it was argued [109] that a Gregory-Laflamme-like instability will arise to dynamically enforce a Kerr-like bound in these cases. While this analysis does not directly apply in five dimensions, entropy arguments suggest an analogous instability still exists and will lead to the formation of a black ring if the angular momentum is too large [73].

While there are several possibilities for instabilities of a black string in six dimensions, it seems that none of these can reproduce the physics of the ergoregion instability which will afflict the non-BPS microstate geometries. This observation relies on the fact that these instabilities have a different character at a very basic level. The ergoregion instability might be termed a radiative instability, in that, the instability is by definition connected to modes that radiate at infinity. In contrast, the four instabilities considered above for black strings can be termed internal instabilities. That is, these instabilities are primarily associated with a rearrangement of the internal or near-horizon structure of the black string. While these instabilities will be accompanied with some radiation at infinity, this will be a secondary effect with these instabilities. Therefore it seems that emulating the ergoregion instability in a nonextremal black string background will require the discovery of a new kind of instability. While we are performing a detailed analysis of the nonextremal D1-D5-P black string, our preliminary results indicate that no such instability arises [192].

We also note in passing that at the same time the microstate geometries should be able to emulate any instabilities found in the black string backgrounds. In particular, the Gregory-Laflamme instability is a robust instability that will afflict these backgrounds for sufficiently large R. In the microstate geometries, one should then find unstable modes carrying KK momentum which are confined near the core of the soliton. We have studied bound states for a test field in the JMaRT solutions, as described in Section 3.7.4. While the modes we identified only arise for nonvanishing KK momentum as desired, they are all stable, *i.e.*, they have real frequencies. Hence they can not serve as the analog of the Gregory-Laflamme instability in the nonsupersymmetric JMaRT solutions. However, the latter would be a gravitational instability, *i.e.*, it should not be expected to appear as a scalar test field, and so this question requires further investigation.

A possible reconciliation of these ideas with the fuzzball proposal would be that the microstate geometries could provide an accurate description of a black hole, but only over a long but finite time. In the context of the AdS_3/CFT_2 duality, some evidence for such a picture has recently been found [194]. With this new point of view, a key question is to determine the timescale over which microstate geometries cannot be distinguished from black holes. One suggestion [194] is that it should be of the order of the recurrence time, which would be exponential in the relevant quantum numbers. An alternative suggestion might be that the timescale is associated with Hawking evaporation which would involve (inverse) powers of the quantum numbers. However, note that both of these suggestions diverge in the classical limit. Hence the ergoregion instability found here seems to be in conflict with both of these suggestions. While the instability timescale is certainly very long in certain parameter regimes, it is a classical timescale, *i.e.*, it is finite in the classical limit. Hence our results would suggest that spinning microstate geometries and black holes should be distinguishable on a large but classically finite timescale.

However, one must ask how characteristic our results for the JMaRT solutions will be of generic microstate geometries. In particular, we note that the CFT states corresponding to the JMaRT solutions are exclusively in the untwisted sector [85, 94, 195]. On the other hand, the majority of microstates accounting for the entropy of the black strings are expected to be in a (maximally) twisted sector [76, 77]. From a geometric point of view, we would observe that the JMaRT solutions have all the same Killing symmetries as the D1-D5-P black holes, while the generic microstate geometry is expected to have a complex nonsymmetric core. Therefore it is not unreasonable to expect that the ergoregion instability timescales found for the JMaRT solutions will not be characteristic of the microstate geometries that make up ‘most’ of the black hole.

One possibility might be the generic non-BPS geometries do not have ergoregions despite the fact that they carry angular momentum. However, we argue that such a scenario is implausible as follows: The fuzzball description would now require that both the horizon and the ergosphere arise as effective surfaces in ‘coarse-graining’. However, quantum fluctuations must then extend out to the ergosphere. In particular, these fluctuations extend to regions of the space-time which should be causally accessible to asymptotic observers on finite classical timescales. Hence it seems inconsistent to say that the underlying microstate geometries are hidden from asymptotic observers in this scenario.

Hence as argued above, if the non-BPS microstate geometries are horizon-free with an ergoregion, they should expect an ergoregion instability. However, it may be that instability timescales calculated for the JMaRT solutions are not representative of those for typical microstate space-times. In particular, the latter should have complicated throats — as seen in their supersymmetric counterparts [78–83, 153] — which would emulate the absorptive behavior of a black hole horizon. Hence it might be expected that the relevant timescales are extremely long. An important question is then whether the instability timescale is classically finite or not. That is, will this timescale diverge as the quantum numbers grow as described above. Certainly finding more generic non-BPS microstate geometries is an essential step towards resolving this issue.

In closing, we note that in the context of the AdS/CFT, a complete description has been produced for half-BPS microstate geometries with AdS_5 [196–198] and AdS_3 [199–201] asymptotics. This framework has given rise to an interesting program of semi-classical quantization [194, 202–204] and a coarse-graining description of space-time geometry [205–209]. With this program in mind, it is useful to recall the role of the smooth horizon-free microstate geometries in Mathur’s ‘fuzzball’ program [76, 77].

The BPS microstate geometries for the D1-D5 system can be derived by studying the F1-P geometries and applying a series of duality transformations [79–83]. There the winding and wavenumbers might be quantized by the geometry but classically the amplitudes of the string excitations are continuous variables. Solutions where select modes are excited with a large amplitude can then be seen as ‘coherent states’ of the underlying quantum theory. Such solutions may be further useful to understand certain properties of typical microstates, *e.g.*, their transverse size [76, 77]. However, ultimately a generic state will have a vast number of modes excited with very few quanta and hence the corresponding ‘space-time’ will not be accurately described by a classical geometry. However, the family of classical geometries still serve as a guide to the classical phase space which must be quantized [202–204]. Of course, this quantization remains a work in progress at present.

3.7 Supplementary material for Chapter 3

3.7.1 WKB matching formulae

In this section we use the usual WKB wavefunctions and WKB connection formulae at the turning points to relate the amplitude of the wavefunctions in the four distinct regions of the scattering problem and, in particular, to derive (3.50). The four WKB regions are (see Figure 3.1): Region I, the innermost forbidden region ($0 < x < x_0$); Region II, the allowed region where V_+ is below Σ_ψ ($x_0 < x < x_1$); Region III, the potential barrier region where V_+ is above Σ_ψ ($x_1 < x < x_2$); and Region IV, the external allowed region where Σ_ψ is below V_- ($x_2 < x < \infty$). The WKB wavefunctions in region I and in region IV were already written in (3.48) and (3.49), respectively, and in regions II and III they are given by

$$
\begin{aligned}
H_{\rm II} &\simeq \frac{1}{m_\psi^{1/2} T^{1/4}} \left\{ C_2 \exp\left[i\, m_\psi \int_{x_1}^{x} \sqrt{T}\, dx \right] + C_3 \exp\left[-i\, m_\psi \int_{x_1}^{x} \sqrt{T}\, dx \right] \right\}, \quad (3.92)\\
H_{\rm II} &\simeq \frac{1}{m_\psi^{1/2} |T|^{1/4}} \left\{ C_4 \exp\left[-m_\psi \int_{x_1}^{x} \sqrt{|T|}\, dx \right] + C_5 \exp\left[m_\psi \int_{x_1}^{x} \sqrt{|T|}\, dx \right] \right\} \quad (3.93)
\end{aligned}
$$

Using the WKB connection formulae in each turning point, x_0, x_1 and x_2, we can find the relations between the amplitudes C_i's $(i = 1, \cdots, 7)$ of the several regions, yielding:

$$
C_2 = C_1 e^{i\gamma}\,, \quad C_3 = C_1 e^{-i\gamma}\,. \tag{3.94}
$$

$$
C_4 = \frac{1}{2}\left(C_2 e^{-i\pi/4} + C_3 e^{i\pi/4} \right)\,, \quad C_5 = i\left(C_2 e^{-i\pi/4} - C_3 e^{i\pi/4} \right)\,, \tag{3.95}
$$

$$
C_6 = \left(\frac{iC_4}{2\eta} + C_5 \eta \right) e^{-i\pi/4}\,, \quad C_7 = \left(-\frac{iC_4}{2\eta} + C_5 \eta \right) e^{i\pi/4}\,, \tag{3.96}
$$

with γ and η defined in (3.51) and (3.52), respectively. Finally, combining these three sets of relations yields (3.50).

3.7.2 Details of the numerical analysis

In this section we discuss some issues related to the numerical computation of the unstable modes. First, we return to the approximation we have used throughout this chapter that the solution to the angular equation (3.16) is well described by the scalar spheroidal harmonics with eigenvalues $\Lambda = l(l+2)$, where l is an integer such that $l \geq |m_\psi| + |m_\phi|$. After showing that this approximation is indeed sufficient, we discuss further details related to the precision of our results.

If ω is treated as fixed, we can actually solve the angular equation quite easily since it is defined on a compact interval. By the symmetry $\theta \to \pi - \theta$, we may reduce the range of integration to $\theta \in [0, \pi/2]$, so that the angular equation is only singular on the boundaries. The boundary conditions at the edges of this interval are determined by the values of m_ψ and m_ϕ chosen. As $\theta \to 0$ with $m_\phi \neq 0$, finiteness of the solution requires that $\chi(0) = 0$, and we may normalize, $\chi'(0) \equiv 1$, by linearity. At the other boundary, nonzero m_ψ requires that χ vanishes. When either of m_ϕ or m_ψ vanish we must modify our boundary conditions as finiteness of the solution requires that χ approaches a constant. To find the eigenvalue Λ we start near $\theta = 0$ where Cauchy data is specified for the solution. The angular equation is then integrated to $\theta \approx \pi/2$ where we check the value of the boundary condition. By adjusting Λ until the $\theta = \pi/2$ boundary condition is satisfied, we arrive at the desired eigenvalue.

The coupled eigenvalue problem defined by (3.16) and (3.19) can be solved iteratively by treating the equations as separate eigenvalue problems. We will parameterize Λ as $\Lambda = l(l+2)$, but no longer assume that l is an integer. To start the solution process, however, we will assume that l is indeed given by an integer and call it l_1. This value is then substituted into the radial equation which is solved according to the method outlined in Section 3.5.1, to obtain the eivenvalue which we call ω_1. The n'th iteration results from substituting l_{n-1} into the radial equation to solve for ω_n. This new value is then used in the angular equation which is solved as above to obtain the improved value, l_n. The first iteration, consisting of (l_1, ω_1) are the solutions we have presented elsewhere in this chapter.

In Figure 3.6, we show that the convergence of this iterative procedure is in fact exponential.

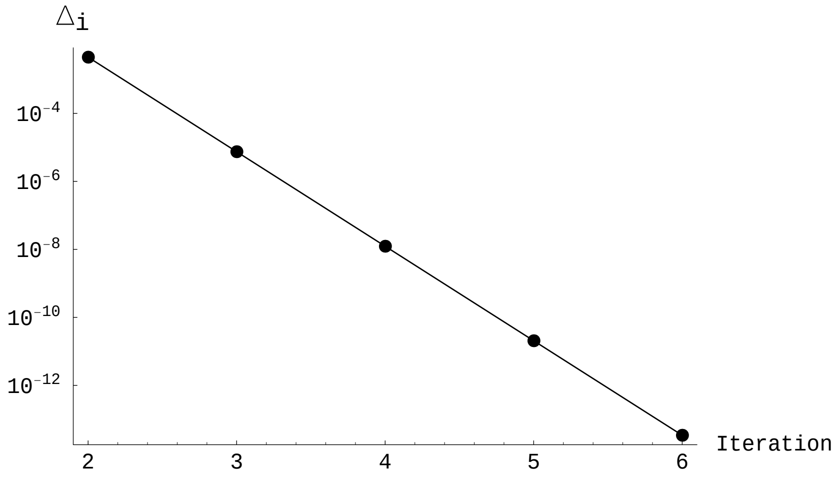

Figure 3.6: Convergence, as defined in eq. (3.97) of the iterative method for solving the coupled eigenvalue problem.

There, we have plotted the amount of convergence in each iteration, which we have defined by

$$\Delta_i^2 = \left|\frac{\omega_i - \omega_{i-1}}{\omega_{i-1}}\right|^2 + \left|\frac{l_i - l_{i-1}}{l_{i-1}}\right|^2 \ , \tag{3.97}$$

as a function of iteration number. Notice that the convergence at the second iteration, *i.e.*, the corrections to the numerical solutions we have presented in this chapter, is already of order $\sim 1\%$, this appears to be a general feature of the numerical solutions. Hence, we are justified in our usage of only the first iteration.

Even though the very small imaginary parts of ω are well described by both the WKB and matched asymptotic approximations, for completeness we show that they are not a numerical artifact due to loss of precision in our numeric routines or a by-product of using the approximate solutions to specify the boundary conditions. In Figure 3.7 we plot the imaginary part of ω for several values of the number of digits of precision used in the calculation. We use the same parameters as before and set $N = 0, l = m_\psi = 4$. We see, as one would expect if the imaginary part were actually nonzero, that the eigenvalue converges to a constant value when the number of digits is larger than the size of the imaginary part.

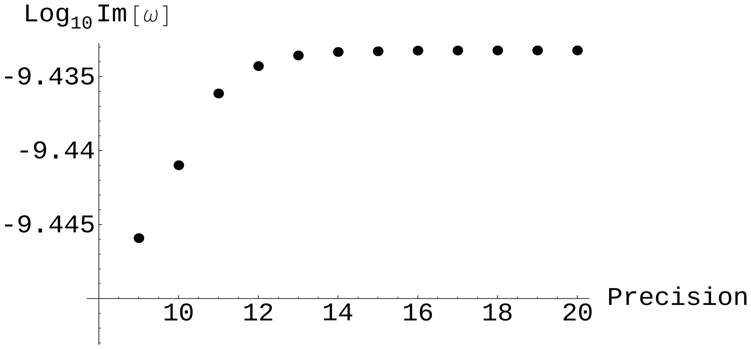

Figure 3.7: Effect of increasing digits of precision used on imaginary part of eigenvalue for outgoing modes.

With only the asymptotic form of the solutions to specify the boundary conditions we are not actually setting the coefficient on the divergent term to zero. Instead, there will always be some amount of the divergent solution in the numerically defined solution. The suppression of the divergent term is dependent on how deep into the asymptotic region we choose to apply the boundary condition. To ensure that these small divergent terms are not causing any errors we study the effect of varying the point at which we apply the boundary conditions. This has been shown in Figure 3.8 on the left and right. In both cases, we again see that the eigenvalue converges to a constant value as we increase the accuracy of the calculation.

3.7.3 Detailed analysis of the instability

The existence of a solution to the matching procedure can be reduced to the requirement that a number of constraints be satisfied. The difficulty one runs into when trying to discuss the general properties of these solutions is that while all the parameters appearing in the various equations are uniquely determined by the set $\{Q_1, Q_5, R, m, n\}$, it is difficult to write explicit expressions for them. In this sense, the fact that the parameters (3.12) can be written in such a simple form is really quite surprising since all are proportional to M, which can at best be

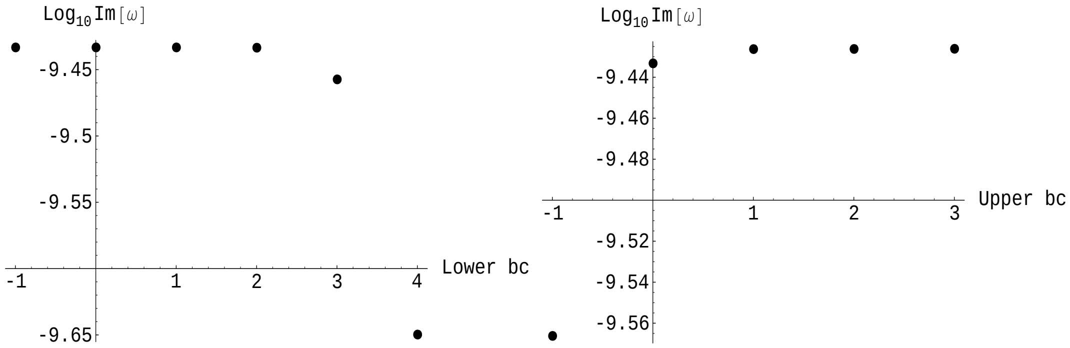

Figure 3.8: On the left, we vary the point at which the inner boundary condition is applied. We parameterize this point by the integer, n, and apply the boundary condition at the point x which is a solution of $(x\kappa^2)/(\zeta^2/x) = 10^{-5+n}$. On the right, we do the same for the outer boundary condition, though now n is defined via $(x\kappa^2)/(\zeta^2/x) = 10^{3+n}$.

defined implicitly in terms of the above parameters.

Hence it is useful to have an approximation for M that allows one to understand the general behavior of the various parameters. Surprisingly, there is quite a simple approximate solution given by

$$M \approx 2(s^{-1} - s)\frac{Q_p}{1 + nm\left(\frac{Q_1+Q_5}{R^2}\right)}\ , \tag{3.98}$$

where we recall that $Q_p = nmQ_1Q_5/R^2$. For most parameter values, this expression is accurate on the order of a few percent. When one of the D-brane charges, say Q_1, grows much larger than $Q_5 \sim R^2$ this approximation can break down, though only by a few percent times $(m - (n+1))$. Similar problems appear when $R^2 \gg Q_1 \sim Q_5$, in this case the error appears to be of the same order. The important thing to note is that it gives the correct scaling of M with the various parameters in all situations. In most cases, except those noted previously when $m \gg n$, it also gives the correct order of magnitude. Treating m as a continuous parameter, the approximation appears to produce the approach to the supersymmetric limit exactly.

Using this, one can approximate, or at least bound, the parameters appearing in the solutions.

$$\begin{aligned}
\varrho &= \frac{c_1^2 c_5^2 c_p^2 - s_1^2 s_5^2 s_p^2}{s_1 c_1 s_5 c_5} \approx \frac{s^{-1}+s}{2}\left(1 + nm\frac{Q_1+Q_5}{R^2}\right) && (3.99)\\
\varepsilon &\leq \frac{1}{R^2}\left(Q_1 + Q_5 + Q_p + M\left(1 - \frac{nms^2}{(s^{-2}-s^2)^2}\right)\right) \\
&\approx \frac{1}{R^2}\left(Q_1 + Q_5 + Q_p + \frac{2Q_p}{1+nm\frac{Q_1+Q_5}{R^2}}\left[\frac{nm(1-s^4)^2 - s^6}{nms(1-s^4)(1+s^2)}\right]\right) && (3.100)\\
\vartheta &\leq \frac{Q_p}{Q_1 Q_5}\left(Q_1 + Q_5 + M\right) \\
&\approx \frac{Q_p}{Q_5} + \frac{Q_p}{Q_1} + 2\frac{Q_p^2}{Q_1 Q_5}\frac{s^{-1}-s}{1+nm\frac{Q_1+Q_5}{R^2}} && (3.101)
\end{aligned}$$

In the above, the inequalities result from writing $s_i^2 \leq s_i c_i = Q_i/M$, in particular they become exact for the supersymmetric limit. From the expression for ε one sees that it is finite, and in fact positive for all $m \geq n+2$. It is only in the supersymmetric limit that $\varepsilon \to -\infty$, which precludes any possible instability. One may also check from these forms that $\varepsilon/\varrho^2 \ll 1$ for all values of the parameters, which can be verified numerically for sets of parameters in which the approximations are less trustworthy. In what follows then we will neglect ε where consistent.

The timescale of the instability is an increasing function of ν which, given the above considerations, is given by

$$\nu \approx -\lambda\frac{Q_p}{\varrho R^2} + \sqrt{\lambda\frac{Q_p}{\varrho R^2}\left(\lambda\frac{Q_p}{\varrho R^2} + 2c\right) + \nu_0^2 - \frac{\varepsilon}{\varrho^2}c^2}\,. \tag{3.102}$$

Unfortunately, we cannot make any definite statements about the size of $Q_p/\varrho R^2$ like we did previously for ε since it can be made arbitrarily large or small just by varying R. At this point we could use the explicit forms for ν_0^2 and c to discuss the general properties of the solutions. Instead we will for now set $\lambda = 0$ to make the discussion more transparent. Nonzero λ will not change the general features of the solutions.

Setting $\lambda = 0$, the above expression for ν simplifies quite a bit

$$\nu \approx \sqrt{\nu_0^2 - \frac{\varepsilon}{\varrho^2}c^2}\,. \tag{3.103}$$

We are now in a position to discuss the behavior of the timescale for various different solutions. Recall that the timescale for the instability is smallest when ν is smallest. Therefore the instability will be strongest when $\nu_0 = l + 1$ is smallest. This, of course, does not mean that we should necessarily consider solutions with $l = 0$, in fact we shall see in a moment that such solutions are not possible. More precisely, the minimum value of l for which all the constraints can be satisfied will lead to the most unstable solution.

Similarly, when c^2 or ε/ϱ^2 is largest the instability will be the strongest. We shall deal with c next, but for now it is sufficient to note that it is only dependent on m and n. Observe from (3.101) that for fixed R, ε/ϱ^2 varies roughly like the inverse of the charges, therefore when one considers limits in which the charges grow, the timescale of the instability diverges. Similar arguments hold when R is vastly different from the charges, we find that ε/ϱ^2 shrinks and the lowering effect of c^2 is diminished. It appears then that the instability will be strongest when $Q_1 \sim Q_5 \sim R^2$.

To discuss the relative effect of c we should return to the constraints. These also simplify when we set $\lambda = 0$ and we may consider the simpler constraint $c - \nu_0 > 0$. The exact form that c takes is dependent on the sign of ζ. By studying the constraints, it turns out that solutions with $\zeta > 0$ will in general exist, but for larger values of l than when $\zeta < 0$. Given the considerations above, the effect of these modes will be subdominant. We therefore focus on $\zeta = -nm_\psi + mm_\phi < 0$ which implies that $m_\psi > m_\phi$. One can then write the constraint as

$$\begin{aligned} c - \nu_0 &= [(m-n)(m_\psi + m_\phi) - (2N+1)] - [l+1] && (3.104) \\ &= (m-(n+1))(m_\psi + m_\phi) - (l - m_\psi - m_\phi) - 2(N+1) > 0\ . && (3.105) \end{aligned}$$

Further, it can be shown that when this is satisfied, the other constraints follow automatically. The last two bracketed terms in the final line are positive, so a solution requires that $m_\psi + m_\phi > 0$, implying that m_ψ must be positive. This is a general result that is also obtained when $\zeta > 0$ or $\lambda \neq 0$. When c is largest, the timescale will be shortest, therefore the lowest harmonic $N = 0$ will lead to the strongest instability. One can also make c large by choosing m_ψ and m_ϕ as large as large as possible, $m_\psi + m_\phi = l$, but taking l large will not necessarily give us a very unstable mode because as noted before it will cause ν_0 to rise which has an opposing effect. Since c^2 enters weighted by ε/ϱ^2, the more important contribution will be that from ν_0

and the net effect is a less unstable mode. Finally, note that m_ϕ and m_ψ appear symmetrically in c, so that the value of ν will be independent of the partition of l into m_ϕ and m_ψ. This does not mean that the timescale will be independent of this partition since it is a weakly shrinking function of $|\zeta|$ for fixed ν. When $|\zeta|$ is maximized the timescale will be the shortest, which is the case when $m_\psi = l$, $m_\phi = 0$.

To summarize then, for a fixed mode that solves the constraints, the instability will be strongest when $Q_1 \sim Q_5 \sim R^2$. On the other hand, when we fix a particular background, the instability with $\lambda = 0$ will be strongest when $l = m_\psi$ is as small as possible and $m_\phi = 0$.

Finally then we may discuss the solutions for which $\lambda \neq 0$. It turns out that the various scalings of the other parameters appears not to be changed. When $\lambda \neq 0$, the constraint $c^2 - \nu_0^2 > 0$ becomes easier to satisfy since c picks up a contribution proportional to $\vartheta\lambda$ while the contribution to ν_0 is smaller. The tougher constraint to satisfy is then the one that implies $\omega^2 > \lambda^2$. When all other parameters are fixed, this places upper and lower bounds on (*i.e.*, we allow negative λ) λ. We will not go into detail here, but instead note one can always find solutions with nonzero λ by going to sufficiently large angular momentum, l.

When studying the characteristic time for the instabilities, one finds that the timescale decreases as λ is raised, but reaches a minimum shortly before reaching the upper bound. For negative values, on the other hand, the timescale is a constant decreasing function of λ. As mentioned, solutions with nonzero λ require larger values of l than when $\lambda = 0$. Though larger l tends to increase the timescale, the overall effect of going to larger l to accommodate nonzero λ can still lead to shorter timescales.

3.7.4 Bound states

The general radial dependence of the scalar field at large distances from the core is determined by the sign of κ^2. When it is positive, the solution oscillates with a power-law falloff. This is the behavior that led to the in and outgoing waves at infinity which we have already discussed. The other two possibilities, where κ^2 is zero or negative, can lead to quite different behavior. For the former there is an exact solution, while the latter may again be solved with a matched expansion.

Marginally bound states: $\kappa^2 = 0$

By considering the special mode with $\omega^2 = \lambda^2$, both the angular and radial equations simplify sufficiently that an exact solution may be found. Such a choice removes all ω dependence from the angular equation allowing it to be solved independently. The result is the eigenvalue equation for the harmonics on an S^3. The exact eigenvalue is $\Lambda = l(l+2)$.

For the radial equation, this choice of mode removes the $\kappa^2 x$ term; the same condition that previously led to the simplification in the near region. The previous solution in the near region (3.72) therefore becomes the exact solution in the entire space-time. This means that asymptotically the equation has a basis of solutions in terms of $r^{-1\pm\nu}$. Ignoring for now the part dependent on the KK momentum, these become r^l and r^{-2-l}. These are simply the terms one expects from a Laplace series in four flat spatial dimensions where the angular momentum creates an effective radial potential.

Asymptotic regularity requires that the $r^{-1+\nu}$ component vanish whenever $\nu > 1$, leaving a field that falls off as $r^{-1-\nu}$. The natural generalization of Friedmann's analysis of ergoregion instabilities to five dimensions would involve studying fields that fall off as r^{-2}, therefore these modes will evade that analysis as long as $\nu > 1$. The requirement that removes the divergent term is similar to that for outgoing modes, except now it is an exact result

$$\nu + |\zeta| \mp \xi \quad = \quad -(2N+1) \, , \tag{3.106}$$

where N is a non-negative integer. Here, however, we allow for either of the Γ functions in the denominator to diverge in eq. (3.74), leading to both possibilities for the sign before ξ. This is in contrast to the search for unstables modes in which we could neglect one of the possibilities since it was found to corresponded to ingoing damped modes. Indeed, since (3.106) contains terms linear in both λ and ω, one must consider both possibilities in order to be consistent with the symmetry under flipping signs as in equation (3.25).

In total then we have three constraints that must be satisfied for these modes. The first, $\omega^2 = \lambda^2$, fixes ω to be an integer, meaning that there are no remaining continuous parameters characterizing the scalar field. For a general background then it is unlikely that the remaining constraints, in particular the one defining N, can be solved by a judicious choice of the integer eigenvalues. On the other hand, fixing the set m_ψ, m_ϕ and λ, there may be families of backgrounds for which these marginally bound states exist.

Bound states: $\kappa^2 < 0$

The final possibility for solutions of the radial equation is $\omega^2 < \lambda^2$, or $\kappa^2 < 0$. As in the case where κ^2 is positive, we are unable to find an exact solution, though progress can be made through approximation. In particular, since the effect of the sign of κ is only relevant at large distances from the core, we need only make slight modifications to the matched asymptotic expansion analysis presented earlier.

To begin, we factor out the sign of κ^2 by redefining $\kappa \to i\kappa$, giving solutions that are real valued exponentials asymptotically. Requiring regularity therefore leaves only the exponentially damped "bound states", localized near the core region. Explicitly, after having made the redefinition in (3.75), a convenient basis of solutions is in terms of modified Bessel functions of the first and second kind.

$$h \;=\; \frac{1}{\sqrt{x}}\left[A_1 I_\nu(\kappa\sqrt{x}) + A_2 K_\nu(\kappa\sqrt{x})\right] \; . \tag{3.107}$$

The first of these diverges at large x and so we require $A_1 = 0$ for regularity. For now though, we leave A_1 arbitrary, setting it to vanish only after we have performed the matching.

In the matching region expanding I_ν and K_ν in the $x^{\pm\nu/2}$ basis gives

$$h \approx \frac{1}{\sqrt{x}}\left[\left(\frac{A_1}{\Gamma(1+\nu)} + \frac{A_2\Gamma(-\nu)}{2}\right)\left(\frac{\sqrt{x}\,\kappa}{2}\right)^{\nu} + \frac{A_2\Gamma(\nu)}{2}\left(\frac{\sqrt{x}\,\kappa}{2}\right)^{-\nu}\right] \; . \tag{3.108}$$

Note that K_ν contains both of these powers of x when expanded in the overlap region. While the contribution of the positive power to K_ν is relatively small, we will keep this contribution until after we perform the matching so that we may see how the approximate solution comes about.

By construction, the solution in the near region (3.72) is unaffected by the redefinition of κ. Immediately then we may proceed to matching the coefficients on powers of x in the overlap region. Setting $A = 1$ in the near region solution, we determine the coefficients A_1, A_2 in the outer region

$$\frac{A_1(\kappa/2)^\nu}{\Gamma(1+\nu)} = \frac{\Gamma(\nu)\Gamma(c)}{\Gamma(a)\Gamma(c-b)} - \frac{\Gamma^2(-\nu)\Gamma(c)(\kappa/2)^{2\nu}}{\Gamma(\nu)\Gamma(b)\Gamma(c-a)} \,, \tag{3.109}$$

$$\frac{A_2\Gamma(\nu)}{2(\kappa/2)^\nu} = \frac{\Gamma(-\nu)\Gamma(c)}{\Gamma(b)\Gamma(c-a)} \,, \tag{3.110}$$

As before, finding the spectrum of solutions now requires that we find values of the free parameters for which these equations are consistent with the boundary conditions. In particular, we now set $A_1 = 0$ and therefore ask that the right hand side of (3.109) vanishes. Again, rather than find such parameters numerically there is an accurate approximation that comes from noting that consistency requires A_2 be nonzero. This implies that the second term in (3.109) must be nonzero and therefore any solution must come from cancellation between the two terms. Since the second term is suppressed by the factor $\kappa^{2\nu}$, a comparable suppression must occur in the first term, again requiring the divergence of a Γ function in the denominator. This gives a quantization condition similar to that found previously

$$\nu + |\zeta| \mp \xi \approx -(2N+1) \,. \tag{3.111}$$

Here again, the terms linear in ω and λ implicit in the above equation – see definitions in eq. (3.20) — imply that both possibilities are required for consistency with the symmetry (3.25), though in practice both may not lead to solutions for which $\omega^2 < \lambda^2$.

When ν is real, this appears to give solutions for ω which are purely real. Note, however, we must be careful in solving the constraint since, given the right combination of background charges, ν^2 could become negative. For an arbitrary frequency in this range, eq. (3.109) will be complex so solutions where ω has both real and imaginary parts may be possible. Such solutions cannot be found with the sort of perturbative expansion used in studying the outgoing modes since now it is the real part of ν which gains a small correction, while the imaginary part is large. We can therefore no longer consider the behavior near the pole on the negative real axis defined by the real part of eq. (3.111). Instead, we have resorted to searching for these solutions by solving (3.109) numerically.

Generically, the root finding algorithm will produce a complex value of ω that sets the equation to zero within a specified precision. Since the imaginary part is many orders of magnitude smaller than the real part one should ensure that it really is nonzero and not a numerical artifact. In Figure 3.9 we show the variation in the size of the imaginary part as a function of the tolerance used in finding the root of (3.109). From this plot we see that the imaginary contribution is indeed just an artifact of trying to solve the complex equation. Surprisingly then it appears we can satisfy (3.109) with a real value of ω, even if that value causes $\nu^2 < 0$. That value corresponds to the solution of the equation resulting from taking the real part of the quantization conditions (3.111).

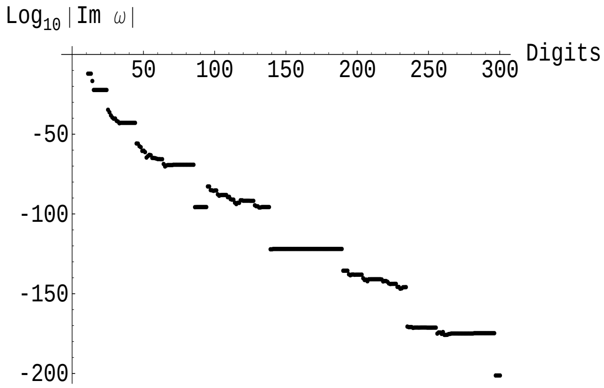

Figure 3.9: Variation of the size of the imaginary part of ω resulting from the numerical solution of (3.109) as the precision is increased.

Since the condition (3.111) is the same as for the outgoing modes, much of the analysis in Section 3.7.3 about the existence of solutions applies. The situation is somewhat more complicated in that one now allows modes with positive ω and there are two possible solutions corresponding to the two signs in (3.111), but the general characteristics of the solutions are the same. In particular, for the outgoing modes it was found that there are upper and lower bounds on the allowable values of λ beyond which $\omega^2 - \lambda^2$ changes sign. In light of these bound states, we see that the full space of solutions may be considered as split into distinct regions based on the value of λ. There is a small-$|\lambda|$ regime, in which one finds the outgoing unstable modes. This is surrounded, at larger values of $|\lambda|$, by a regime where the bound states arise.

This separation of the two types of modes according to the parameter λ makes clear the difference in their origin. In particular, one can always find outgoing unstable modes that do not carry KK momentum, they need only be supplied with sufficient angular momentum. This is in accord with our interpretation of these solutions as the unstable modes predicted by Friedman which result from the existence of the ergoregion. In contrast, bound states will always result as long as $|\lambda|$ is large enough. This includes modes which carry no angular momentum, thus indicating the important characteristic of these solutions is their KK momentum and the effective five-dimensional mass it induces.

Having established the existence of these bound states we should question just how close to the core region they are bound. The solutions are damped exponentially and so have characteristic size

$$\begin{aligned} x_{bs}^{-1} \sim \kappa^2 &= (\lambda^2 - \omega^2)\frac{r_+^2 - r_-^2}{R^2} \,, && (3.112) \\ &\approx 2(\lambda^2 - \omega^2)\frac{Q_1 Q_5}{(s^{-1}+s)R^2(R^2 + nm(Q_1+Q_5))} \,. && (3.113) \end{aligned}$$

To arrive at the final line we have used the approximation for M (3.98) found in Section 3.7.3. The boundary of the ergoregion, on the other hand, is given by the vanishing of the norm of the Killing vector ∂_t (3.13). We ignore the a_1, a_2 dependent contributions appearing in f to give an outer bound on the size of the ergoregion, given approximately by $r_{er}^2 \sim Mc_p^2$. In terms of the variable x this means

$$x_{er}^{-1} \gtrsim \frac{s^{-2} - s^2}{nm(s^{-2} - s^2)^2 c_p^2 - s^2} \,. \qquad (3.114)$$

Whenever Q_1 and Q_5 are much smaller than R^2, the size of the bound state scales as $x_{bs}^{-1} \sim Q_1 Q_5 / R^4 \ll 1$. On the other hand, for large Q_1 and Q_5 we have $x_{bs}^{-1} \sim Q_i/R^2$ where Q_i is the smaller of the two. In other words, the size of the bound state is strongly dependent on the background. When the charges are large, the bound state will be mostly contained within the ergoregion, while for small charges the exponential tail of the bound state can extend far outside.

Finally we can consider the possibility that the bound states have negative energy, which requires a detailed analysis of the energy integral (3.7). Examining the integrand evaluated on bound state solutions, we see that it may become negative near where the modulus of the scalar field peaks if the latter occurs inside the ergoregion. Though there are bound states for arbitrarily large values of $|\lambda|$, the total energy will not be negative for all of these. Instead, the modes that tend to exhibit negative energy densities (in the ergoregion) only appear for a limited range of $|\lambda|$, which is just beyond the small-$|\lambda|$ regime discussed above. That is, for values of λ near where the ergoregion instability appears. When this is the case, the maximum of the modulus of the scalar field is inside the ergoregion and the phase velocity in the compactified direction $\Sigma_y = \omega/\lambda$ is negative, *i.e.*, in the direction opposite to which the background is boosted.

Chapter 4

Bouncing Braneworlds Go Crunch!

In the present chapter, we will focus on one small aspect of the braneworld description of cosmology. In particular, we are interested in a certain family of cosmological solutions [210] which were recently proposed in the context of the Randall-Sundrum (RS) scenario [39, 40]. Recall that the RS model introduces a codimension-one brane into a five-dimensional bulk space-time with a negative cosmological constant. The gravitational back-reaction due to the brane results in gravitational warping which produces massless graviton excitations localized near the brane. Fine tuning of the brane tension allows the effective four-dimensional cosmological constant to be zero (or nearly zero). Brane cosmologies where the evolution is essentially that of a four-dimensional Friedmann-Robertson-Walker (FRW) universe can be constructed with a brane embedded in either AdS [41–56] or an AdS black hole [57–62, 211, 212].

In either of the above cases, however, the cosmological evolution on the brane is modified at small scales. In particular, if the bulk space is taken to be an AdS black hole *with charge*, the universe can 'bounce' [210]. That is, the brane makes a smooth transition from a contracting phase to an expanding phase. From a four-dimensional point of view, singularity theorems [99] suggest that such a bounce cannot occur as long as certain energy conditions apply. Hence a key ingredient in producing the bounce is the fact that the bulk geometry may contribute a negative energy density to the effective stress-energy on the brane [213]. At first sight these bouncing braneworlds are quite remarkable, since they provide a context in which the evolution evades any cosmological singularities yet the dynamics are still controlled by a simple (orthodox) effective action. In particular, it seems that one can perform reliable calculations without deliberating on the effects of quantum gravity or the details of the ultimate underlying theory. Hence several authors [214–221] have pursued further developments for these bouncing braneworlds. In particular, ref. [221] presents a critical examination of the phenomenology of these cosmologies.

In the following we re-examine these bouncing brane cosmologies, paying careful attention to the global structure of the bulk space-time. We find that generically these cosmologies are in fact singular. In particular, we show that a bouncing brane must cross the Cauchy horizon in the bulk space. However, the latter surface is unstable when arbitrarily small excitations are introduced in the bulk space-time. The remainder of the chapter is organized as follows: We review the construction of the bouncing braneworld cosmologies in Section 4.1. Section 4.2 presents a discussion of the global structure of the full five-dimensional space-time and the instability associated with the Cauchy horizon. We conclude in Section 4.3 with a brief discussion of our results.

4.1 Construction of a bouncing braneworld

We consider a four-dimensional brane coupled to five-dimensional gravity with the following action

$$\mathcal{I} = \frac{1}{16\pi G_5}\int_{\mathcal{M}} d^5x\sqrt{-g}\left[R_5 + \frac{12}{L^2} - \frac{1}{4}F^2\right] - \frac{3}{4\pi G_5\lambda}\int_{\mathcal{B}} d^4x\sqrt{-\gamma} + \int_{\mathcal{B}} d^4x\sqrt{-\gamma}\mathcal{L}\,. \quad (4.1)$$

Here, R_5 denotes the Ricci scalar for the bulk metric, $g_{\mu\nu}$, and $F_{\mu\nu}$ is the field strength of a bulk gauge field. The (negative) bulk cosmological constant is given by $\Lambda_5 = -6/L^2$, while the brane tension is $T = \frac{3}{4\pi G_5\lambda}$. The length scales L and λ are introduced here to simplify the following analysis. The induced metric on the brane is denoted by γ_{ab}. With the last term in the action (4.1), we have allowed for the contribution of extra field degrees of freedom which are confined to the brane, *e.g.*, the standard model fields in a RS2 scenario [40].

The bulk equations of motion are satisfied by the five-dimensional charged AdS black hole solution with metric

$$ds_5^2 = -V(r)\,dt^2 + \frac{dr^2}{V(r)} + r^2 d\Sigma_k^2\,, \tag{4.2}$$

where

$$V(r) \equiv \frac{r^2}{L^2} + k - \frac{\mu}{r^2} + \frac{q^2}{3r^4} \tag{4.3}$$

and the gauge potential is $A_t = \frac{q}{2r^2}$. In the metric above, $d\Sigma_k^2$ denotes the line element on a three-dimensional sphere, flat space or hyperbolic plane for $k = +1, 0$ or –1, respectively (with unit curvature for the cases $k = \pm 1$). The parameters μ and q appearing in the solution are related to the ADM mass and charge of the black hole — see, *e.g.,* [221, 222]. Note that this solution contains a curvature singularity at $r = 0$, but if μ is large enough, there are two horizons at radii $r = r_\pm$ solving $V(r_\pm) = 0$. A Penrose diagram illustrating the maximal analytic extension of such a black hole space-time is given in Figure 4.1. In different parameter regimes, the positions of these two horizons may coincide (or vanish, *i.e.*, $r_\pm$ become complex) to produce an extremal black hole (or a naked singularity). We will not consider these cases in the following.

The brane is modelled in the usual thin-brane approximation. That is, its worldvolume is a hypersurface, $\mathcal{B}$, which divides the bulk space-time, $\mathcal{M}$, into two regions. At this hypersurface, the bulk metric is continuous but not differentiable. Using the standard Israel junction conditions [223] (see also [224]), the discontinuity in the extrinsic curvature is interpreted as a δ-function source of stress-energy due to the brane. Then, defining the discontinuity in the extrinsic curvature across $\mathcal{B}$ as $\mathcal{K}_{ab} \equiv K^+_{ab} - K^-_{ab}$, the surface stress-tensor is given by

$$S_{ab} = \frac{1}{8\pi G_5}\left(\mathcal{K}_{ab} - \gamma_{ab}\,\mathcal{K}^c{}_c\right)\ . \tag{4.4}$$

In the case of an empty brane with only tension (*i.e.*, a brane on which no internal degrees of freedom are excited), one has $S_{ab} = -T\gamma_{ab}$.

The construction of the braneworld cosmology [211, 212] then proceeds by taking two copies of the AdS black hole geometry, identifying a four-dimensional hypersurface $r = a(\tau)$, $t = b(\tau)$ in each, cutting out the space-time regions beyond these hypersurfaces and ‘gluing’

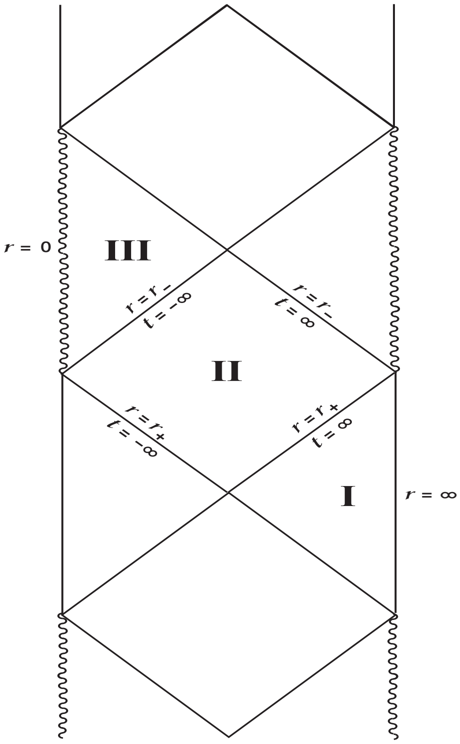

Figure 4.1: Penrose diagram for maximally extended AdS Reissner-Nordström black hole.

the two remaining space-times along these surfaces. While asymmetric constructions are possible (see *e.g.*, [221]), we will focus on the case where the two bulk space-time geometries are characterized by the same physical parameters (μ, q, L). With this choice, the calculation of the surface stress-tensor simplifies, since $\mathcal{K}_{ab} = 2K^+_{ab}$. Note, however, that the gauge fields are chosen with opposite signs on either side of the brane. Then the flux lines of the bulk gauge field extend continuously over the brane, starting from a positively-charged black hole on one side and ending on the negatively-charged one on the other. In this case, the brane carries no additional charges. We will return to consider a charged brane in the discussion section. Since the black hole geometry includes two separate, asymptotically AdS regions, an economical approach to this construction would be to glue together two mirror surfaces in each of the asymptotic regions.[1]

Of course, the hypersurface described above must be determined to consistently solve the Einstein equations (or alternatively, the Israel junction conditions (4.4)) for a physically reasonable surface stress-tensor. Here we follow the analysis of ref. [211, 212]. Identifying the time coordinate on the brane as the proper time, τ, fixes

$$V(a)\,\dot{b}^2 = \frac{\dot{a}^2}{V(a)} + 1\ . \tag{4.5}$$

The induced metric then takes a standard FRW form:

$$ds^2 = \gamma_{ab}\,dx^a dx^b = -d\tau^2 + a(\tau)^2 d\Sigma_k^2\ . \tag{4.6}$$

Again, the brane worldvolume in the bulk space-time (4.2) is given by $r = a(\tau)$ and $t = b(\tau)$ and so the Israel junction conditions (4.4) imply

$$\frac{\left(V(a) + \dot{a}^2\right)^{1/2}}{a} = \frac{1}{\lambda} + \frac{4\pi G_5}{3}\rho\ , \tag{4.7}$$

where the ‘dot’ denotes ∂_τ, and we have included a homogeneous energy density ρ for brane matter. Stress-energy conservation would imply that the latter satisfies $\dot{\rho} + 3\frac{\dot{a}}{a}\,(\rho + p) = 0$, where p is the pressure due to brane matter.

---

[1] Note that this periodic construction is distinct from the RS1 models [39], *e.g.*, there is a single positive tension brane here, rather than two branes one of which has a negative tension.

A conventional cosmological or FRW constraint equation for the evolution of the brane is produced by squaring eq. (4.7):

$$\left(\frac{\dot{a}}{a}\right)^2 + \frac{k}{a^2} = \frac{1}{\ell^2} + \frac{\mu}{a^4} - \frac{q^2}{3a^6} + \left(\frac{1}{T\lambda}\right)^2 \left(2T\rho + \rho^2\right) \ . \tag{4.8}$$

Here, we have defined a 'vacuum' curvature scale on the brane as

$$\frac{1}{\ell^2} \equiv \frac{1}{\lambda^2} - \frac{1}{L^2} \ . \tag{4.9}$$

Implicitly, ℓ^2 is assumed to be positive here, which leads to the cosmological evolution being asymptotically de Sitter. However, this assumption is inconsequential for analysis of the cosmological bounce which follows. We can also write out the effective cosmological and Newton constants in the four-dimensional braneworld as

$$\Lambda_4 \equiv \frac{3}{8\pi G_4}\frac{1}{\ell^2} = \frac{T}{2}\left(1 - \left(\frac{\lambda}{L}\right)^2\right) \ , \qquad\qquad G_4 \equiv \frac{G_5}{\lambda} \ , \tag{4.10}$$

where the latter comes from matching the term in eq. (4.8) linear in ρ to the conventional FRW equation in four dimensions: $\left(\frac{\dot{a}}{a}\right)^2 + \frac{k}{a^2} = \frac{8\pi G_4}{3}\rho$. Of course, the FRW constraint in this braneworld context also comes with an unconventional term quadratic in ρ [41–56].

The bulk geometry introduces various sources important in the cosmological evolution of the brane. The mass term, μ/a^4, behaves like a conventional contribution coming from massless radiation. The charge term, $-q^2/a^6$, introduces a more exotic contribution with a *negative* energy density. This is another example of the often-noted result that the bulk contributions to the effective stress-energy on the brane [225, 226] may be negative — see, *e.g.*, [213].

Many exact and numerical solutions for the Friedmann equation (4.8) can be obtained in various situations, *e.g.*, [214–220]. However, one gains a qualitative intuition for the solutions in general by rewriting eq. (4.8) in the following form:

$$0 = \dot{a}^2 + U(a) \ , \tag{4.11}$$

where

$$\begin{aligned} U(a) &= V(a) - \frac{a^2}{\lambda^2} \qquad (4.12) \\ &= k - \frac{\mu}{a^2} + \frac{q^2}{3a^4} - \frac{a^2}{\ell^2} \end{aligned}$$

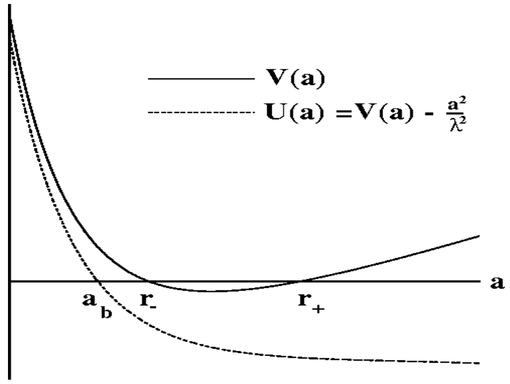

Figure 4.2: Effective potential, $U(a)$, appearing in eq. (4.11) for the evolution of the scale factor, $a(\tau)$. The turning point, a_b, occurs inside the Cauchy horizon r_-.

and for simplicity we have assumed an empty brane, *i.e.*, $\rho = 0$. In this form, we recognize the evolution equation as the Hamiltonian constraint for a classical particle with zero energy, moving in an effective potential $U(a)$. In this case, the transition regions where the braneworld cosmology 'bounces' are identified with the turning points of the effective potential. We have also expressed the latter in terms of the metric function $V(a)$ in eq. (4.12) because we will want to discuss the position of the turning points relative to the position of the 'horizons', *i.e.*, $r_\pm$. Recall that we assume the bulk solution corresponds to a black hole with a nondegenerate event horizon. That is, we will assume that there are two distinct solutions, $r_\pm$, to $V(r) = 0$. Then, there are two physically distinct possibilities for a bounce.

The first only occurs with $k = +1$, *i.e.*, with a spherical brane world, and positive ℓ^2 (or equivalently $\Lambda_4 > 0$). In this case, at large a, the effective potential becomes large and negative. The next most important contribution at large a is the constant term k and hence if $k = +1$, the potential may have a zero at large a. This bounce is typical of those one might find in a de Sitter-like space-time, *e.g.*, [227, 228]. It is driven by the spatial curvature and occurs as long as the effective energy density from the bulk black hole contributions or braneworld degrees of freedom is not too large. The turning point occurs at some large a_{dS} and in particular, it is not difficult to show that $a_{dS} > r_+$. That is, the brane bounces before reaching the black hole. In fact the presence of the black hole with or without charge is really irrelevant to this kind of

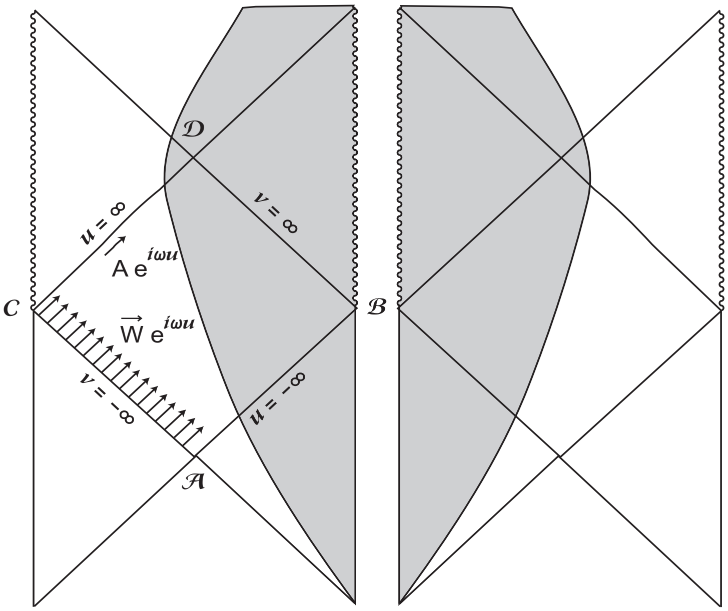

Figure 4.3: Penrose diagram for a bouncing braneworld model with ingoing modes at the event and Cauchy horizons. The grey areas are those regions of space-time that are cut out in the construction, with identification performed along the boundary.

bounce. For example, setting $\mu = 0 = q$ in eq. (4.12) produces a de Sitter cosmology on the empty brane.

The second type of bounce is generic for a wide range of parameters. It occurs at small a where the positive q^2/a^4 term dominates the potential (4.12), *i.e.*, where the exotic negative energy dominates the Friedmann constraint (4.8). As is clear from the first line of eq. (4.12), $U(a) < V(a)$ and therefore the turning point occurs at a_b, inside the position of the Cauchy horizon, *i.e.*, $a_b < r_-$, as illustrated in Figure 4.2. The latter result will be essential in the following discussion.

The Penrose diagram for the bouncing braneworld cosmologies is shown in Figure 4.3. In the 'cut and paste' procedure outlined above, the singularity on the right side of the first black hole is cut out, but the singularity on the left remains. Hence the remaining portion of the $r = r_-$ surface is still a Cauchy horizon.

Note that in Figure 4.3, the brane trajectory enters the region between the horizons across the segment $\mathcal{AB}$ and exits across the opposite segment $\mathcal{CD}$. One can verify that this occurs in all cases using eqs. (4.7) and (4.5). From the latter, we find that

$$\dot{t} = \pm \frac{a}{V(a)} \left(\frac{1}{\lambda} + \frac{4\pi G_5}{3} \rho \right) \; . \tag{4.13}$$

If the brane tension and the energy density, ρ, are both assumed to be always positive, then the last factor is always positive. Furthermore, for $r_- < a < r_+$, $V(a) < 0$. Hence the right hand side above is nonzero and has a definite sign for the entire range $r_- < a < r_+$. Therefore $\dot{t}$ cannot change sign along the brane trajectory within the black hole interior. It then follows that if a trajectory starts at a point on $\mathcal{AB}$ with $(t, r) = (\infty, r_+)$, then it must run across the black hole interior to a point on $\mathcal{CD}$ with $(t, r) = (-\infty, r_-)$ — see Figures 4.1 and 4.3.

4.2 Instability analysis

In the previous section, we reviewed the construction of a broad family of bouncing braneworld cosmologies [210]. A key result was that the turning point for the brane's trajectory in the bulk geometry was inside the Cauchy horizon of the charged AdS black hole. However, previous studies in classical general relativity found that the Cauchy horizon is unstable when generic perturbations are introduced for charged black holes in asymptotically flat [108, 229, 230], or de Sitter [231–233] spaces. Below, we will show that the same instability arises in the asymptotically AdS case as well. This is problematic for the bouncing braneworld cosmologies, as generically the contracting brane will reach a curvature singularity before it begins re-expanding.

In the following, we demonstrate the instability of the Cauchy horizon to linearized perturbations in the bulk. Our approach will be two-fold. We begin by examining linearized fluctuations of a massive Klein-Gordon field propagating in the background. Secondly, we consider gravitational and electromagnetic perturbations. In both cases, it is found that an observer crossing the Cauchy horizon would measure an infinite flux from these modes. The expectation is then that the full nonlinear evolution, including the back-reaction on the background metric, will produce a curvature singularity.

Many of the expressions appearing in the linearized analysis involve the surface gravities of the two horizons in the background. The surface gravities are given, as usual, by

$$\kappa_\pm = \frac{1}{2}\left|\frac{dV}{dr}\right|_{r=r_\pm} . \tag{4.14}$$

An important observation in the following is that $\kappa_+/\kappa_- < 1$, which follows from $r_- < r_+$. Now it will be convenient to define the event and Cauchy horizons implicitly by reexpressing the metric function (4.3) as

$$V(r) = \frac{(r^2 - r_+^2)(r^2 - r_-^2)(r^2 + r_0^2)}{L^2 r^4} . \tag{4.15}$$

This expression also defines r_0 as determining the complex roots of $V(r)$. Further, the analysis is facilitated by introducing some new coordinates to describe the background geometry (4.2). In particular, we define the radial tortoise coordinate

$$r_* \equiv \frac{1}{2\kappa_+}\log\frac{|r - r_+|}{r + r_+} - \frac{1}{2\kappa_-}\log\frac{|r - r_-|}{r + r_-} + \frac{r_0^3 L^2}{(r_0^2 + r_-^2)(r_0^2 + r_+^2)}\tanh^{-1}\frac{r}{r_0} , \tag{4.16}$$

which is chosen to satisfy $dr_* = dr/V(r)$. The focus of the following analysis will be the behavior of linearized perturbations in the range $r_- < r < r_+$ (*i.e.*, region II in Figure 4.1). In this region, we have $r_* \to \pm\infty$ as $r \to r_\mp$. Finally, it will be useful to work with null coordinates,

$$u = r_* - t , \qquad v = r_* + t , \tag{4.17}$$

with which the line element becomes $ds^2 = V(r)du\,dv + r^2 d\Sigma_k^2$.

The massive Klein-Gordon equation in the charged black hole background (4.2) may be expanded as

$$-\frac{1}{V(r)}\partial_t^2\Phi + V(r)\partial_r^2\Phi + \frac{1}{\sqrt{-g}}\partial_r\left(\sqrt{-g}\,V(r)\right)\partial_r\Phi + \frac{1}{r^2}\nabla_k^2\Phi - M^2\Phi = 0 , \tag{4.18}$$

where we write ∇_k^2 for the Laplacian on the three-dimensional space Σ_k appearing in the line element (4.2). The eigenvalue problems for ∂_t^2 and ∇_k^2 each have known solutions with eigenvalues, say, $-\omega^2$ and $-n_k^2$. Hence by separation of variables, the Klein-Gordon equation is reduced to a single ordinary differential equation for $\Phi(r)$,

$$-\partial_{r_*}^2\tilde{\Phi} + V(r)\left(\frac{n_k^2}{r^2} + M^2 + \frac{3V'}{2r} + \frac{3V}{4r^2}\right)\tilde{\Phi} = \omega^2\,\tilde{\Phi} , \tag{4.19}$$

where we have introduced the tortoise coordinate (4.16) and rescaled $\tilde{\Phi} = r^{3/2}\Phi$.

As we approach the Cauchy horizon, the second term on the left hand side of eq. (4.19) vanishes, leading to oscillatory solutions $\exp(\pm i\omega r_*)$. Now, the flux seen by an observer freely falling across the horizon, with five-velocity U^μ, is proportional to the square of the scalar $\mathcal{F} = U^\mu \partial_\mu \Phi$. $\mathcal{F}$ then includes a contribution proportional to $e^{\kappa_- u}\partial_u \tilde{\Phi}$ near the Cauchy horizon. Since the solutions of eq. (4.19) are oscillatory as $r \to r_-$, we have that this term, and hence $\mathcal{F}$, diverges. Similar divergences appear in the observed energy density for these linearized perturbations, and so the expectation is that when back-reaction is included, the metric will develop a curvature singularity.

Next we proceed to a more rigorous analysis of metric and Maxwell field perturbations, following the method of Chandrasekhar and Hartle [108, 229, 230]. We are simply establishing the existence of unstable modes and so, for simplicity, we fix $k = 0$ and consider an "axial" perturbation of one of the flat space coordinates. However, the extension of this analysis to general perturbations and backgrounds is straightforward.

The unperturbed bulk metric (4.2) is

$$ds^2 = -V(r)\,dt^2 + \frac{dr^2}{V(r)} + \frac{r^2}{L^2}(dx^2 + dy^2 + dz^2)\ , \tag{4.20}$$

where $V(r)$ is as given in eq. (4.3) with $k = 0$. We now focus on a class of perturbations where this metric is modified by replacing

$$dz \to dz + q_t(t,r)dt + q_r(t,r)dr\ . \tag{4.21}$$

Similarly for the Maxwell field, we introduce perturbations: $\delta\mathbf{F} = (f_{tz}(t,r)\mathbf{d}t + f_{rz}(t,r)\mathbf{d}r) \wedge \mathbf{d}z$. The linearization of the bulk Einstein and Maxwell equations about the background solution may be reduced to a single Schrödinger-like equation:

$$\begin{aligned} \left(\frac{d^2}{dr_*^2} + \omega^2\right) F &= \frac{V}{r}\left(\frac{4q^2}{r^5} - \frac{V}{4r} + \frac{V'}{2}\right) F\ , && (4.22) \\ &= W(r)\,F\ . && (4.23) \end{aligned}$$

In this equation, we have defined $F \equiv r^{1/2} f_{tz}$ and assumed an $e^{-i\omega t}$ dependence for all fields. To apply the standard results of scattering theory below, it is important to note that the effective potential, W, is bounded, negative and integrable throughout the black hole interior.

Further, we note that the effective potential vanishes as $\exp(\pm\kappa_\pm r_*)$ for $r_* \to \mp\infty$. The other components of the perturbation are related to F by

$$\begin{aligned} f_{rz} &= \frac{i}{\omega}\partial_r(F/r^{1/2})\,, \\ Q_{tr} &= -4i\frac{q\,L^2}{\omega\,r^{11/2}}F\,, \end{aligned} \tag{4.24}$$

where $Q_{tr} = \partial_t q_r - \partial_r q_t$. Note that the linearized equations only fix the metric perturbations, q_r and q_t, up to infinitesimal coordinate transformations of z, but Q_{tr} provides a gauge invariant combination which is completely determined.

To simplify our notation we will rename $x = r_*$. We then introduce a solution, F_+ to eq. (4.23) normalized so that near the event horizon, *i.e.*, $x \to -\infty$, we have

$$F_+(x,\omega) = e^{i\omega x}\,, \tag{4.25}$$

representing a mode that falls in through the event horizon at $\mathcal{A}C$. The Wronskian of any two solutions of the Schrödinger equation is conserved, so we may evaluate

$$[F_+(x,\omega), F_+(x,-\omega)] = 2i\omega \tag{4.26}$$

near the horizon. This second solution, $F_+(x,-\omega)$ is then linearly independent of $F_+(x,\omega)$, and represents an outgoing mode at the event horizon. Using these particular solutions as a basis, we may write the full solution to (4.23) as

$$F(x,t) = \int_{-\infty}^{\infty}\frac{d\omega}{2\pi}\left[\overleftarrow{W}(\omega)F_+(x,-\omega) + \overrightarrow{W}(\omega)F_+(x,\omega)\right]e^{-i\omega t}\,. \tag{4.27}$$

At present, we are only interested in the ingoing modes along $\mathcal{A}C$, whose profile is determined by $\overrightarrow{W}(\omega)$. The outgoing modes may be similarly dealt with, but extra analysis would be required to show they lead to a divergent flux. We will return to this point near the end of the section.

We are free to choose any reasonable initial profile for the ingoing modes. However, one restriction which we impose on the initial frequency distribution $\overrightarrow{W}(\omega)$ of ingoing modes is that an observer falling across the event horizon at $\mathcal{AB}$ measures a finite flux. The flux for such an observer contains a term $\mathcal{F} \sim e^{-\kappa_+ u}\partial_u F$. Hence considering eq. (4.27), we require that $\vec{W}(\omega)$ have at least one pole with $\mathcal{I}m(\omega) \leq -\kappa_+$.

The initially-ingoing modes are scattered by the potential in region II, leading to both ingoing and outgoing modes at the Cauchy horizon. It is useful therefore to have another basis of solutions that describes purely in and outgoing modes at the Cauchy horizon. As before, we normalize our solutions so that when $x \to \infty$

$$F_-(x,\omega) = e^{-i\omega x} \, , \tag{4.28}$$

is purely ingoing at the Cauchy horizon. The second independent solution is taken to be $F_-(x,-\omega)$, and represents an outgoing mode.

Since both sets of modes form a basis for the full solution, they must be linearly related. In particular, there must be an $A(\omega)$ and $B(\omega)$ such that

$$F_+(x,\omega) \quad = \quad A(\omega)F_-(x,-\omega) + B(\omega)F_-(x,\omega) \, . \tag{4.29}$$

The full solution then becomes

$$\begin{aligned} F(x,t) &= \int_{-\infty}^{\infty} \frac{d\omega}{2\pi} \vec{W}(\omega) \left[A(\omega)F_-(x,-\omega) + B(\omega)F_-(x,\omega)\right] e^{-i\omega t} \, , && (4.30) \\ &\to \int_{-\infty}^{\infty} \frac{d\omega}{2\pi} \vec{W}(\omega) \left[A(\omega)e^{i\omega u} + B(\omega)e^{-i\omega v}\right] \, , && (4.31) \end{aligned}$$

near the Cauchy horizon.

Clearly, the dominant contribution to the flux at the Cauchy horizon results from

$$\mathcal{F} \sim e^{\kappa_- u} \int_{-\infty}^{\infty} d\omega \, \omega \, \vec{W}(\omega) A(\omega) e^{i\omega u} \, . \tag{4.32}$$

In terms of the Schrödinger equation describing the perturbations, it is the modes that are “transmitted” across the potential that constitute this potentially-divergent flux. These modes skim along just outside the Cauchy horizon heading towards the brane. This integral may be computed by closing the contour in the upper-half-plane. To do so requires a knowledge of the the analyticity of $A(\omega)$ in the upper half plane, which can be achieved using arguments similar to those in [108, 229, 230, 234].

By calculating the Wronskian of F_+ with F_- and evaluating near the Cauchy horizon we can write

$$\begin{aligned} [F_+(x,\omega), F_-(x,\omega)] &= 2i\omega A(\omega)\ , && (4.33) \\ [F_+(x,\omega), F_-(x,-\omega)] &= -2i\omega B(\omega)\ . && (4.34) \end{aligned}$$

Investigating the analytic properties then comes down to considering the analyticity of the solution $F_+(x,\omega)$ and $F_-(x,\pm\omega)$. We will do so by transforming the Schrödinger equation into an integral equation that can be solved iteratively. Requiring that the iterates be analytic will give the desired boundary on the domain of analyticity.

We'll deal exclusively with $F_+(x,\omega)$, though the other solutions will be similar. Using the Green's function

$$G(x-x') = \frac{\sin\omega(x-x')}{\omega}\theta(x-x')\ , \tag{4.35}$$

the Schrödinger equation becomes an inhomogeneous Volterra equation

$$F_+(x,\omega) = e^{i\omega x} + \int_{-\infty}^{x} \frac{\sin\omega(x-x')}{\sigma} W(x') F_+(\omega,x')\,dx'\ . \tag{4.36}$$

Equations such as this can be solved by an iterative procedure that will break-down where the solution is no longer an analytic function of ω. Specifically, we take our solution to be

$$F_+(x,\omega) = \sum_{n=0}^{\infty} F_+^{(n)}(x,\omega)\ , \tag{4.37}$$

where $F_+^{(0)} = \exp(i\omega x)$ and

$$\begin{aligned} F_+^{(n)}(\omega,x) &= \int_{-\infty}^{x} \frac{\sin\omega(x-x_1)}{\omega} V(x_1) F_+^{(n-1)}(\omega,x_1)\,dx_1\ , && (4.38) \\ &= \frac{e^{i\omega x}}{(-2i\omega)^n} \int_{-\infty}^{x_0} dx_1 \ldots \int_{-\infty}^{x_{n-1}} dx_n \prod_{i=1}^{n} \left\{ \left[e^{-2i\omega(x_{i-1}-x_i)} - 1 \right] V(x_i) \right\} && (4.39) \end{aligned}$$

To find the domain in which F_+ is analytic, we use a theorem from analysis [234] that states a function expressed as

$$F(\omega) = \int_{-\infty}^{x} G(\omega,x')\,dx' \tag{4.40}$$

will be analytic in z if the integrand is analytic in ω, continuous in x' and the integral is uniformly convergent for large negative x. Clearly, $F_+^{(0)}$ is analytic in ω and continuous in x', so one need only show that the integral defining $F_+^{(1)}$ is uniformly convergent for large negative x to prove $F_+^{(1)}$ is analytic in ω. Having shown this, one may proceed by induction to show that all the $F_+^{(n)}$ are analytic.

Proving analyticity requires the integral converge uniformly, but only in the limit $x \to -\infty$. It is precisely in this limit that the potential, $W(x)$, takes a particularly simple form that allows the convergence to be demonstrated. In fact, for x large and negative we have $W(x) \sim e^{2\kappa_+ x}$, but this behavior is common to all the previous studies of Cauchy horizon instabilities [108, 229, 230, 234]. The details of the proof of uniform convergence in [230, 234] are quite involved so we do not reproduce them here. It suffices to note that all that is required of the potential is the exponential vanishing near the event horizon already noted and that it be bounded and integrable in the interior. With these conditions satisfied, their results apply immediately.

The crux of the argument leading to analyticity is to notice that in the iterates there are terms proportional to $\exp(-2i\omega(x_{i-1} - x_i)) \sim \exp(2i\omega x)$ at large negative x. When $\mathcal{I}m(\omega)$ is positive this can lead to divergences in the integrals that may not be sufficiently damped by the vanishing of the potential. This places a bound

$$\mathcal{I}m(\omega) < \kappa_+ \tag{4.41}$$

on the domain for which the integral converges. Using contour rotation, analyticity can be extended to the entire plane with the exception of a cut on the positive imaginary axis starting at $i\kappa_+$ and extending upward [234]. In fact, this argument can be further refined to show that there is a series of poles on the imaginary axis at $\omega = in\kappa_+$, where $n = 1, 2, \ldots$ [230]. Obviously, similar arguments will hold when one considers the functions $F_-(x, \pm\omega)$, though of course uniform convergence must now be checked near the Cauchy horizon. The result is that $F_-(x, \omega)$ is an analytic function of ω in the entire plane with the exception of poles along the positive imaginary axis at $\omega = in\kappa_-$.

Finally then we are in a position to consider the analyticity of $A(\omega)$. Since $A(\omega)$ is just given by the Wronskian of $F_+(x, \omega)$ and $F_-(x, \omega)$, it's domain of analyticity is just given by the intersection of the domains for the two functions. In particular, it's range of analyticity extends upward to $\omega = i\kappa_+$, where there is a pole. For simplicity, we'll further assume that $\overrightarrow{W}(\omega)$ is analytic in the strip $[0, i\kappa_+]$ and that it is nonzero for $\omega = i\kappa_+$. With these assumptions, the leading term in (4.32) is from the residue of the pole at $\omega = i\kappa_+$:

$$\mathcal{F} \sim e^{(\kappa_- - \kappa_+)u} \left\{ i\kappa_+ \overrightarrow{W}(i\kappa_+) 2\pi i \, \text{Res}\left(A(i\kappa_+)\right) \right\} \; . \tag{4.42}$$

Since $\kappa_- > \kappa_+$, this flux always diverges as $u \to \infty$. Relaxing our assumptions on the analyticity of $\overrightarrow{W}(\omega)$ in the upper half plane could lead to additional divergent contributions to the flux, but we will not consider those here.

Note that the brane and boundary conditions at the brane played no role in the scattering analysis above. While the brane will affect the complete scattering of modes inside the event horizon, the basic source of the instability is the same piling up of infalling modes on the Cauchy horizon found in previous examples [108, 229–232]. Hence we disregard the details of the scattering of modes at the brane, just as the original discussion of the instability for the Reissner-Nordström black hole [108, 229, 230] ignored the presence of a collapsing star forming the black hole.

However, for completeness, let us briefly discuss the boundary conditions which must be imposed on the perturbations at the brane. First, the metric perturbations must be matched across the brane surface so that no additional contributions are induced in the surface stress-energy (4.4). In particular, the axial perturbation (4.21) considered above induces a new $K_{\tau z}$ component in the extrinsic curvature, and this component must be continuous across the brane. Similarly, continuity is imposed on the Maxwell field strength. More precisely, to ensure that no electric charges or currents are implicitly induced on the brane, we require that all components $n^\mu F_{\mu\nu} t^\nu$ are continuous, where n^μ and t^ν are the unit normal and any tangent vector to the brane. Finally, since we are working with perturbations to the field strength directly, and not the gauge potential, we must demand continuity of the tangential components, $t_1^\mu F_{\mu\nu} t_2^\nu$, to ensure there are no magnetic charges or currents induced, *i.e.*, $\mathbf{dF} = 0$.

We close this section with a discussion of the initially-outgoing modes defined by the distribution $\overleftarrow{W}(\omega)$ in eq. (4.27). In Figure 4.3, we will primarily consider modes entering the interior region on the left through the lower portion of $\mathcal{AB}$. In this case, to contribute to the instability at the Cauchy horizon $\mathcal{CD}$, these modes must be reflected by the curvature (*i.e.*, by the effective potential in eq. (4.23) to become ingoing). This scattering leads to a different analytic structure in eq. (4.31) for $A(\omega)$, describing the u-dependent modes at the Cauchy horizon. In the "un-cut" space-time with no brane in place, this structure is identical to that obtained for the contribution of the initially-ingoing modes to $B(\omega)$. Of course, inserting the brane in the black hole interior produces a more complicated scattering problem, the details of which would depend on the precise brane trajectory. For example, the outgoing flux would receive additional contributions from perturbations transmitted across the brane from the right hand side of Figure 4.3, as well as from initially-ingoing modes which are back-scattered by the brane. We did not attempt a detailed study of these contributions.

Now, following the standard analysis with no brane in place, we find the contribution to the flux of ingoing modes by considering the Wronskian of $F_+(x, -\omega)$ and $F_-(x, \omega)$. This leads to analyticity in the semi-infinite strip $(-i\kappa_+, i\kappa_-)$. If we assume that $\overleftarrow{W}(\omega)$ is analytic in the strip $(0, i\kappa_-)$, then we would find, upon closing the contour in the upper-half-plane, that the contribution to the flux is finite. However, it is consistent with the requirement that an observer crossing $\mathcal{AC}$ measure a finite flux, to allow $\overleftarrow{W}(\omega)$ to have poles in the range $\kappa_+ \leq \mathcal{I}m(\omega) < \kappa_-$. With such a choice, there will be divergent contributions to the flux, provided that the residue of A is nonzero at these poles. This effect differs from that discussed above in that the leading contribution to the flux comes from a pole in the initial frequency distribution rather than the scattering coefficient $A(\omega)$. A similar discussion played an important role in demonstrating the instability of the Cauchy horizon of de Sitter-Reissner-Nordström black holes over the entire range of physical parameters [233].

4.3 Discussion

One of the most interesting features of the braneworld cosmologies presented in ref. [210] is that, while they seem to evade any cosmological singularities, their evolution is still determined by a simple effective action, albeit in five dimensions. However, our present analysis indicates that instabilities arise in the five-dimensional space-time, and that the brane will generically encounter a curvature singularity before bouncing. The two essential observations leading to this result were: i) the turning point for the brane cosmology occurs inside the Cauchy horizon of the maximally-extended geometry of the charged AdS black hole and ii) a standard analysis within classical general relativity shows that the Cauchy horizon is unstable against even small excitations of the bulk fields.

Our analysis was at the level of linearized perturbations and hence did not take into account any back-reaction. We therefore cannot conclusively say whether the infinite flux will actually cause a curvature singularity to form near the Cauchy horizon. In a series of papers, Poisson and Israel [235–237] addressed this question for four-dimensional solutions with an inner Cauchy horizon. They found that the presence of infinitely blueshifted modes *and* an arbitrarily small flux of modes falling across the Cauchy horizon causes a classically unbounded inflation of the effective internal gravitational-mass. This mass inflation causes curvatures to grow without bound in a vicinity of the Cauchy horizon. The fluxes studied by Poisson and Israel had their origin in the radiative tail produced in the gravitational collapse which formed the black hole. The bouncing brane models are constructed from eternal black holes so would not have this particular source, however the main properties of mass inflation are insensitive to the precise nature of the blueshifted flux [238], so on can expect the same conclusion to follow.

Note that from these results we cannot conclude that the brane does not bounce, but rather due to the appearance of curvature singularities, the evolution can not be reliably studied with the original low energy action (4.1). Of course, one may ultimately have reached this conclusion since the full bulk space-time still includes a curvature singularity at $r = 0$ — see Figure 4.3. However, while the latter remains distant from the brane, those at the Cauchy horizon are of more immediate concern as they intersect the brane's trajectory.

In the discussion of metric and gauge field perturbations in Section 4.2, we fixed $k = 0$ and limited ourselves to modes that depended only on t and r to simplify the discussion. One may be concerned by the fact that these modes have infinite extent in the three-dimensional flat space and so we present a brief discussion of the full analysis. Generalizing our results to the most general perturbation is straightforward but tedious. For an arbitrary linearized perturbation, the separation of variables would naturally lead to considering Fourier components in the (x, y, z) directions with a factor $\exp(i\vec{n} \cdot \vec{x})$. Since we require a superposition of these modes for many different $\vec{n}$ to localize the perturbation, we cannot simply rotate in the flat space to remove the dependence on one of the spatial coordinates. Thus the general analysis necessarily involves an ansatz for the perturbations dependent on all five coordinates, which, of course, requires extending the perturbations to additional components of both the metric and gauge field. Appropriate linear combinations of these perturbations would decouple, giving a set of Schrödinger-like equations, similar to that found above. While the potentials in each of these equations is different, there are typically simple relationships between them implying relations between the solutions — for further discussion of these relations, see [108, 229, 230]. Then it is sufficient to solve only one of the equations, and the analysis, and the results, are essentially the same as presented above

Of course, our preliminary analysis with massive Klein-Gordon modes included all of the spatial modes, and further applied for all of the possible values of k, specifying the spatial curvature on the brane. In all cases, there was an infinite flux of these modes at the Cauchy horizon. While further analysis of the full scattering and boundary conditions would be required to make this consideration of fluxes rigorous, the end result would be the same. Hence we are confident that the results for the metric and gauge field perturbations with $k = 0$ also carry over for $k = \pm 1$.

Recall that, as discussed in Section 4.1, an apparently economical approach to constructing these bouncing cosmologies would be to cut and paste along two mirror surfaces in each of the separate asymptotically AdS regions of the black hole geometry. In such a periodic construction the nature of the singular behavior would be slightly different. As discussed around eq. (4.13), the brane trajectory is unidirectional in the coordinate time, t. Hence in Figure 4.3, if a brane enters the event horizon to the right of the bifurcation surface $\mathcal{A}$, then it must exit through the Cauchy horizon to the left of $\mathcal{D}$. However, the same result requires that a brane trajectory entering to the left of $\mathcal{A}$ exits to the right of $\mathcal{D}$. Therefore in the periodic construction above, the two mirror trajectories must cross at some point in the region $r_- < r < r_+$, as illustrated in Figure 4.4. Hence the evolution is singular in that the fifth dimension collapses to zero size in a finite proper time. One redeeming feature of this collapse is that the curvature remains finite, and hence one might imagine that there is a simple continuation of the evolution in which this ‘big crunch’ is matched onto a ‘big bang’ geometry. Similar collapsing geometries have been a subject of great interest in the string theory community recently — see, *e.g.*, [239–254]. Resolving precisely how the space-time evolves beyond such a 'big crunch' is an extremely difficult question and as yet string theory seems to have produced no clear answer. In particular, it seems that these geometries are also subject to gravitational instabilities [255–257] not dissimilar to those found here. In the present context, the situation is further complicated as the precise matching procedure for the background geometry is obscure. Naively, one might be tempted to continue beyond the collapse point $\mathcal{E}$ with the doubly shaded region in Figure 4.4. However, a closer examination shows that the brane would have a negative tension in this geometry. The other natural alternative is to match the crunch at $\mathcal{E}$ to the big bang emerging from $\mathcal{F}$, but the gap in the embedding geometry would seem to complicate any attempts to make this continuation precise. In any event, it is clear that once again these knotty questions can not be resolved using the low energy action (4.1) alone but, rather, one would have to embed this scenario in some larger framework, *e.g.*, string theory.

Much of our discussion has focused on bouncing cosmologies stemming from an empty four-dimensional brane, but the analysis and the results are easily extended to other cases. One simple generalization would be for higher-dimensional cosmologies following, *e.g.*, [219, 220]. The instability found here would also appear in the asymmetric constructions discussed in ref. [221].

A more interesting generalization to consider is adding matter excitations on the brane. As long as the energy density is positive, such matter contributions will not affect the result that the brane crosses the Cauchy horizon. At first sight, it would also seem that reasonable brane matter cannot prevent the bounce. The negative energy contribution arising from the bulk charge is proportional to $1/a^6$. For a perfect fluid (in four dimensions), this would require the stiffest equation of state consistent with causality [258], *i.e.*, $p = \rho$. For example, a coherently rolling massless scalar field would yield $\rho \propto 1/a^6$. Hence it would seem that the term $-q^2/a^6$ would dominate the ρ contribution coming from brane matter and a bounce would be inevitable. However, ref. [221] recently pointed out the ρ^2 contribution in the FRW constraint (4.8) can prevent a bounce. In fact, with any equation of state $p = w\rho$ with $w \geq 0$, this contribution can dominate the bulk charge contribution. Hence with a sufficiently large initial energy density on the brane, a big crunch results on the brane. This crunch corresponds to the brane trajectory

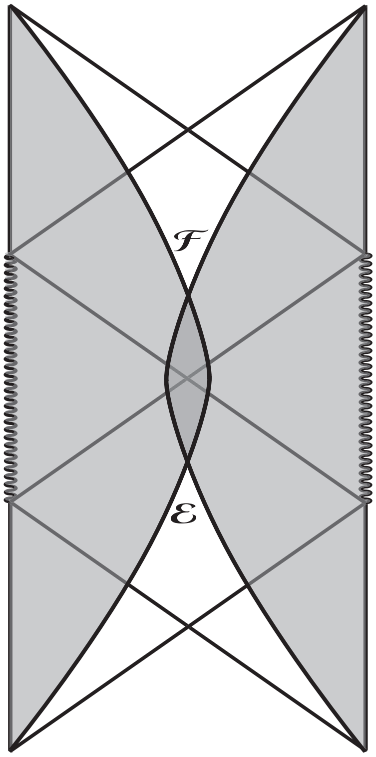

Figure 4.4: Penrose diagram for periodic construction of the braneworld cosmology.

falling into the bulk singularity at $r = 0$. It then follows that the brane must cross the Cauchy horizon in this case as well, and we expect singularities to develop there with generic initial data.

More broadly, mirage cosmologies [57–62] are induced by the motion of a brane in a higher-dimensional space-time. A general warning which the present analysis holds for these models is that Cauchy horizons are quite generally unstable. Hence if a particular solution involves a brane traversing such a surface in the bulk space-time, one should expect that these cosmologies will encounter singularities for generic initial data.

At this point, we observe that in the literature much of the discussion of these brane cosmologies treats the brane as a fixed point of a Z_2 orbifold, rather than making a symmetric construction as discussed in Section 4.1. As discussed there, one must flip the sign of the gauge potential in the background solution on either side of the brane in order that the brane is transparent to field lines. In contrast for a Z_2 orbifold, the field lines end on the brane. As there is no natural coupling of a one-form potential to a three-brane in five dimensions, the model must be extended to include charged matter fields on the brane. One comment is that as the action (4.1) does not explicitly include these degrees of freedom or their coupling to the Maxwell field, we cannot be sure that the analogous construction to that presented in Section 4.1 will yield a consistent solution of all of the degrees of freedom. One might also worry that the simplest solutions would have additional instabilities associated with having a homogeneous charge distribution throughout the brane.

Chapter 5

Conclusion

While instabilities may seem to be ubiquitous in higher-dimensional theories of gravity, their existence need not be viewed negatively. Indeed, it is often problems such as these that are the impetus for the new directions in physics that lead to important discoveries. A classic example of this are the singularity theorems of Hawking and Penrose — for a review see [259] — in which the development of singularities *i.e.*, points in space-time where general relativity breaks down are a common prediction of general relativity itself. The quest for a theory that resolves these singularities has fueled some of the progress in string theory and quantum gravity.

Likewise, though in a more modest sense, one is led in new directions by the results we have presented here. The discovery of instabilities of static black strings led to many insights, including the existence of new nonuniform static solutions of general relativity [65, 67, 68]. The same can be said of the unstable boosted solutions considered in Chapter 2. The construction and interpretation of the corresponding nonuniform boosted solutions is an ongoing project [129]. However, these are not the only new solutions expected.

One of the interesting observations of Section 2.3.1 was that, at least in the large-ring limit, the black ring configuration is essentially determined by the energy density and tension of the static black string. Hence this invalidates arguments restricting black rings to five dimensions based on the interplay of the gravitational potential and centripetal barrier, which have the same radial dependence in precisely five dimensions. Rather it would seem that there should be black ring solutions in any number of dimensions greater than four. This confirms the original intuition presented in [104] that the existence of black rings did not depend on the dimension of the space-time (as long as $D > 4$). Of course, explicitly constructing these solutions remains a challenging open problem. It seems these are simply one part of a rich multitude of solutions and physics which remains to be discovered in higher dimensions.

The fuzzball proposal of Mathur and collaborators [76, 77] is an interesting approach to understanding black hole entropy. To provide a satisfactory explanation for black holes in general we wish to go beyond the BPS sector where the program is much less developed. In particular, one must understand the analog of the ergoregion instability presented in Chapter 3 in the geometry dual to a coarse grained ensemble of the JMaRT geometries.

Further, we face the challenge of constructing a more or less complete family of microstate geometries. The existence of the JMaRT solutions indicate that at least certain non-BPS states can be described by classical geometries. However, it is not at all clear how large a class of non-supersymmetric smooth horizon-free geometries exists. Going beyond the present special class of solutions will probably call for the development of new solution-generating techniques, but the JMaRT geometries offer hope that a broader class of nonsupersymmetric solutions can be found. This will certainly be an intriguing direction for further research and will undoubtedly lead to interesting new insights and discoveries.

Bouncing cosmologies have long been of interest [260, 261]. Much of their appeal lies in their potential to provide a calculable framework to describe the origins of the universe. Apart from those discussed in Chapter 4, braneworlds and higher dimensions have inspired many attempts to model a bouncing cosmology, including: pre-big bang cosmology [262]; cyclic universes [263–265] based on a Lorentzian orbifold model [239–248]; braneworld cosmologies induced by cyclic motion in more than one extra dimensions [266, 267];[1] universes with higher form fluxes [269–282], which are related to S-brane solutions [283–286]; braneworld cosmologies [287] with an extra internal time directions [288, 289]. However, as well as the

---

[1] Ref. [268] gives a closely related construction embedded in string theory. Note, however, that from the point of view of the Einstein frame in four dimensions, there are no sources of negative energy density and the universe is static.

model discussed, none of these works has yet provided a compelling scheme which is free of pathologies or obstructions to prediction. We may take solace from the absence of any simple bounce models in that it appears that understanding the early universe and, in particular, the big bang singularity demands that we greatly expand our understanding of quantum gravity and string theory.

BIBLIOGRAPHY

[1] G. Nordstrom, Phys. Z. **13**, 1126 (1912).

[2] G. Nordstrom, Phys. Z. **15**, 504 (1914).

[3] T. Kaluza, Sitzungsber. Preuss. Akad. Wiss. Berlin (Math. Phys.) **1921**, 966 (1921).

[4] A. Pais, *'Subtle is the Lord... ' The Science and the Life of Albert Einstein* (Clarendon, 1982).

[5] T. Appelquist, A. Chodos, and P. G. O. Freund, *Modern Kaluza-Klein Theories* (Addison-Wesley, 1987).

[6] O. Klein, Z. Phys. **37**, 895 (1926).

[7] H. Mandel, Z.F. Physik **39**, 136 (1926).

[8] A. Einstein and P. Bergmann, Annals Math. **39**, 683 (1938).

[9] B. DeWitt, *Relativity, Groups, Topology* (Gordon and Breach, 1964), p. 725.

[10] A. Trautman, Rept. Math. Phys. **1**, 29 (1970).

[11] R. Kerner, Annales Poincare Phys. Theor. **9**, 143 (1968).

[12] Y. M. Cho and P. G. O. Freund, Phys. Rev. **D12**, 1711 (1975).

[13] Y. M. Cho, J. Math. Phys. **16**, 2029 (1975).

[14] Y. M. Cho and P. S. Jang, Phys. Rev. **D12**, 3789 (1975).

[15] L. N. Chang, K. I. Macrae, and F. Mansouri, Phys. Rev. **D13**, 235 (1976).

[16] E. Cremmer and J. Scherk, Nucl. Phys. **B108**, 409 (1976).

[17] J. F. Luciani, Nucl. Phys. **B135**, 111 (1978).

[18] E. Cremmer, B. Julia, and J. Scherk, Phys. Lett. **B76**, 409 (1978).

[19] P. G. O. Freund and M. A. Rubin, Phys. Lett. **B97**, 233 (1980).

[20] E. Witten, Nucl. Phys. **B186**, 412 (1981).

[21] E. Witten, In *Appelquist, T. (Ed.) et al.: Modern Kaluza-Klein Theories*, 438-511. (In *Shelter Island 1983, Proceedings, Quantum Field Theory and the Fundamental Problems of Physics*, 227-277) and preprint - Witten, E. (83,rec.Jan.84) 78 P. (see book index).

[22] R. M. Wald, *General Relativity* (The University of Chicago Press, 1984).

[23] J. D. Bekenstein, Phys. Rev. **D7**, 2333 (1973).

[24] S. W. Hawking, Commun. Math. Phys. **43**, 199 (1975).

[25] J. Polchinski, Phys. Rev. Lett. **75**, 4724 (1995), hep-th/9510017.

[26] A. Strominger and C. Vafa, Phys. Lett. **B379**, 99 (1996), hep-th/9601029.

[27] A. W. Peet, Class. Quant. Grav. **15**, 3291 (1998), hep-th/9712253.

[28] S. R. Das and S. D. Mathur, Ann. Rev. Nucl. Part. Sci. **50**, 153 (2000), gr-qc/0105063.

[29] J. R. David, G. Mandal, and S. R. Wadia, Phys. Rept. **369**, 549 (2002), hep-th/0203048.

[30] J. M. Maldacena, Adv. Theor. Math. Phys. **2**, 231 (1998), hep-th/9711200.

[31] E. Witten, Adv. Theor. Math. Phys. **2**, 253 (1998), hep-th/9802150.

[32] O. Aharony, S. S. Gubser, J. M. Maldacena, H. Ooguri, and Y. Oz, Phys. Rept. **323**, 183 (2000), hep-th/9905111.

[33] Super-Kamiokande, Y. Fukuda *et al.*, Phys. Rev. Lett. **81**, 1562 (1998), hep-ex/9807003.

[34] S. Willenbrock, (2004), hep-ph/0410370.

[35] H. E. Haber and G. L. Kane, Phys. Rept. **117**, 75 (1985).

[36] I. Antoniadis, Phys. Lett. **B246**, 377 (1990).

[37] N. Arkani-Hamed, S. Dimopoulos, and G. R. Dvali, Phys. Lett. **B429**, 263 (1998), hep-ph/9803315.

[38] I. Antoniadis, N. Arkani-Hamed, S. Dimopoulos, and G. R. Dvali, Phys. Lett. **B436**, 257 (1998), hep-ph/9804398.

[39] L. Randall and R. Sundrum, Phys. Rev. Lett. **83**, 3370 (1999), hep-ph/9905221.

[40] L. Randall and R. Sundrum, Phys. Rev. Lett. **83**, 4690 (1999), hep-th/9906064.

[41] P. Binetruy, C. Deffayet, and D. Langlois, Nucl. Phys. **B565**, 269 (2000), hep-th/9905012.

[42] N. Kaloper, Phys. Rev. **D60**, 123506 (1999), hep-th/9905210.

[43] T. Nihei, Phys. Lett. **B465**, 81 (1999), hep-ph/9905487.

[44] C. Csaki, M. Graesser, C. F. Kolda, and J. Terning, Phys. Lett. **B462**, 34 (1999), hep-ph/9906513.

[45] J. M. Cline, C. Grojean, and G. Servant, Phys. Rev. Lett. **83**, 4245 (1999), hep-ph/9906523.

[46] T. Shiromizu, K.-i. Maeda, and M. Sasaki, Phys. Rev. **D62**, 024012 (2000), gr-qc/9910076.

[47] P. Kanti, I. I. Kogan, K. A. Olive, and M. Pospelov, Phys. Lett. **B468**, 31 (1999), hep-ph/9909481.

[48] P. Kanti, I. I. Kogan, K. A. Olive, and M. Pospelov, Phys. Rev. **D61**, 106004 (2000), hep-ph/9912266.

[49] P. Binetruy, C. Deffayet, U. Ellwanger, and D. Langlois, Phys. Lett. **B477**, 285 (2000), hep-th/9910219.

[50] E. E. Flanagan, S. H. H. Tye, and I. Wasserman, Phys. Rev. **D62**, 044039 (2000), hep-ph/9910498.

[51] C. Csaki, M. Graesser, L. Randall, and J. Terning, Phys. Rev. **D62**, 045015 (2000), hep-ph/9911406.

[52] R. Maartens, D. Wands, B. A. Bassett, and I. Heard, Phys. Rev. **D62**, 041301 (2000), hep-ph/9912464.

[53] P. Kanti, K. A. Olive, and M. Pospelov, Phys. Lett. **B481**, 386 (2000), hep-ph/0002229.

[54] P. Kanti, K. A. Olive, and M. Pospelov, Phys. Rev. **D62**, 126004 (2000), hep-ph/0005146.

[55] N. Deruelle and T. Dolezel, Phys. Rev. **D62**, 103502 (2000), gr-qc/0004021.

[56] A. Kehagias and K. Tamvakis, Phys. Lett. **B515**, 155 (2001), hep-ph/0104195.

[57] A. Kehagias and E. Kiritsis, JHEP **11**, 022 (1999), hep-th/9910174.

[58] I. Savonije and E. P. Verlinde, Phys. Lett. **B507**, 305 (2001), hep-th/0102042.

[59] J. P. Gregory and A. Padilla, Class. Quant. Grav. **19**, 4071 (2002), hep-th/0204218.

[60] A. Padilla, (2002), hep-th/0210217.

[61] S. Nojiri, S. D. Odintsov, and S. Ogushi, Int. J. Mod. Phys. **A17**, 4809 (2002), hep-th/0205187.

[62] P. Singh and N. Dadhich, (2002), hep-th/0208080.

[63] R. Gregory and R. Laflamme, Phys. Rev. Lett. **70**, 2837 (1993), hep-th/9301052.

[64] R. Gregory and R. Laflamme, Nucl. Phys. **B428**, 399 (1994), hep-th/9404071.

[65] G. T. Horowitz and K. Maeda, Phys. Rev. Lett. **87**, 131301 (2001), hep-th/0105111.

[66] B. Kol, (2004), hep-th/0411240.

[67] S. S. Gubser, Class. Quant. Grav. **19**, 4825 (2002), hep-th/0110193.

[68] T. Wiseman, Class. Quant. Grav. **20**, 1137 (2003), hep-th/0209051.

[69] W. Israel, Phys. Rev. **164**, 1776 (1967).

[70] W. Israel, Comm. Math. Phys. **8**, 245 (1968).

[71] M. Heusler, Helv. Phys. Acta **69**, 501 (1996), gr-qc/9610019.

[72] M. Heusler, *Black Hole Uniqueness Theorems* (Cambridge University Press, 1996).

[73] R. Emparan and H. S. Reall, Phys. Rev. Lett. **88**, 101101 (2002), hep-th/0110260.

[74] J. L. Hovdebo and R. C. Myers, Phys. Rev. **D73**, 084013 (2006), hep-th/0601079.

[75] R. Emparan, JHEP **03**, 064 (2004), hep-th/0402149.

[76] S. D. Mathur, Fortsch. Phys. **53**, 793 (2005), hep-th/0502050.

[77] S. D. Mathur, (2005), hep-th/0510180.

[78] O. Lunin and S. D. Mathur, Nucl. Phys. **B623**, 342 (2002), hep-th/0109154.

[79] V. Balasubramanian, J. de Boer, E. Keski-Vakkuri, and S. F. Ross, Phys. Rev. **D64**, 064011 (2001), hep-th/0011217.

[80] J. M. Maldacena and L. Maoz, JHEP **12**, 055 (2002), hep-th/0012025.

[81] O. Lunin and S. D. Mathur, Nucl. Phys. **B610**, 49 (2001), hep-th/0105136.

[82] O. Lunin, J. Maldacena, and L. Maoz, (2002), hep-th/0212210.

[83] M. Taylor, (2005), hep-th/0507223.

[84] O. Lunin, JHEP **04**, 054 (2004), hep-th/0404006.

[85] S. Giusto, S. D. Mathur, and A. Saxena, Nucl. Phys. **B701**, 357 (2004), hep-th/0405017.

[86] S. Giusto, S. D. Mathur, and A. Saxena, Nucl. Phys. **B710**, 425 (2005), hep-th/0406103.

[87] I. Bena and N. P. Warner, (2004), hep-th/0408106.

[88] I. Bena and N. P. Warner, (2005), hep-th/0505166.

[89] P. Berglund, E. G. Gimon, and T. S. Levi, (2005), hep-th/0505167.

[90] I. Bena and P. Kraus, Phys. Rev. **D72**, 025007 (2005), hep-th/0503053.

[91] I. Bena, P. Kraus, and N. P. Warner, Phys. Rev. **D72**, 084019 (2005), hep-th/0504142.

[92] H. Elvang, R. Emparan, D. Mateos, and H. S. Reall, JHEP **08**, 042 (2005), hep-th/0504125.

[93] A. Saxena, G. Potvin, S. Giusto, and A. W. Peet, (2005), hep-th/0509214.

[94] V. Jejjala, O. Madden, S. F. Ross, and G. Titchener, Phys. Rev. **D71**, 124030 (2005), hep-th/0504181.

[95] G. T. Horowitz, (1992), hep-th/9210119.

[96] M. Cvetic, Nucl. Phys. Proc. Suppl. **56B**, 1 (1997), hep-th/9701152.

[97] J. P. S. Lemos, (1996), hep-th/9701121.

[98] D. Youm, Phys. Rept. **316**, 1 (1999), hep-th/9710046.

[99] S. Hawking and G. Ellis, *The Large Scale Structure of Spacetime* (Cammbridge University Press, 1973).

[100] W. L. Smith and R. B. Mann, Phys. Rev. **D56**, 4942 (1997), gr-qc/9703007.

[101] M. Banados, Phys. Rev. **D57**, 1068 (1998), gr-qc/9703040.

[102] D. R. Brill, J. Louko, and P. Peldan, Phys. Rev. **D56**, 3600 (1997), gr-qc/9705012.

[103] S. Holst and P. Peldan, Class. Quant. Grav. **14**, 3433 (1997), gr-qc/9705067.

[104] R. C. Myers and M. J. Perry, Ann. Phys. **172**, 304 (1986).

[105] C. V. Vishveshwara, Phys. Rev. **D1**, 2870 (1970).

[106] F. J. Zerilli, Phys. Rev. **D2**, 2141 (1970).

[107] W. Press and S. Teukolsky, Astrophys. J. **185**, 649 (1973).

[108] S. Chandrasekhar, *The Mathematical Theory of Black Holes* (Oxford, 1983).

[109] R. Emparan and R. C. Myers, JHEP **09**, 025 (2003), hep-th/0308056.

[110] E. Sorkin, Phys. Rev. Lett. **93**, 031601 (2004), hep-th/0402216.

[111] O. Aharony, J. Marsano, S. Minwalla, and T. Wiseman, Class. Quant. Grav. **21**, 5169 (2004), hep-th/0406210.

[112] H. S. Reall, Phys. Rev. **D64**, 044005 (2001), hep-th/0104071.

[113] D. J. Gross, M. J. Perry, and L. G. Yaffe, Phys. Rev. **D25**, 330 (1982).

[114] H. Kudoh, (2006), hep-th/0602001.

[115] R. C. Myers, Phys. Rev. **D60**, 046002 (1999), hep-th/9903203.

[116] B. Kol, JHEP **10**, 049 (2005), hep-th/0206220.

[117] D. R. Terno, Phys. Rev. Lett. **93**, 051303 (2004), hep-th/0403142.

[118] H. Kudoh and T. Wiseman, Phys. Rev. Lett. **94**, 161102 (2005), hep-th/0409111.

[119] B. Kleihaus, J. Kunz, and E. Radu, (2006), hep-th/0603119.

[120] H. Kudoh and U. Miyamoto, Class. Quant. Grav. **22**, 3853 (2005), hep-th/0506019.

[121] T. Harmark and N. A. Obers, Class. Quant. Grav. **21**, 1709 (2004), hep-th/0309116.

[122] T. Harmark and N. A. Obers, Nucl. Phys. **B684**, 183 (2004), hep-th/0309230.

[123] T. Harmark and N. A. Obers, (2005), hep-th/0503020.

[124] B. Kol, E. Sorkin, and T. Piran, Phys. Rev. **D69**, 064031 (2004), hep-th/0309190.

[125] E. Sorkin, B. Kol, and T. Piran, Phys. Rev. **D69**, 064032 (2004), hep-th/0310096.

[126] T. Harmark, Phys. Rev. **D69**, 104015 (2004), hep-th/0310259.

[127] D. Gorbonos and B. Kol, JHEP **06**, 053 (2004), hep-th/0406002.

[128] D. Gorbonos and B. Kol, Class. Quant. Grav. **22**, 3935 (2005), hep-th/0505009.

[129] J. L. Hovdebo and R. C. Myers, in preparation .

[130] B. Kol and E. Sorkin, (2006), hep-th/0604015.

[131] H. Elvang and R. Emparan, JHEP **11**, 035 (2003), hep-th/0310008.

[132] A. M. Polyakov, Nucl. Phys. **B268**, 406 (1986).

[133] H. Kleinert, Phys. Lett. **B174**, 335 (1986).

[134] U. Lindstrom, Phys. Lett. **B218**, 315 (1989).

[135] R. H. Price and K. S. Thorne, Phys. Rev. **D33**, 915 (1986).

[136] K. Thorne, R. Price, and D. Macdonald, *Black Holes: The Membrane Paradigm* (Yale University Press, 1986).

[137] G. Arcioni and E. Lozano-Tellechea, Phys. Rev. **D72**, 104021 (2005), hep-th/0412118.

[138] G. Arcioni and E. Lozano-Tellechea, (2005), hep-th/0502121.

[139] M. Nozawa and K.-i. Maeda, Phys. Rev. **D71**, 084028 (2005), hep-th/0502166.

[140] R. Gregory and R. Laflamme, Phys. Rev. **D51**, 305 (1995), hep-th/9410050.

[141] S. F. Ross and T. Wiseman, Class. Quant. Grav. **22**, 2933 (2005), hep-th/0503152.

[142] S. S. Gubser, JHEP **02**, 040 (2005), hep-th/0411257.

[143] J. J. Friess and S. S. Gubser, JHEP **11**, 040 (2005), hep-th/0503193.

[144] T. Harmark and N. A. Obers, JHEP **09**, 022 (2004), hep-th/0407094.

[145] H. Elvang, R. Emparan, D. Mateos, and H. S. Reall, Phys. Rev. Lett. **93**, 211302 (2004), hep-th/0407065.

[146] H. Elvang, R. Emparan, D. Mateos, and H. S. Reall, Phys. Rev. **D71**, 024033 (2005), hep-th/0408120.

[147] J. P. Gauntlett and J. B. Gutowski, Phys. Rev. **D71**, 025013 (2005), hep-th/0408010.

[148] J. P. Gauntlett and J. B. Gutowski, Phys. Rev. **D71**, 045002 (2005), hep-th/0408122.

[149] S. Chandrasekhar, *Ellipsoidal Figures of Equilibrium* (Yale University Press, 1969).

[150] G. T. Horowitz and H. S. Reall, Class. Quant. Grav. **22**, 1289 (2005), hep-th/0411268.

[151] P. K. Townsend, (1997), gr-qc/9707012.

[152] O. Lunin and S. D. Mathur, Phys. Rev. Lett. **88**, 211303 (2002), hep-th/0202072.

[153] O. Lunin and S. D. Mathur, Nucl. Phys. **B615**, 285 (2001), hep-th/0107113.

[154] A. A. Tseytlin, Mod. Phys. Lett. **A11**, 689 (1996), hep-th/9601177.

[155] J. C. Breckenridge, R. C. Myers, A. W. Peet, and C. Vafa, Phys. Lett. **B391**, 93 (1997), hep-th/9602065.

[156] J. C. Breckenridge *et al.*, Phys. Lett. **B381**, 423 (1996), hep-th/9603078.

[157] M. Cvetic and D. Youm, Nucl. Phys. **B476**, 118 (1996), hep-th/9603100.

[158] W. Press and S. Teukolsky, Nature **238**, 211 (1972).

[159] T. Damour, N. Deruelle, and R. Ruffini, Lett. Nuovo Cim. **15**, 257 (1976).

[160] V. Cardoso, O. J. C. Dias, J. P. S. Lemos, and S. Yoshida, Phys. Rev. **D70**, 044039 (2004), hep-th/0404096.

[161] Y. Zel'dovich, Pis'ma Zh. Eksp. Teor. Fiz. **14**, 270 (1971).

[162] Y. Zel'dovich, Zh. Eksp. Teor. Fiz. **62**, 2076 (1972).

[163] J. Friedman, Commun. Math. Phys. **63**, 243 (1978).

[164] N. Comins and B. Schutz, Proc. R. Soc. Lond. **A364**, 211 (1978).

[165] S. Yoshida and E. Eriguchi, MNRAS **282**, 580 (1996).

[166] S. F. Ross, JHEP **10**, 112 (2005), hep-th/0509066.

[167] G. T. Horowitz, JHEP **08**, 091 (2005), hep-th/0506166.

[168] S. Detweiler, Phys. Rev. **D22**, 2323 (1980).

[169] V. Cardoso and O. J. C. Dias, Phys. Rev. **D70**, 084011 (2004), hep-th/0405006.

[170] V. Cardoso and S. Yoshida, JHEP **07**, 009 (2005), hep-th/0502206.

[171] V. P. Frolov and A. Zelnikov, Phys. Rev. **D63**, 125026 (2001), hep-th/0012252.

[172] M. Cvetic and F. Larsen, Phys. Rev. **D56**, 4994 (1997), hep-th/9705192.

[173] S. A. Teukolsky, Astrophys. J. **185**, 635 (1973).

[174] V. P. Frolov and D. Stojkovic, Phys. Rev. **D67**, 084004 (2003), gr-qc/0211055.

[175] V. P. Frolov and D. Stojkovic, Phys. Rev. **D68**, 064011 (2003), gr-qc/0301016.

[176] M. Vasudevan, K. A. Stevens, and D. N. Page, Class. Quant. Grav. **22**, 1469 (2005), gr-qc/0407030.

[177] A. Starobinsky, Sov. Phys. JETP **37**, 28 (1973).

[178] A. Starobinsky and S. Churilov, Sov. Phys. JETP **38**, 1 (1973).

[179] W. G. Unruh, Phys. Rev. **D14**, 3251 (1976).

[180] V. Cardoso, O. J. C. Dias, and S. Yoshida, Phys. Rev. **D72**, 024025 (2005), hep-th/0505209.

[181] M. Abramowitz and A. Stegun, *Handbook of mathematical functions* (Dover Publications, 1970).

[182] S. Wolfram, *The Mathematica Book*, 5th ed. (Wolfram Media, 2003).

[183] E. Witten, Nucl. Phys. **B195**, 481 (1982).

[184] D. Brill and G. T. Horowitz, Phys. Lett. **B262**, 437 (1991).

[185] D. Brill and H. Pfister, Phys. Lett. **B228**, 359 (1989).

[186] J. Callan, Curtis G. and J. M. Maldacena, Nucl. Phys. **B472**, 591 (1996), hep-th/9602043.

[187] J. M. Maldacena and A. Strominger, Phys. Rev. **D55**, 861 (1997), hep-th/9609026.

[188] S. R. Das and S. D. Mathur, Nucl. Phys. **B478**, 561 (1996), hep-th/9606185.

[189] S. R. Das and S. D. Mathur, Nucl. Phys. **B482**, 153 (1996), hep-th/9607149.

[190] G. T. Horowitz and A. Strominger, Phys. Rev. Lett. **77**, 2368 (1996), hep-th/9602051.

[191] J. M. Maldacena, Phys. Rev. **D55**, 7645 (1997), hep-th/9611125.

[192] V. Cardoso, O. Dias, J. Hovdebo, and R. Myers, in preparation .

[193] D. Marolf and B. C. Palmer, Phys. Rev. **D70**, 084045 (2004), hep-th/0404139.

[194] V. Balasubramanian, P. Kraus, and M. Shigemori, Class. Quant. Grav. **22**, 4803 (2005), hep-th/0508110.

[195] O. Lunin and S. D. Mathur, Commun. Math. Phys. **227**, 385 (2002), hep-th/0103169.

[196] H. Lin, O. Lunin, and J. Maldacena, JHEP **10**, 025 (2004), hep-th/0409174.

[197] S. Corley, A. Jevicki, and S. Ramgoolam, Adv. Theor. Math. Phys. **5**, 809 (2002), hep-th/0111222.

[198] D. Berenstein, JHEP **07**, 018 (2004), hep-th/0403110.

[199] D. Martelli and J. F. Morales, JHEP **02**, 048 (2005), hep-th/0412136.

[200] J. T. Liu, D. Vaman, and W. Y. Wen, (2004), hep-th/0412043.

[201] J. T. Liu and D. Vaman, (2004), hep-th/0412242.

[202] G. Mandal, JHEP **08**, 052 (2005), hep-th/0502104.

[203] L. Grant, L. Maoz, J. Marsano, K. Papadodimas, and V. S. Rychkov, JHEP **08**, 025 (2005), hep-th/0505079.

[204] L. Maoz and V. S. Rychkov, JHEP **08**, 096 (2005), hep-th/0508059.

[205] D. Berenstein, (2005), hep-th/0507203.

[206] P. G. Shepard, JHEP **10**, 072 (2005), hep-th/0507260.

[207] V. Balasubramanian, J. de Boer, V. Jejjala, and J. Simon, (2005), hep-th/0508023.

[208] V. Balasubramanian, V. Jejjala, and J. Simon, (2005), hep-th/0505123.

[209] P. J. Silva, JHEP **11**, 012 (2005), hep-th/0508081.

[210] S. Mukherji and M. Peloso, Phys. Lett. **B547**, 297 (2002), hep-th/0205180.

[211] P. Kraus, JHEP **12**, 011 (1999), hep-th/9910149.

[212] C. Barcelo and M. Visser, Phys. Lett. **B482**, 183 (2000), hep-th/0004056.

[213] D. N. Vollick, Gen. Rel. Grav. **34**, 1 (2002), hep-th/0004064.

[214] A. J. M. Medved, JHEP **05**, 008 (2003), hep-th/0301010.

[215] A. J. M. Medved, (2002), hep-th/0205251.

[216] A. J. M. Medved, Class. Quant. Grav. **21**, 2749 (2004), hep-th/0307258.

[217] D. H. Coule, Class. Quant. Grav. **18**, 4265 (2001).

[218] S. Foffa, Phys. Rev. **D68**, 043511 (2003), hep-th/0304004.

[219] Y. S. Myung, Class. Quant. Grav. **20**, 935 (2003), hep-th/0208086.

[220] A. Biswas, S. Mukherji, and S. S. Pal, Int. J. Mod. Phys. **A19**, 557 (2004), hep-th/0301144.

[221] P. Kanti and K. Tamvakis, Phys. Rev. **D68**, 024014 (2003), hep-th/0303073.

[222] A. Chamblin, R. Emparan, C. V. Johnson, and R. C. Myers, Phys. Rev. **D60**, 064018 (1999), hep-th/9902170.

[223] W. Israel, Nuovo Cim. **B44S10**, 1 (1966).

[224] C. Misner, K. Thorne, and J. Wheeler, *Gravitation* (Freeman, 1973).

[225] T. Shiromizu, K.-i. Maeda, and M. Sasaki, Phys. Rev. **D62**, 024012 (2000), gr-qc/9910076.

[226] M. Sasaki, T. Shiromizu, and K.-i. Maeda, Phys. Rev. **D62**, 024008 (2000), hep-th/9912233.

[227] F. Leblond, D. Marolf, and R. C. Myers, JHEP **06**, 052 (2002), hep-th/0202094.

[228] F. Leblond, D. Marolf, and R. C. Myers, JHEP **01**, 003 (2003), hep-th/0211025.

[229] R. Matzner, N. Zamorano, and V. Sandberg, Phys. Rev. **D19**, 2821 (1979).

[230] S. Chandrasekhar and J. Hartle, Proc. R. Soc. London **A384**, 301 (1982).

[231] F. Mellor and I. Moss, Phys. Rev. **D41**, 403 (1990).

[232] F. Mellor and I. Moss, Class. Quant. Grav. **9**, L43 (1992).

[233] P. R. Brady, I. G. Moss, and R. C. Myers, Phys. Rev. Lett. **80**, 3432 (1998), gr-qc/9801032.

[234] J. Hartle and D. Wilkins, Commun. Math. Phys. **38**, 47 (1974).

[235] E. Poisson and W. Israel, Phys. Rev. Lett. **63**, 1664 (1989).

[236] E. Poisson and W. Israel, Phys. Lett. **B233**, 74 (1989).

[237] E. Poisson and W. Israel, Phys. Rev. **D41**, 1796 (1990).

[238] e. . Frolov, V. P. and e. . Novikov, I. D., *Black hole physics: Basic concepts and new developments* , Dordrecht, Netherlands: Kluwer Academic (1998) 770 p.

[239] G. T. Horowitz and A. R. Steif, Phys. Lett. **B258**, 91 (1991).

[240] C. R. Nappi and E. Witten, Phys. Lett. **B293**, 309 (1992), hep-th/9206078.

[241] J. Khoury, B. A. Ovrut, N. Seiberg, P. J. Steinhardt, and N. Turok, Phys. Rev. **D65**, 086007 (2002), hep-th/0108187.

[242] N. Seiberg, (2002), hep-th/0201039.

[243] N. A. Nekrasov, Surveys High Energ. Phys. **17**, 115 (2002), hep-th/0203112.

[244] S. Elitzur, A. Giveon, D. Kutasov, and E. Rabinovici, JHEP **06**, 017 (2002), hep-th/0204189.

[245] B. Craps, D. Kutasov, and G. Rajesh, JHEP **06**, 053 (2002), hep-th/0205101.

[246] M. Berkooz, B. Craps, D. Kutasov, and G. Rajesh, JHEP **03**, 031 (2003), hep-th/0212215.

[247] S. Elitzur, A. Giveon, and E. Rabinovici, JHEP **01**, 017 (2003), hep-th/0212242.

[248] B. Pioline and M. Berkooz, JCAP **0311**, 007 (2003), hep-th/0307280.

[249] J. Simon, JHEP **06**, 001 (2002), hep-th/0203201.

[250] J. Simon, JHEP **10**, 036 (2002), hep-th/0208165.

[251] H. Liu, G. W. Moore, and N. Seiberg, JHEP **06**, 045 (2002), hep-th/0204168.

[252] H. Liu, G. W. Moore, and N. Seiberg, JHEP **10**, 031 (2002), hep-th/0206182.

[253] A. Hashimoto and S. Sethi, Phys. Rev. Lett. **89**, 261601 (2002), hep-th/0208126.

[254] L. Cornalba and M. S. Costa, Phys. Rev. **D66**, 066001 (2002), hep-th/0203031.

[255] G. T. Horowitz and J. Polchinski, Phys. Rev. **D66**, 103512 (2002), hep-th/0206228.

[256] A. Lawrence, JHEP **11**, 019 (2002), hep-th/0205288.

[257] M. Fabinger and J. McGreevy, JHEP **06**, 042 (2003), hep-th/0206196.

[258] Y. Zel'dovich, Zh. Exsperim. i Teor. Fiz. **41**, 1609 (1961).

[259] S. W. Hawking and G. F. R. Ellis, *The large scale structure of space-time* (Cambridge University Press, 1973).

[260] A. Einstein, Sitzungsber. Preuss. Akad. Wiss. , 235 (1931).

[261] R. Tolman, Phys. Rev. **38**, 1758 (1931).

[262] M. Gasperini and G. Veneziano, Phys. Rept. **373**, 1 (2003), hep-th/0207130.

[263] P. J. Steinhardt and N. Turok, Phys. Rev. **D65**, 126003 (2002), hep-th/0111098.

[264] A. J. Tolley, N. Turok, and P. J. Steinhardt, Phys. Rev. **D69**, 106005 (2004), hep-th/0306109.

[265] J. Khoury, P. J. Steinhardt, and N. Turok, Phys. Rev. Lett. **92**, 031302 (2004), hep-th/0307132.

[266] P. Brax and D. A. Steer, (2002), hep-th/0207280.

[267] C. P. Burgess, P. Martineau, F. Quevedo, and R. Rabadan, JHEP **06**, 037 (2003), hep-th/0303170.

[268] S. Kachru and L. McAllister, JHEP **03**, 018 (2003), hep-th/0205209.

[269] H. Lu, S. Mukherji, C. N. Pope, and K. W. Xu, Phys. Rev. **D55**, 7926 (1997), hep-th/9610107.

[270] H. Lu, S. Mukherji, and C. N. Pope, Int. J. Mod. Phys. **A14**, 4121 (1999), hep-th/9612224.

[271] R. Poppe and S. Schwager, Phys. Lett. **B393**, 51 (1997), hep-th/9610166.

[272] K. Behrndt and S. Forste, Phys. Lett. **B320**, 253 (1994), hep-th/9308131.

[273] K. Behrndt and S. Forste, Nucl. Phys. **B430**, 441 (1994), hep-th/9403179.

[274] F. Larsen and F. Wilczek, Phys. Rev. **D55**, 4591 (1997), hep-th/9610252.

[275] A. Lukas, B. A. Ovrut, and D. Waldram, Nucl. Phys. **B495**, 365 (1997), hep-th/9610238.

[276] C. Grojean, F. Quevedo, G. Tasinato, and I. Zavala, JHEP **08**, 005 (2001), hep-th/0106120.

[277] C. P. Burgess, F. Quevedo, S. J. Rey, G. Tasinato, and I. Zavala, JHEP **10**, 028 (2002), hep-th/0207104.

[278] C. P. Burgess, P. Martineau, F. Quevedo, G. Tasinato, and I. Zavala C., JHEP **03**, 050 (2003), hep-th/0301122.

[279] L. Cornalba and M. S. Costa, Class. Quant. Grav. **20**, 3969 (2003), hep-th/0302137.

[280] A. Buchel, P. Langfelder, and J. Walcher, Annals Phys. **302**, 78 (2002), hep-th/0207235.

[281] A. Buchel, P. Langfelder, and J. Walcher, Phys. Rev. **D67**, 024011 (2003), hep-th/0207214.

[282] L. Cornalba, M. S. Costa, and C. Kounnas, Nucl. Phys. **B637**, 378 (2002), hep-th/0204261.

[283] M. Gutperle and A. Strominger, JHEP **04**, 018 (2002), hep-th/0202210.

[284] C.-M. Chen, D. V. Gal'tsov, and M. Gutperle, Phys. Rev. **D66**, 024043 (2002), hep-th/0204071.

[285] M. Kruczenski, R. C. Myers, and A. W. Peet, JHEP **05**, 039 (2002), hep-th/0204144.

[286] N. Ohta, Phys. Lett. **B558**, 213 (2003), hep-th/0301095.

[287] Y. Shtanov and V. Sahni, Phys. Lett. **B557**, 1 (2003), gr-qc/0208047.

[288] F. J. Yndurain, Phys. Lett. **B256**, 15 (1991).

[289] G. R. Dvali, G. Gabadadze, and G. Senjanovic, (1999), hep-ph/9910207.